Republic of Iraq
Ministry of Higher Education and Scientific Research
Babylon University
Collage of Materials Engineering
Department of Metallurgy

Improvement of Mechanical Behavior and Corrosion of Cu-25%Zn-4%Al Shape Memory Alloy

A Dissertation
Submitted to the Council of the Collage of
Materials Engineering / University of Babylon in Partial fulfillment of the Requirements for the Master Degree in Materials Engineering / Metallurgy

by
Israa Nayyef Kadhim Obais

Supervised by

Prof. Dr .Ali Hubi Haleem   Asst. Prof. Dr. Zuheir Talib Khulief

2021A.D   **1442A.H**

بِسْمِ اللَّهِ الرَّحْمَنِ الرَّحِيمِ

۞ وَيَسألُونَكَ عَنِ الرُّوحِ قُلِ الرُّوحُ مِنْ أَمْرِ رَبِّي وَمَا أُوتِيتُم مِّن الْعِلْمِ إِلاَّ قَلِيلاً ۞

صدق الله العلي العظيم

{ سورة الإسراء / آية 85}

Acknowledgments

First of all, profusely all thanks be for (**ALLAH , the most gracious**) of all creations who enable me to achieve this work. I would like to express my gratitude and appreciation to my supervisor, **(Prof. Dr. Ali Hubi Haleem and Asst. Prof. Dr. Zuheir Talib Khulief)** for guidance , advice and enthusiastic encouragement throughout my study.

I greatly thankful my department , Metallurgical Engineering and my College Materials Engineering for their assistance .

Many thanks are to everyone work in metallic and nonmetallic laboratories in Materials Engineering College / University of Babylon. Finally special thanks are to my family, thank you for being in my life.

Israa

Dedication

To My Family ..

To My Supervisors..

To My Teachers..

To My Friends..

With Respect….

Israa

Supervisors Certificate

We certify that this thesis entitled **"Improvement of Mechanical Behavior and Corrosion of Cu-25%Zn-4%Al Shape Memory Alloy"** is Prepared by (**Israa Nayyef Kadhim Obais**) under our supervision at the Department of Metallurgical Engineering**/** College of Materials Engineering / University of Babylon in partial fulfillment of the requirements for the Master Degree in Materials Engineering / Metallurgy .

Signature:

Name: Prof. Dr. Ali Hubi Haleem

(supervisor)

Date: / / 2021

Signature:

Name: Asst. Prof. Dr .Zuheir Talib Khulief

(supervisor)

Date: / / 2021

Abstract:

Due to the industrial and technological applications of copper-based shape memory alloys consist of Cu-25 wt% Zn-4 wt% Al exhibit an interesting research topic, also having many important characterises and advantages, including low cost compared to nickel-titanium alloy, easily of manufacture and the ability to recover its original shape. In this work, study the influence of different amounts of nickel (Ni), boron (B), and boron oxide (B_6O) additions to the alloy on its mechanical and chemical behaviore . This present study is divide in two parts. In the first part, the microstructure, phase characteristics, transformation temperatures, shape memory effect, and electrochemical properties of Cu –Zn – Al SMAs with Ni and B alloying additions has been investigated. Cu–25Zn–4Al SMAs were produced by powder metallurgy technique with and without the additions of 0.5, 0.7, and 1 wt.% of Ni or B. After mixing the powders for 4hr, the alloys were prepared using 675MPa compact pressure. The alloys were subjected to sintering process in tube furnace under "controlled atmosphere of argon with three steps. The first step at 350°C for 2hr; the second step at 550°C for 2hr; the third step at 900°C for 4hr. After that, many tests were carried out such as, X-ray diffraction, , DSC, SME, corrosion test For alloy before and after addition the elements (Ni) and (B).

The XRD and the microstructure analysis showed that all alloys compositions consisted of the predominating of two phases which phase CuZn(α) represent martensite and β phase (Cu5Zn8) represent the austenite. The results of transformation temperatures DSC test showed that the transformation temperatures (Af,As) for unmodified Cu – Zn – Al alloy is (0228.32 °C, 0326.93 °C),while the highest transformation temperature for modified Cu – Zn – Al-1% Ni alloy and modified Cu – Zn – Al-1% B are (274.64 °C, 335.38 °C) and (273.88 °C, 343.68 °C) respectively. The results of shape memory effect showed that modified Cu – Zn – Al-1% Ni and Cu – Zn – Al-1% B alloy

composition was higher than the unmodified Cu – Zn – Al SMA , where the results of SME were 29.1% at 1% wt.(Ni) and 23.65% at 1% wt.(B).

The corrosion test was carried out for the prepared alloys before and after addition with potentiodynamic polarization technique , and the results showed that the corrosion resistance improved by 36% at 1 wt% Ni and 25% at 1 wt% B. The corrosion rate was (0. 033 mpy) and (0.039 mpy), respectively, knowing that the corrosion rate of the base alloy is (0.052 mpy) . The energy dispersal X-ray spectroscopic examination of the sintered shape-memory alloy before and after addition of Ni and B was conducted to the surface of the samples after the corrosion process, in order to obtain the chemical composition of the protective layer covering the surface, the most important of which are (Al_2O_3), (Cu_2O) and (NiO).

Cu – Zn – Al SMA The second part studies influence of different amounts (1,3, and 5 wt. %) of boron oxide (B_6O) on the mechanical properties of the samples prepared modified Cu – Zn – Al – Ni or Cu – Zn – Al – B alloy . The results showed that the best value of the fine hardness (Hv.) are 176.6 and 165.8 for samples with the chemical composition of Cu-25Zn-4Al-1Ni- 3%B_6O and Cu-25Zn-4Al-1B- 3%B_6O alloy respectively. Wet sliding wear process also investigated for the samples prepared for 1 , 3, and 5 wt.% B_6O for modified Cu – Zn – Al –1Ni or Cu – Zn – Al –1B alloy compositions in tap water at 2, 5, and 10 N normal load at room temperature, and the results showed that 3% boron oxide B_6O gives the best wear resistance of the alloys prepared during this study.

Table of Content

Chapter three: Experimental Part

List of the figure

Chapter one : Introduction

Chapter Two : Theoretical Part & Literature Review

List of Tables

Chapter one : Theoretical Part

Chapter Tow : Theoretical Part & Literature Review

Chapter Three : Experimental Work

Chapter Four : Results and Discussions

List of Latin Symbols

Symbol	Meaning	Units
t	Time	Hour
T	Temperature	℃
Wt	Percentage of Weight	%
Pc	Compacting pressure	MPa
W	Weight	g
C.R	Corrosion Rate	(mpy)
P	Porosity	%
A	area of the surface	(cm^2)
E_{corr}	Corrosion potential	(mV)

List of Greek Symbols

Symbol	Meaning	Units
α	Martensite phase	-
β	Austenite phase	-
ρ	Density	g/cm^3

List of Subscripts & Superscripts

Symbol	Meaning	Units
Hv	Vickers hardness	Kg/mm
Icorr	corrosion current density	(μA/cm2).
ρ	density of the sample	(g/cm3)

List of Abbreviations

Symbol	Meaning
ASTM	American Society for Testing and Materials
XRD	x-ray diffraction
XRF	x-ray florescence
LOM	Light optical microstructure
EDS	Energy Dispersion Spectroscopy
SEM	Scanning Electron Microscopy
SMA	Shape Memory Alloys
PRV	pressure relief valve
SME	shape memory effect
TWSME	Two Way Shape Memory Effect
DSC	Differential Scanning Calorimeter
VHN	Vickers hardness number

Chapter One

Introduction

Chapter One

Introduction

1.1 General Review

Shape memory materials (SMM) are those category of materials which have the memorize or retain their previous form when they are subjected to certain stimulus in terms of thermal, mechanical, electrical, chemical, light and magnetic variations. Out of these materials SMAs have widely used due to its relatively higher values of specific strength, corrosion resistance, wear resistance, fatigue properties and good actuation response [1].

The first reported steps towards the discovery of the shape memory effect SME) were taken in the 1930s, when a shape memory behavior was studied in 1932 by ¨ Olander in his study of "rubber like effect" in samples of gold-cadmium is ok 1938 by Greninger and Mooradian in his study of brass alloys (copper-zinc). Many years later in 1951 Chang and Read first reported the term "shape recovery". Copper, zinc, aluminium alloys are formed between 60% to 80% copper, 15% to 30% consists of zinc, 3% to 10% of aluminium in various proportions [2] . The prepared shape memory alloys based on copper, zinc and aluminum provides a scope for dense, compact articles having good mechanical properties and other properties associated with the shape-memory effect [3]. In such processes the prepared powder is encapsulated, cold compacted, hot pressed and extruded. However, these ‘methods are not adapted to all practical requirements and the finished articles often leave something to be desired in their mechanical properties. The necessary characteristics of these alloys is to ensure the long-time operation of a shape memory alloy. Cu-Zn-Al alloy has been considered for many applications as a consequence of low density, high thermal conductivity, high specific modulus, good creep and fatigue resistance [3] .

1.2. Types of Shape Memory Alloys (SMAs)

SMA can be categorized based on a wide-ranging variety of classifications: Mode of actuation (thermal, magnetic) operating temperature and primary alloying elements. Table (1-1) also shows some of the important SMAs [4].

Table (1-1) The properties of different types of SMAs [5,6].

Characteristics	Ni-Ti	Cu-Al-Ni	Cu-Zn-Al
Yield strength(MPa)	580	400	80 -200
Ultimate tensile strength (MPa)	830	800	500 -600
Ductility (%)	54	7-5	15
Specific heat($J/K\cdot m^3$)	$2.980x10^6$	$3.52x10^6$	3.06×10^6
Thermal conductivity (J/K.M.S)	10	75	120
Electrical Conductivity ($1/\Omega.m$)	2×10^6	9×10^6	14.2×10^6
One-way effect(%)	8	7	4.5
Two-way effect(%)	5	1.6	1
Melting point (°C)	1250	1050	1020
Corrosion Resistance	Excellent	Good	Fair
Biological Compatibility	Excellent	Bad	Bad

1.3. Applications of Shape Memory Alloys

Over the past the development in material science was determined by the discovery of new material properties. Today shape memory alloys (SMAs) are already commercially applied in several technical fields such as automotive, aerospace, medicine and they can be very successfully used as actuators or connectors in electronic devices[7] . SMAs are gaining special attention particularly in the aerospace and biomedical applications. A recent well-known project in the aerospace applications of the shape memory alloys involves bending in the variable-geometry chevron (VGC) [8]. The alloys have also been exploited in the mechanical and electromechanical control systems, for example a precise mechanical response to the small and repeated temperature changes. Shape memory alloys are also used in a wide range of the medical and dental applications (healing broken bones, misaligned teeth)[9].

1.3.1. Fluid connectors and Safety valves

Cu-Zn-Al shape memory alloy used for the application of fluid line connectors are essential to liquid cooling loops . CuZnAl alloy consider selection, installation, and maintenance of a system's fluid connections to prevent leaks and ensure system longevity. Fluid connectors can be considered either fittings or couplings, which are common hardware components in a liquid cooling system. Both connect cooling loop components such as valves, pumps, liquid cold plates, heat exchangers, hoses, etc. A coupling enables quick connection and disconnection a line without fluid loss or introducing air into a system[10]. A coupling is a better fluid connector for systems that require fast assembly or routine maintenance , while a safety valve is a valve that acts as a fail-safe. An example of safety valve is a pressure relief valve (PRV), which automatically releases a substance from a boiler, pressure vessel, or other system, when the pressure or temperature exceeds preset limits. Pilotoperated relief valves are a specialized type of pressure safety valve, a leak tight, lower cost [10]. Figure (1-1) shows applications SMAs in the fluid connectors and safety valves . .

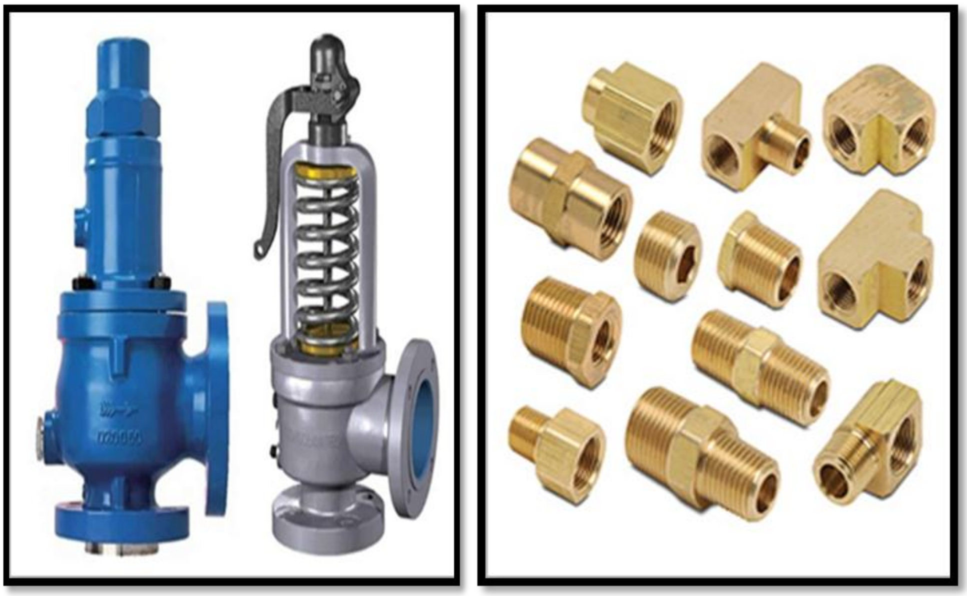

Figure (1-1) Applications of SMAs in the fluid connectors and safety valves[10, 11]

1.3.2. Aerospace applications of SMAs

SMAs are being explored as vibration dampers for launch vehicles and commercial jet engines. The large amount of hysteresis observed during the superelastic effect allow SMAs to dissipate energy and dampen vibrations Designers and other Engineers in various fields ,they have worked on the ways to develop the convert thermal energy into mechanical work via the crystallographic phase variant of SMAs[10]. Designers have utilized both the pseudo elastic effects and shape memory effect of shape memory alloys in finding solutions to the engineering problems of the aerospace industry [10]. SMA beams force chevrons to change shape and move in to aspecific direction in which the noise of the engine will be reduced. At higher altitudes where the temperature decreases, SMA beams become colder and force the chevrons to return to their original shape to increase the fuel efficiency. There is also strong interest in using SMAs for a variety of actuator applications in commercial jet engines, which would significantly reduce their weight and boost efficiency [11]. Figure (1-2) showns application of SMAs in the configuration of the Boeing VGC variable-geometry chevron .

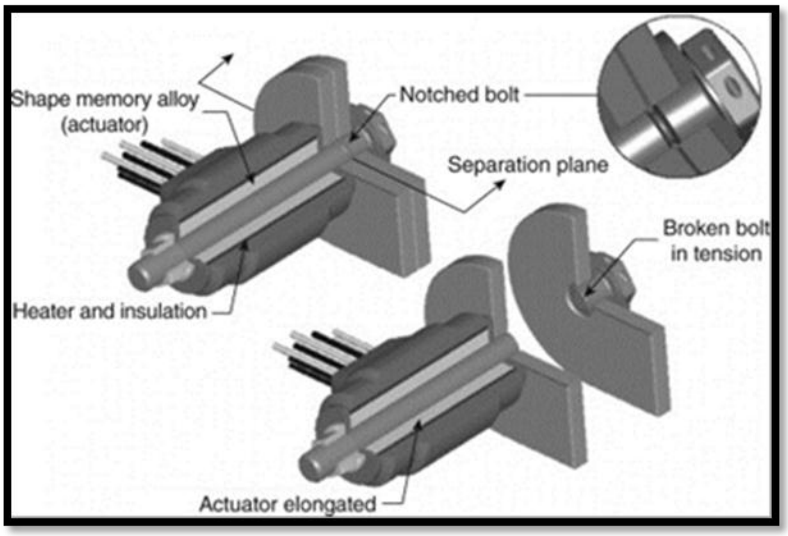

Figure (1-2) :Configuration of the use of shape memory alloys (SMAs) in aerospace engineering[11]

1.3.3. Cellulars phone Industry

The major applications for these alloys are in the field of cellular phone antennas .The cellular phone is now ubiquitous being in view in almost every public arena. The cellular phone area, formerly of stainless steel, is now universally manufactured from superelastic NiTi alloy due to the great resistance to permanent set on bending and accidental damage. Significant cold work is often used to enhance the low temperature superelasticity. Ni-rich chemistry or ternary addition is also used to achieve this desired property [13] . Figure (1.3) represent application , of SMAs in the cellulars phone .

Figure (1.3): Superelastic antenna for a cellular phone [14].

1.4. Objectives of The Present Study

The aim of this study is to investigate Cu-25Zn-4Al shape memory alloys prepared by powder metallurgy route. Several parameters have been taken in to consideration such as:

1. To systematically investigate the effect of the Ni and B addition on the microstructures shape memory properties and corrosion behaviour of unmodified Cu- Zn- Al shape memory alloy .
2. To systematically investigate the effect of the B_6O addition on the mechanical and wear resistance of Ni and B modified Cu- Zn- Al shape memory alloy .
3. Study the effect of addition alloying elements on the transformation temperature of martensite .

Chapter two

Theoretical & Literature Review

Chapter Two

Theoretical Part & Literature Review

2.1. Introduction

This chapter deals with metals and alloys selected in fabrication of the shape memory alloys (SMAs) , namely with copper zinc aluminum (CuZnAl) alloy and thermal equilibrium phase diagram of the alloy . In addition, there is a clear overview on the characteristics of shape memory alloys, thermomechanical behavior, wet wear resistance and corrosion of shape memory alloys. Powder metallurgy and its basic steps will be presented. Furthermore, theoretical considerations of powder metallurgy technique for copper base alloys taking into consideration types of compaction and sintering processes have been presented also the type of corrosion occurs in metallic materials .

2.2. Shape Memory Alloys (SMAs)

A wide variety of SMAs have been investigated over the last seven decades. New composition have been fabricated by adding different alloying elements to existing alloys, providing a catalog of SMAs with a variety of properties [15] . Such a wide selection give designers a great flexibility in tailoring SMA properties to match the constraints of a given commercial applications [16]. Shape memory alloys can be classified based on a wide variety of categories including primary alloying elements, mode of actuation (magnetic, thermal) operating temperature, and desired behavior. In the following section will briefly discuss the types of shape memory alloys , and we will focuse on CuZnAl, the alloy of this work.

2.2.1 Ti-Ni Shape Memory Alloy

In the early 1960s, Buehler and co-workers first explored the shape memory effect an (SME) in equiatomic NiTi alloy [17]. This alloy , commonly referred as "Nitinol", has been investigated extensively [17]. Nitinol is an alloy of nickel and titanium in approximately 50:50 ratios [18]. It is superelastic and can tolerate large strains without being irreversibly deformed[19]. The major physical properties of the basic binary NiTi system and some of the mechanical properties of the alloy in the annealed condition are listed in Table (2.1) [20].

Table (2.1): Properties of Binary Ni - Ti Shape Memory Alloys [21]

Properties	Value of properties	Austenite	Martensite
Melting Temperature deg. °C	1300	------	------
Density g/cu.cm	6.45	------	------
Resistivity micro-ohms*cm	------	~ 100	~70
Thermal conductivity W / cm * deg . °C	------	18	8.5
Corrosion Resistance	Similar to 300series Steel or titanium alloy	------	------
Shape memory strain	8.5% maximum	-------	-------
Young Modulus GPa	------	83	28 -41
Yield Strength MPa	------	195-690	70-140
Ultimate Tensile Strength Mpa	895	------	------
Transformation Temperatures °C	- 200 to 110	------	------

Ti - rich NiTi and Ni-rich NiTi differs from equiatomic NiTi the additional Ti increases the transformation temperatures of alloy . While , increasing Ni content decreases the transformation temperatures of alloy . These alloys exhibit pseudoelasticity over a wide range due to the effect of precipitation, which increase the hardness of the matrix [21].

2.2.2. Iron-base Shape Memory Alloy

Iron based shape memory alloys have been largely investigated during the last years. They are known to exhibit less SME than many other alloys types. Fe Mn Si alloy is a example of iron based SMAs that widely studied [23]. It was recently found that the SME in Fe Mn Si based alloys can be greatly improved by addition of small amounts of Nb and C [24].

2.3 Copper Based Shape Memory Alloys

Copper-based shape memory alloys have some advantages, such as low cost and simple fabrication procedure, compared to Ti-Ni alloys. The ternary Cu-Zn-Al and Cu-Al-Ni alloys have been extensively studied and they are also now commercially available [25].There are other commercial alloys include Cu-Al-Mn and Cu-Al-Be alloys. However, the applications of these alloys have been much limited mainly for two reasons: the first reason , the poor ductility and workability of the polycrystalline alloys resulting from the coarse grains [25] .

Cu-Al-Ni alloys have a good thermal stability and higher operating temperatures than the Cu-Zn-Al alloys, they may become one candidate for practical high-temperature shape-memory alloys[26]. Indeed, the workability of the Cu-Al-Ni alloys can be significantly improved by adding small amounts of alloying elements to the alloys [25].

It is well known that many copper alloys such as CuAl, Cu-Zn-Al, Cu-Al-Ni and Cu-Al-Mn exhibit shape memory properties [27]. Cu-based SMAs have attracted much attention due to their good shape memory capacity, narrow temperature region of transformation, ease of fabrication and low production cost [27]. For the alloys of the ternary Cu-Zn-Al system, the shape memory effect is only observed within a certain range of composition which generally contains 16 to 30% of Zn and 4 to 8% of

Al . Depending on alloy composition and temperature, three equilibrium phases (α, β and γ) may occur[28]. However, β phase is the only phase that exhibits the shape memory effect of practical importance. The β phase in the Cu-Zn-Al alloys is disordered at high temperatures and has a Bcc lattice[26,27]. During the cooling process and depending on the alloy composition the parent β-phase can order in two different superlattice structures β2 and β3 [28]. By stress-induced or thermally, the β2 or β3 austenite phases transform into the β2 ' or β3 ' martensitic phases[28].

Cu-Zn-Al alloys are usually quenched to retain the β phase for further transformation to martensite .Figure (2.1) Effect of alloying elements on Cu–Zn–Al characterization [28].

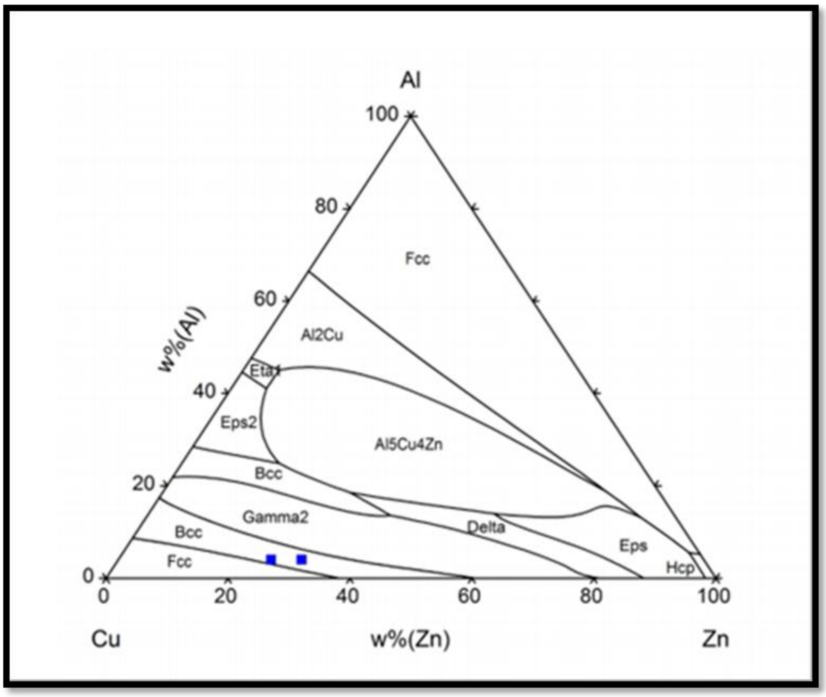

Figure: (2.1) Effect of alloying elements on Cu–Zn–Al characterization[28].

Cu–Zn–Al alloys are the most studied Cu-based alloys and have been explored for use in applications such as fasteners, springs, couplings and thermal actuators where the use of other alloys would be technically and economically ineffective [26,27]. Cu–Zn–Al alloys have relatively higher strain recovery compared to other Cu-based alloys. However, similar to other Cu-based alloy grades [28]. Grain refinement has been proffered as a technique for the improvement of mechanical and shape memory properties of Cu-based SMAs . The use of micro-alloying elements such as B, Ti, V, Ce, Fe, Co, Be and Zr have been the most reported of these approaches; and many of the investigations show that their presence has influence on the microstructure, transformation and shape memory properties of Cu-based SMAs [31]. B and Fe are the least expensive of these micro-alloying elements and have been reported to be very efficient grain modifiers [31]. However there have been divergent opinions on the optimum concentrations of these micro-alloying elements and the mechanisms for effecting grain modification in Cu-based SMAs in general and Cu–Zn–Al SMAs in particular. For instance, Wang et al. [31] reported that 0.01% B was the optimum concentration required to achieve grain refinement in Cu–Zn–Al alloy [32] stated that B concentration within the range of 0.05–0.08% was sufficient for effective grain refinement. Fe concentration for effective grain modification and enhanced mechanical properties has also been subject of research discuss recently [33].

2. 4 Shape Memory Property and Superelasticity

The phenomenon of shape memory property was observed in 1920 by Johnson from observations of a copper and zinc alloys. In 1938 Greninger and Mooradian published a comprehensive article of the properties of SMAs [34]. The first attempt to explain the shape memory effect on NiTi is attributed to Zijdervled and associates, who established in 1966 that the unique properties were due to a crystalline transition induced by temperature change or application of stress [35].

Several alloys have been discovered that exhibit the shape memory effect, as listed in Table (2.2). The majority of these alloys can be generalized into three major categories: Ni-Ti-based, Cu-based, and those containing precious metals. Only the Cu-Zn-Al, Cu-Al-Ni, and Ni-Ti alloys are presently of commercial importance[36].

Table (2.2) :Alloys exhibiting the shape memory effect **[36].**

Alloy	***Austenite Structure***
Au-Cd	B2
Cu-Zn	B2
In-Ti	FCC
Ni-Ti	B2
Cu-Zn-Al	B2, DO3
Ti-Nb	BCC (disordered)
Au-Cu-Zn	No data
Cu-Zn-Sn	B2
Cu-Zn-Si	B2
Cu-Al-Ni	DO3
Ag-Cd	No data
Cu-Sn	B2
Cu-Zn-Ga	B2
Ni-Al	B2
Fe-Pt	LI_2
U-Nb	BCC (disordered)
Ti-Pd-Ni	B2
Fe-Mn-Si	FCC (disordered

SMA presents two well - defined crystallographic phases, austenite and martensite. Martensite is a phase that, in the absence of stress, is stable only at low temperatures. The austenite phase is the parent state of the metal alloy. The two crystal lattices stable under certain thermodynamic conditions for a given alloy, characterize the two ultimate products of the martensitic reaction, so that after its completion, the whole volume of material is represented only by one or another phase. In the low temperature (martensite) phase, the alloy can be easily bent and shaped, as the metal is reheated (austenite), its original shape and stiffness are restored [37].

2.5 Characteristics of Shape Memory Alloys

2.5.1 Shape Memory Effect(SME)

Shape Memory Effect (SME) is the ability to remember a predetermined shape even after several deformation. The shape changes with temperature variation are mainly attributed to martensite phase trasformation. Shape memory effect is a phenomenon such that even though a specimen is deformed below austenite start temperature As, it regains its original shape by virtue of the reverse trasformation upon heating to a temperature above austenite finish temperature (Af) [36] . In particular, Ni–Ti alloys exhibits the SME when specimens are deformed below martensite finish temperature (Mf) or at temperature between (Mf) and (As), above which the martensite becomes unstable. Depending upon the temperature range, the SME phenomenon are slightly different, as schematically shown in Figure. 2.2 supposed, to simplify the model [37].

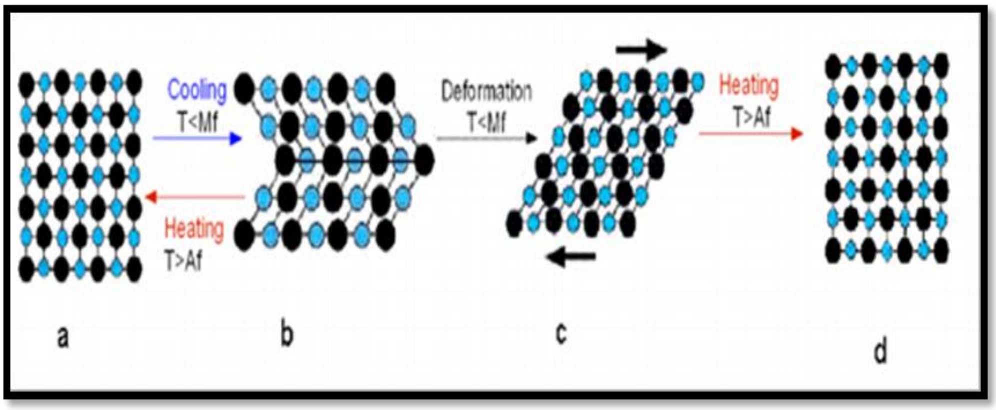

Figure. 2.2: parent phase, b-self–accomodeted in martensite, c-deformation in martensite(twenning and detweening), d-upon heating to a temperature above Af (reverse trasformation) [37].

Consider a single crystal in parent phase (T ≤ Mf)(a). Supposed to cool the single crystal to a temperature below Mf (b). Then, martensite are formed in a self-accommodation manner(c). Thus, if an external stress is applied, and if the stress is high enough, it will become a single variant of martensite under stress. Such a high mobility of the twin boundary, in which a single variant of martensite change into the twin orientation by shear. When the speciemen is heated to a temperature above Af, reverse trasformation occurs [38]. Figure (2.3) that shown shape memory effect microscopically

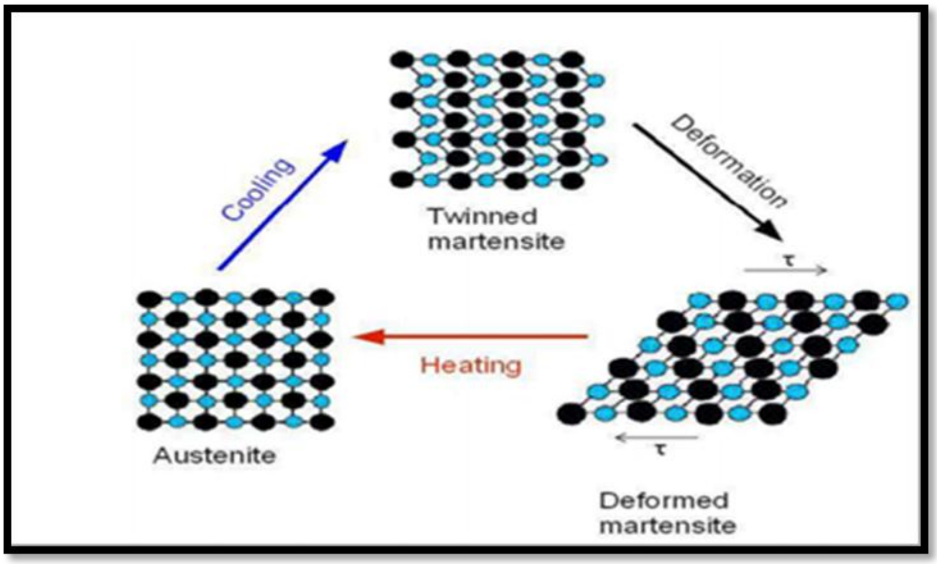

Figure (2.3): Shape memory effect shown microscopically[39].

Austenite is cooled to form twinned Martensite without undergoing a shape change, when is deformed by moving twin boundaries. Heating either state will return the originally austenitic structure and shape [39].

The reverse transformation induced by heating recovers the inelastic strain; since martensite variants have been reoriented by stress, the reversion to austenite produces a large transformation strain having the same amplitude but the opposite direction with the inelastic strain and the SMA returns to its original shape of the austenitic phase (d) [39] .

This is the mechanism of SME. In particular, the above described phenomenon is called One–Way Shape Memory Effect (OWSME). One Way Shape Memory Effect is an intrinsic property of SMAs[39], the macroscopically behavior is schematically of OWSME is explained in Figure(2.4) [39].

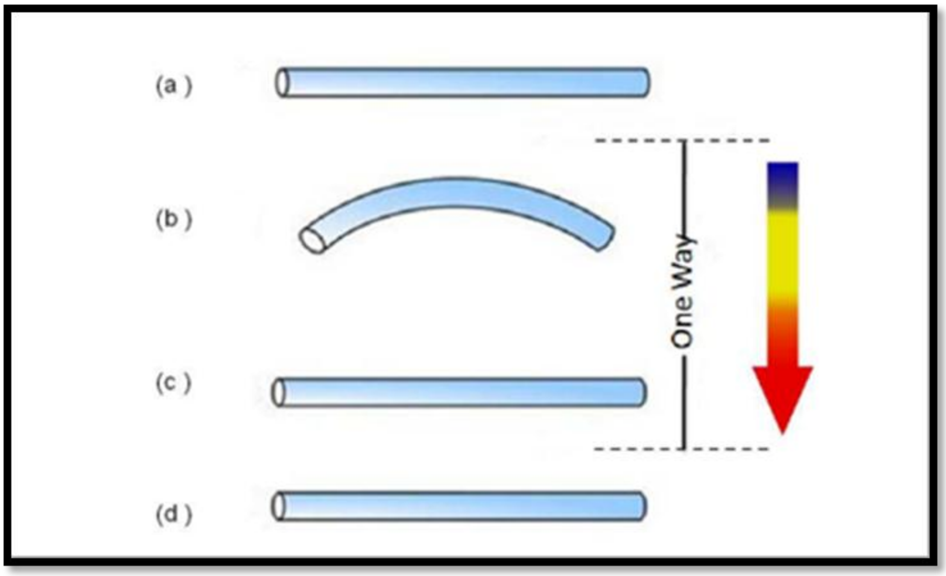

Figure (2.4): Macroscopically mechanism of one way shape memory effect: (a) Martensite, (b) Loaded and Deformed in martensite phase T≤ Mf, (c) Heated above T G As (austenite),(d) Cooling to martensite T≤ M [39].

2.5.1.1 Two Way Shape Memory Effect (TWSME)

The mechanism of SME describe above, only the shape of the austenitic phase is remembered. However, it is possible to remember the shape of the martensitic phase under certain condition. This behavior is a common property of SMA, it is called Two Way Shape Memory Effect (TWSME), in contrast to One Way Shape Memory Effect (OWSME) [40,41].

TWSME is not intrinsic property as the (OWSME) to SMA, but it can be exhibited after specific thermomechanical treatments .TWSME refers to the reversible and spontaneous shape change of materials with thermal cycling, in other words, this property permetted to SMA a spontaneous shape change on both heating and cooling[46] .

Once that the material has learned the behavior, it is possible to modify the shape of the material, in a reversible way between two different ones and without applied stress or load, only by changing of temperature across Af and Mf. The first report of Two–Way shape memory effect is done by Delay ,then by Wang and Buehler for a Ti-Ni alloy; a schematic representation of the macroscopic observed behavior of TWSME is shown in Figure (2.5) [46] .

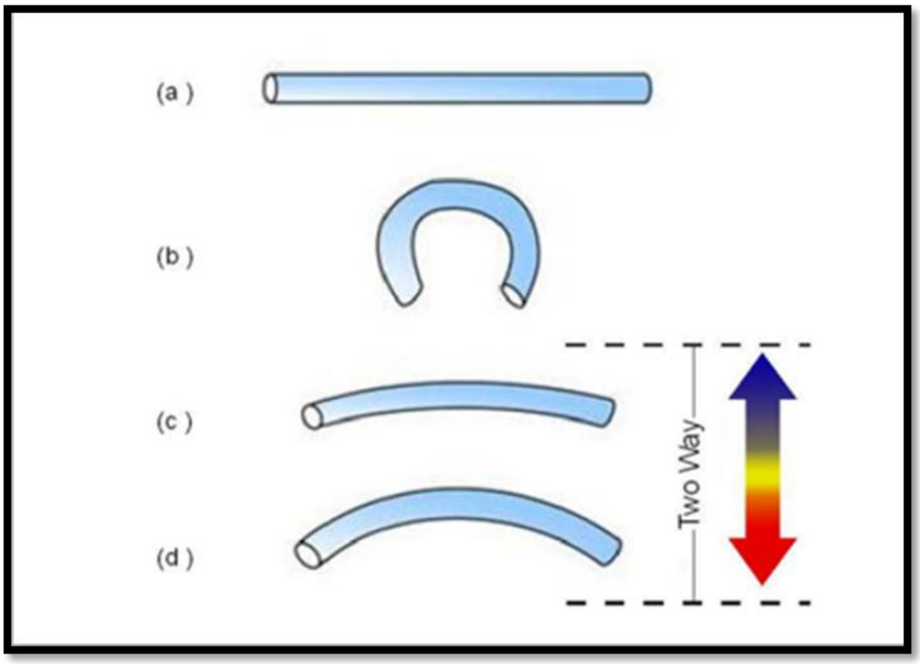

Fig. 2.5: Macroscopically Mechanism of Two Way Shape Memory Effect: (a) Martensite state, (b) Several deformation with an irreversible amount, (c) Heated, (d) Cooled [42] .

At microscopic level, the reason for which a specimen remembers the shape is explanetion as follows. Upon heavy deformation in martensitic phase, dislocations are introduced so as to stabilezed the configuration of martensitic phase. These dislocation exist even in the parent phase after reverse martensite upon heating [42] .

In particular, there are three key microstructural forms for SMA The first is austenite, the second is martensite. The third is a stress–biased martensite, is created either by stressing martensite below Mf, or by stressing austenite near but above Af. This key microstructure is preferred in which becomes learned by the alloy during training process. Therefore, this structure promotes the TWSME[42].

At low temperature, a SMA can be seemingly "plastically" deformed, but this "plastic" strain can be recovered by increasing the temperature. This is called the shape memory effect (SME), Fig. 2.6 (a). At a high temperature , a large deformation can be recovered simply by releasing the applied force, and this behaviour is called Superelasticity, Figure (2.6 b) [43].

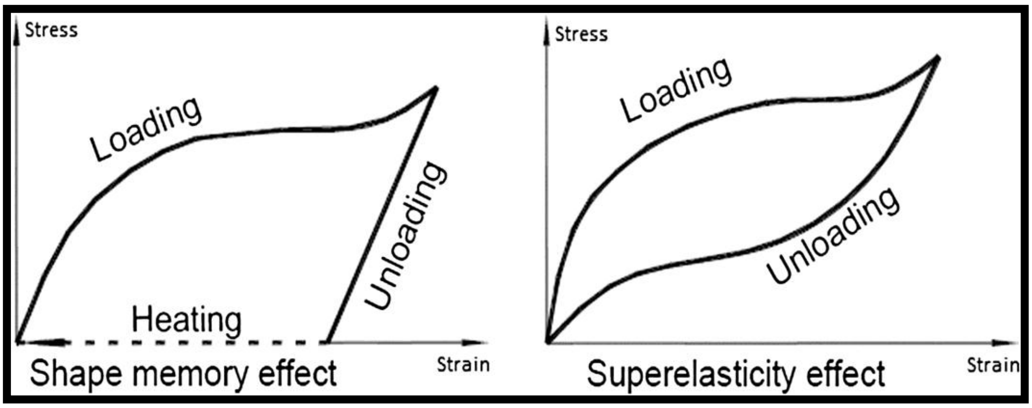

Figure: (2.6) Shape memory behaviour. (a) Shape memory effect; (b) superelasticit[43]

The shape memory effect in metals is a very interesting phenomenon. Just imagine taking a piece of metal and deform it completely and then restore it to its original shape with the application of heat. Taking a shape memory alloy spring and hanging a weight on one end of the spring can easily illustrate this[43]. After the spring has been stretched, heat the spring with a hot air gun and watch it return to its original length with the weight still attached. These materials undergo a thermomechanical change as they pass from one phase to another . In addition to the family of nickel–titanium alloys , there are other alloys that exhibit the shape memory effect. These alloys are silver–cadmium, gold– cadmium, copper–aluminum–nickel, copper–tin, copper–zinc, combinations of copper–zinc with silicon or tin or aluminum, indium–thallium, nickel–aluminum, iron–platinum, manganese–copper, and iron–manganese–silicon[44].

When a SMA is in austenite phase, it exhibits a highly elastic behavior. This allows the alloy to deform up to 7% and then fully recover the resulting strain by simply removing the load. This behavior is known as the pseudoelastic effect or pseudoelasticity; though pseudoelasticity is an important characteristics of SMAs, typical applications of these materials require use of the shape memory effect, which is a result of temperature induced transformation .The value of this transformation temperature depends on the composition of the alloy [45] .

The basis for the shape memory effect is that the materials can easily transform to martensite phase. Shape memory effect is associated with the crystallographically reversible nature of the martensitic transformation which appears in shape memory alloys. The shape memory and super elasticity effects are characteristic of thermo elastic transformation [46].

2.5.2 Phase Transformation

Phase transformation in crystallike materials can be classified into two groups; one is diffusional transformation and the other, diffusionless or displacive transformation[46]. In the case of diffusional transformation, atoms leave one crystal structure to form another structure by diffusion[47]. For this reason, a high temperature is generally necessary to ensure that the mobility of atoms is high, otherwise the transformation is too sluggish[46]. Meanwhile, it is possible for the atoms to alter the crystal structure without leaving the original crystal by their coordinated displacive movements. This does not require long range diffusion of atoms and takes place in a relatively short time. Martensitic transformation belongs to this second category of diffusionless transformation and is characterized by well-coordinated shear dominant atomic displacement, as shown in Figure (2.7) [46].

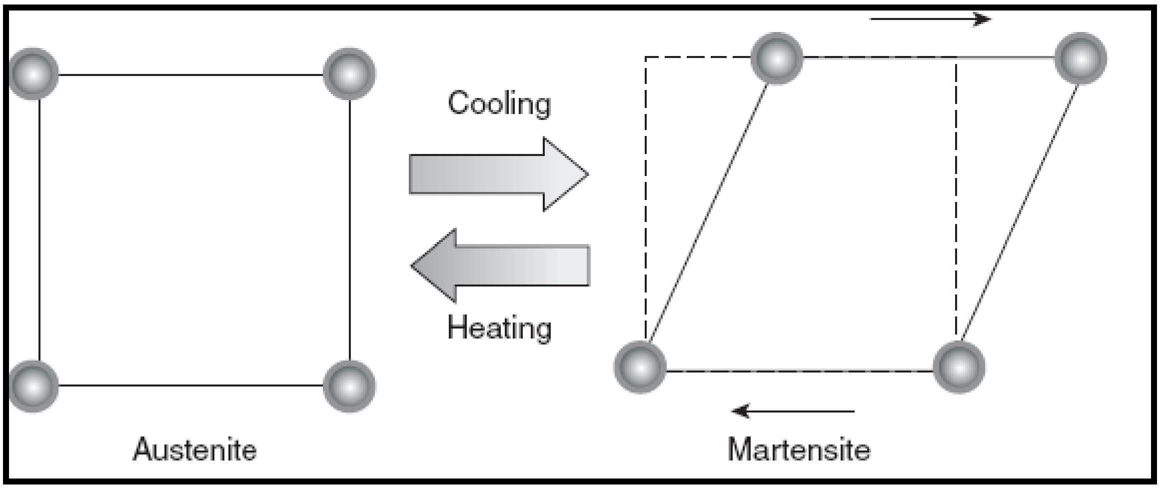

Figure : (2.7) Schematic illustration of change in unit cell shape on martensitic transformation [46] .

The characteristic properties of shape memory alloys are all due to the phase transformations in the alloy from martensite to austensite due to the change in the temperature. When the alloy is heated to higher temperatures, martensite transforms to austensite The starting temperature of austenite formation is As and finish temperature is Af. Similarly the starting and finishing martensite temperatures are Ms and Mf respectively. The transformations are characterized by these four temperatures (Figure 2.8) which are composition dependent. The different between the heating transition and the cooling transition gives rise to the hysteresis effect where some of the mechanical energy is lost in the process [47] .

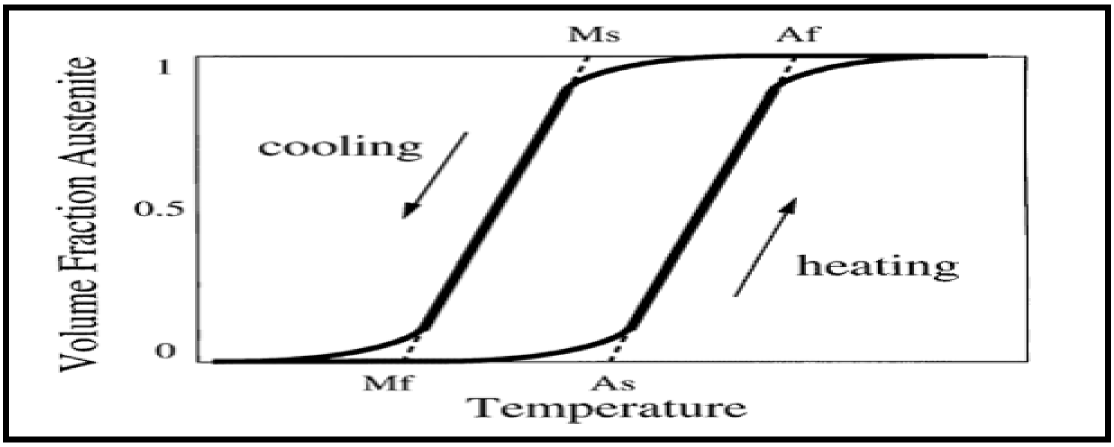

Figure 2.8 Martensite-Austenite transformation temperature[47]

2.5.3 Super Elasticity (Pseudo Elasticity)

The superelasticity (SE) pseudoelastic material may return to its previous shape (hence, shape memory) after the removal of even relatively high applied strains [48].A superelastic alloy deforms reversibly to very high strains (up to 10%) by the creation of a stress-induced phase. When the load is removed, the new phase becomes unstable and the material recovers its original shape [47]. Unlike shape-memory alloys, no change in temperature is needed for the alloy to recover its initial shape. is characterized by the closed loop hysteresis in the stress-strain diagram and is explained by the mechanism of stress-induced martensitic transformation SE, which occurs at a temperature above Af, which is caused by a stress-induced martensitic transformation upon loading and by the subsequent reverse transformation upon unloading[47]. It is observed that due to the associated strain energy which they are used as damping material and energy storage devices. The crystalline structure of martensite has two forms, twinned and detwinned, which give the SMA its pseudoelastic property [48] .

2. 5. 4 Martensitic Transformations:

The martensitic transformation is one of the maximum pervasive phase modifications found to arise in some of material systems inclusive of metallic, polymeric and ceramic structures[49]. This transformation is a diffusionless solid to solid shear transformation from a better temperature phase which ends within side the formation of martensite[49]. Martensitic modifications may be thermoelastic (nucleation independent)or non-thermoelastic (nucleation dependent modifications in ferrous alloys)[47]. Diffusion transformation provide an explanation for wherein a information phases can simplest be created through shifting atoms at random over lengthy range .Long rang diffusions is perfect due to the fact the information phases is in various chemical synthesis as compared to the matrix from which it's miles created. Since then atomics migrations is desired , the proceed of this form of variations is depend on each instances and temperatures. In disparity , diffusionless transformation the atoms are cooperatively rearranged into a new greater stables crystals systems however with out changing the chemical substances natures of the matrix ,and the atomics migrations is now no longer needing[48]. Diffusionless transformation usually continue in a time–in dependents models due to the fact its rely simplest on temperature so the known as thermals transformation[48] .Martenesitic transformation is shaped upon cooling from a highs temperatures phases named the parents phases or austenitic phases to the rooms temperatures segment that is the martensites segment. The expressions "Martensite" and "austenite " are initially supposed to refers simplest metal phases however the greater generalized definition relating to the type of transformation product and now no longer the particular material. In bodily metallurgy, the time period martensite is used to explain any diffusionless transformation product. [48]. Martensitics transformation are firsts orders transformation which imply that heats release while martensites is created .The transformation from determine section to martensites may be looked after in parts, the lattices invariants shear and Bain strains. The Bain strains or lattices deformations encompass all of the atomics actions essential to create the information systems from the antique structure [48]. As the interface progresses one atomics layers, each atoms had to actions in little quantities as proven in Figure (2.9) . The ends effects of a majority of these small organized motions are the information martensites systems .The motions essential to create the information systems are named as Bain strains[49].Martensitic transformation may be defined in Figure(2.9) [49].

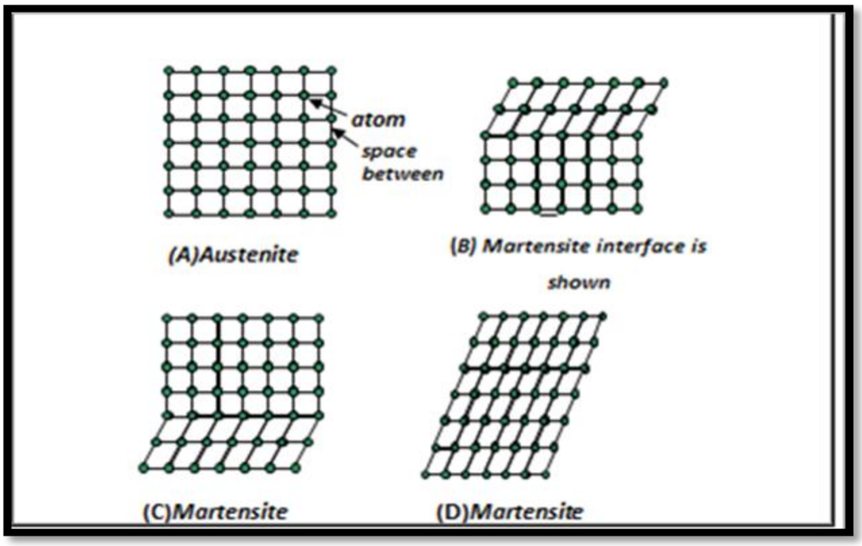

Figure(2.9): The Transformation from Austenite to Martensite .A. Austenitic Phase ,B. and C. Interface Advance and D. Completely Martensitic Phase[49].

2. 5. 5. Martensite Structure and Morphology

The formation of martensite as shown in micrographs to be a random operation and that is shown clearly in Figure (2.10) . It has been shown that the martensitic phase is more often looks like lens and extending for the whole grain diameter [50] .

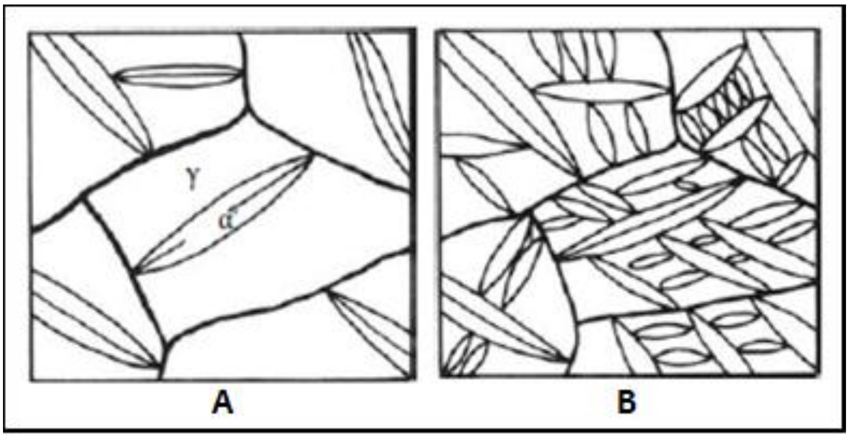

Figure(2. 10) : (A), (B) Growth of martensite with increasing cooling below Ms [51].

2.6 Thermomechanical Behavior

The mechanical properties of shape memory alloys vary greatly within the temperature range where the transformation occurs [52]. As you can see in Figure (2.11), this Figure shows a simple stress-strain curve for Nitinol alloys tested under loads below and above the transformation temperature range [53]. Martensite is prone to different degrees of deformation under lower stress, while the yield strength and yield strength of austenite (high temperature phase) are much higher. After the stress is relieved, the sample "remembers" its undeformed shape and returns to its original shape when the material becomes austenite. This shape recovery is not observed in the austenite phase under stress and heating, because no phase transformation has occurred. The stress-strain behavior is shown in Figure (2.11c), where the material is tested at a temperature just above the transition temperature. At this temperature, martensite can be induced by stress. It then deforms immediately and shows an increasing deformation under constant stress, as shown by AB. However, after the discharge, the material returns to austenite under lower stress, as shown by the line CD, the shape recovery is not due to heating, but due to reduced stress. This effect makes the material extremely elastic. It is called pseudo-elasticity [54].

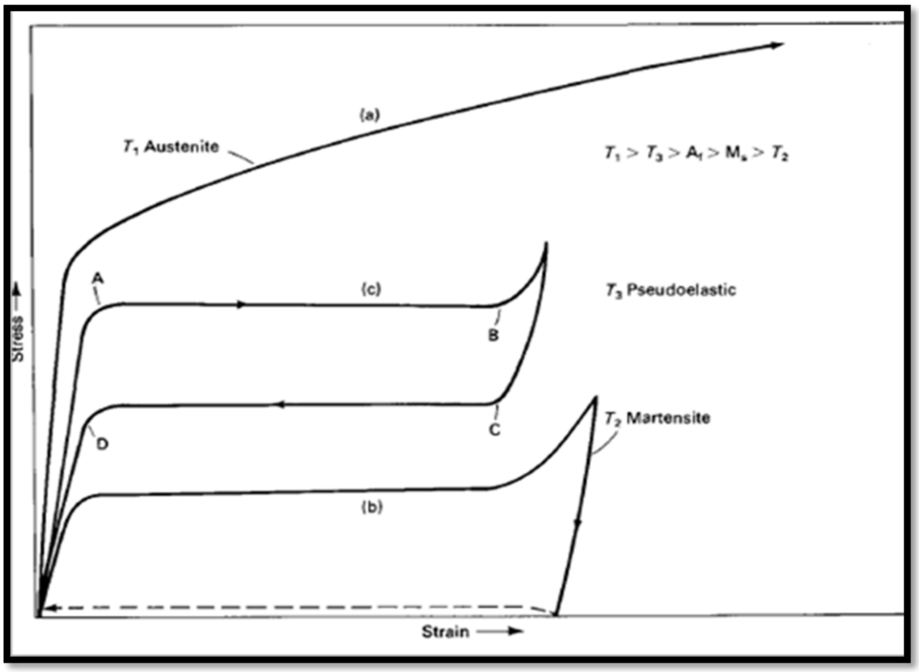

Figure (2.11) Typical stress-strain curves at different temperatures relative to the transformation, showing (a) Austenite. (b) Martensite. (c) Pseudoelastic behavior[55].

2.7.Commercial Shape Memory Alloys

Commercial copper-based alloys with shape memory function include ternary alloys Cu-Zn-Al and Cu-Al-Ni or their manganese-containing quadruple variants [56]. Elements such as boron, cerium, cobalt, iron, titanium, vanadium, etc. and zirconium is also added for abrasive particles. The melting of copper-based shape memory alloys is similar to that of aluminum bronze [43]. Most alloys on the market are induction cast. In order to avoid zinc evaporation and aluminum oxidation, it is necessary to use protective flux on the melt, and use nitrogen or inert gas for protection during the casting process [43]. Powder metallurgy and rapid crystallization are also used to produce fine-grained alloys without additives [43].Conventional substances have tended to have their homes dictated with the aid of using the product design and on this recognize the layout can be idea of because the belongings driver. This is a greater reactive method that concentrates on marketplace wishes and highlights the want for application relevant research. The simplest alloy structures which have completed a degree of industrial exploitation are the NiTi alloys and the copper-base alloys[43]. Properties of the 2 structures are quite different .The NiTi alloys have extra form memory strain as much as 8% as opposed to 4 to 5% for the copper-base alloys have a tendency to be a great deal greater thermally strong and feature tremendous corrosion resistance as compared to the copper-base alloys. Medium the corrosion resistance and susceptibility to stress-corrosion cracking, and feature a great deal better ductility. On the other hand, the copper-base alloys are a great deal much less expensive, and may be melted and extruded and feature a much broader variety of capacity transformation temperatures[54].

Cu-Zn-Al Alloys, while quenched rapidly and directly into the martensitic phase, are susceptible to the martensite stabilization impact[57].This effect reasons the opposite transformation to shift towards better temperatures. Therefor delays and might absolutely inhibit the form recovery. For alloys with Ms temperatures above the ambient, slow cooling or step quenching with intermediate aging withinside the parent Beta-phase state ought to be adopted [57].The Ni-Ti and Cu-Zn-Al alloys all found technical applications. Nitinol is extensively used for the manufacture of surgical devices and implants due to its biocompatibility[59]. Cu-Zn-Al alloys are frequently used in a extensive variety of engineering applications nonmedical applications due to their wonderful thermal and electric conductivity and their higher ductility[59]. Cu-Al-Ni in addition to iron primarily based totally alloys inclusive of

Fe-Mn-Si, Fe-Cr-Ni-Si-Co,Fe-Ni-Mn, orFe-Ni-C alloys have additionally been investigated in regard to their shape-memory properties [59].

2.8. Method of Powder-Metallurgy

Powder metallurgy is the production of metals powder and converting them to useful shape. It is material processing technique in which particulate materials are consolidating to semi-finished and finished product [34]. This technology is producing a parts by mixing , compacting and sintering metal powders. The performance of metal powders during processing and the properties of the products are dependent upon the characteristics of the metal powders that are used, including particle shape, particle size, compressibility of powders, density, particle size distribution, flow rate of powder and purity of powders[34]. Also, it depends upon compacting pressure , sintering temperature and soaking time of sintering [34].

2.8.1 Mixing and Blending of Powders

Blending is an operation of intermingling of powders having the same composition, while mixing is defined as intermingling of powders having several or more different materials . Mixing is extremely desirable in the preparation of alloys from elemental powders. Additives such as binders or lubricate are usually included in both types of processes to facilitate pressing and achieve the required green strength and controlled porosity in the final product[61]. Mixing of powders is a more complex process which relies on the movement of mass of one powder component into that of another powder component. This movement is dependent upon powder material , particle size , shape and surface conditions[38]. The main purpose of mixing is to produce a uniform distribution of powder and to control the powder characteristics. It must produce a homogenous mixture in the least possible time[38]. The time of mixing may vary from a few minutes to 24 hours or more depending upon the results desired. Mixing may be either dry or wet. Wet mixing is used to produce a uniform mixture of powder particles[38]. It may be obtained by the addition of alcohol or acetone as a liquid medium,after completion of mixing, the liquid medium is removed by drying the mixture in air or in an a suitable able temperature [61].

2.8.2 Compacting The Powders

The main purpose of the compacting process is the forming of metal powders into compacts of the desired shape with sufficient strength to withstand ejection from the dies and subsequent handling up to the completion of sintering, without breakage or damage [47] . The pressure used for producing green compact of the component depends upon the material , the characteristics of the powders used and the product. The compacting process must be designed so as the pressure will be uniformly distributed in the affected area [47].

2.8.3 Sintering The Compacts

Sintering is the process of transforming the powder into a solid body by using heat, the idea of sintering is to join particles together for the purpose of increasing strength by bonding the particles together. Bonding the particles together implies the formation of bonds in the areas where neighboring particles are deformed at their points of contact by applying pressure[63]. During sintering these areas of metallurgical contact grow and the strength of the sintered body progressively increases [63]. Sintering processes can be divided into; solid state sintering and liquid phase sintering. Solid state sintering occurs when the powder compact condensed wholly in a solid state at the sintering temperature, while liquid phase sintering occurs when a liquid phase is present in the powder compact during sintering. Sintering of solid-state can be divided into four stages as shown in Figure (2.12) [64].

First stage; at the contact point between particles necks formed which continues to grow. Second stage; with enough neck growth, the pore channel becomes more cylindrical in nature, small neck size has a high curvature gradient leading to fast sintering. Third stage; the pores between particles are reduced in size; final stage: grain boundaries are developed between particles in place of necked regions [65].

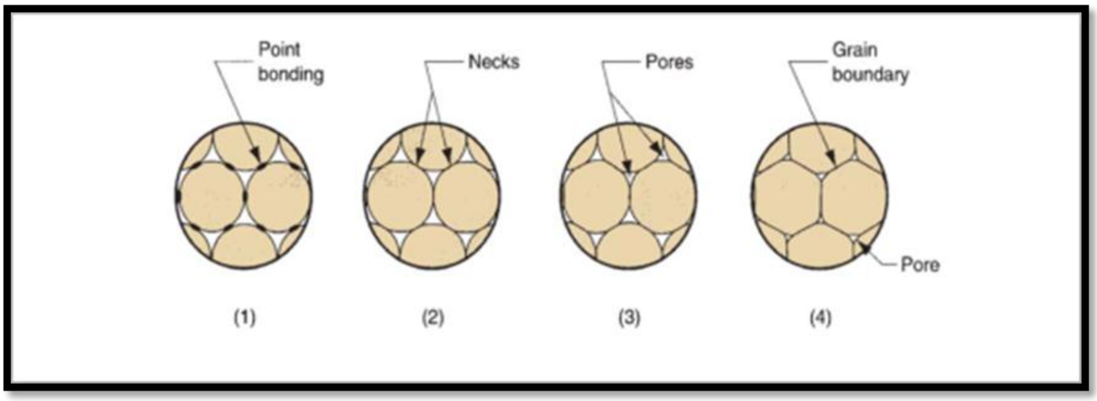

Figure (2.1 2) : Changes during Sintering of Metallic Powders [65].

The driving force of solid state sintering is the difference in free energy or chemical potential between the free surface of the particles and contact points of linked particles. In general, density, mechanical strength, ductility, electrical and thermal conductivity of the depends upon sintering process [51].

2.9. Wear Resistance of Shape Memory Alloys

The wear studies on shape memory alloys achieved until these days have nearly absolutely centered at the form memory alloy NiTi. The work achieved on cu-primarily based totally form memory alloys is the via way of means of wang et al. in 1992 [70].In this work , the authors studied the wear and tear of a Cu-25Zn-4Al alloy. It has been found that the alloy with martensitic microstructure gives a higher wear resistance than that of the β segment [70]. Studies on bulk TiNi suggest that the high put on resistance of TiNi is attributed to its superelastic behaviour. Unlike traditional materials, superelastic TiNi undergoes a large elastic recovery after deformation. Thus when a pressure is applied, the austenite segment transforms to a premartensitic phase after which to martensitic segment, observed via way of means of large deformation[69]. As the load is removed, a reverse transformation happens and the initially induced deformation recovers[69]. Recent studies has shown that TiNi alloy reveals higher put on resistance in comparison to different traditional engineering materials which includes steels, Ni-primarily based totally and Co-primarily based totally tribo-alloys[69].Shape memory alloy provides the superelasticity when it's far deformed with the aid of using a determined pressure, in a temperature range wherein thermoelastic martensitic is formed. When the pressure is removed, the deformation disappears and spontaneously returns to the unique phase [68] . From a mechanical factor of view, wear of metal materials, described as the removal of material from surface because of cyclic mechanical contact both from sliding touch in adhesive and abrasive wear or particle impulsion in erosion wear, originates from plastic deformation. Plastic deformation and accumulation of plastic deformation because of cyclic loading will provoke microcrackss withinside the surface and finally wear particles will form. Therefore the wear and tear resistance of a ductile material may be evaluated with the aid of using its capacity of plastic deformation under sliding conditions[69]. Under given touch loading conditions, if plastic deformation is difficult to be generated in a material, then this material is expected to possess high wear resistance[70].

2.10 . Corrosion of Shape Memory Alloy

Shape memory alloys (SMAs) have been introduced to biomedical fields due to its unique functions of shape memory effect and superelasticity. NiTi- SMAs are now widely used for practical biomedical applications[71] . Amongst the maximum interesting medical alloys evolved withinside the last few years are the NiTi-alloys with almost equiatomic nickel and titanium distribution. This offers them with several advantages. The most important are their form memory effect, their superelasticity and an awesome biocompatibility where , those alloys are effectively implemented in orthopaedic surgery[72]. This demonstrates that the form memory alloys have extra corrosion resistance than conventional alloys because of wonderful elastic behavior of polycrystalline structure. Since SMAs discover a wide application withinside the marine, aerospace applications and it is also used withinside the medical application like stents[73].The corrosion resistance of the implant alloy is a totally critical determinant of its biocompatibility. The nature of the surroundings and the surface remedies have a marked have an effect on corrosion [74]. n sensible applications, as the alloys are uncovered to different corrosion media for an extended length of time. They are at risk of corrosion and pitting. Therefore, the study of corrosion capability and pitting capability of the alloys are necessary earlier than they are placed into biomedical and industrial applications.

2.11. Literature review

A literature review is conducted to addition knowledge about the copper zinc aluminum (CuZnAl) shape memoryalloy and previous papers in the area of the shape memory effect.

In (2002), Pena et al. [69] studied the effect of microstructure on sliding wear in CuZnAl in their different phases .The weight losses for the different alloys in function of the present phase ,and the Ms of alloy are studied . After the characterization of wear surface by means of optical microscopy, scanning electron microscopy and differential scanning calorimetric. It is observed that wear behavior of this alloy depends on the shape memory properties . On the other hand, it is observed that β alloys with low Ms have the worst wear behavior . We can observe that the wear behaviour of this alloy depends on the shape memory properties. For the β shape memory alloys a lineal relation of weight loss with Ms transformation temperatures are obtained. For the martensitic phase and β+ martensitic phase the relation weight loss–Ms is not evident.

In (2005), Sampath [77] prepared Cu-11Al-3.82Ni form reminiscence alloy through melting it to 1050˚C .Different quantities of Zr have been used as grain refining additions to the melt. The consequences confirmed that Zr lessen grain length to 70%.Zr will increase the martensite transformation temperatures to 32˚C ,however similarly addition of Zr lower Ms to underneath room temperature . The addition of Zr decreases the hardness. The consequences unveil discount withinside the grain length of 89.18% with the improved tensile strength of 667 ± 30 MPa and ductility of 23.95 ± 0.86% and great form recuperation ratio of 100% with the addition of Zr as much as 0.3 wt%. Increase in transformation temperatures is observed with the addition of Zr.

In (2006), Kuo et al. [79] Studied the corrosion conduct of Cu–Al and Cu–Al–Be (0.55–1.0 wt % B) shape-reminiscence alloys in 0.5 M H2SO4 solution at room temperature. The consequences of anodic polarization test display that the anodic dissolution rates of alloys reduced barely with growing the concentrations of aluminum or beryllium. The addition of a small quantity of beryllium turned into effective to prevent the intergranular corrosion. The effect of beryllium addition at the prevention of intergranular corrosion is possibly attributed to the diffusion of beryllium atoms into grain boundaries, which in turn deactivates the grain boundaries.

In (2008), Mallik and smapth [80] studied Cu–Al–Mn shape memory alloys with 10–14.5 wt.% of Al and 0–10 wt.% of Mn, They reported that the transformation temperatures, shape memory effect and superelasticity of these alloys are highly sensitive to variations in composition. It is found that with the increase in the amount of aluminum the morphology of martensite and its transformation temperatures change. On the other hand, an increase in the amount of manganese stabilizes the martensite and enhances the superelasticity of the alloys.

In (2009), Abid Ali [59] studied martensite transformation of porous Cu-Zn-Al shape memory alloy during direct quenching heat treatment using X-ray diffraction technique to identify phase transformation . Direct quenching heat treatment includes heating the sintered samples up to 850˚C for 1hour and quenching in iced water. To reveal microstructure of formed martensite phase for prepared specimens after grinding and polishing have been examined by optical microscopy and scanning electron microscopy . Shape memory effect is calculated by measuring of hardness indentation after quenching and after shape recovery treatment using image analysis of light optical microscopy .It appears that direct quenching heat treatment leads to form fully martensite microstructure in CuZnAl alloy.

In (2010), Abid Ali & Khulief [82] Studied dry sliding wear and corrosion conduct of Cu + 13wt% Al +3.8 wt% Ni organized with the aid of using powder metallurgy. Corrosion conduct in 5 wt% NaOH solution primarily based totally up on potentiostatic (Tafel) has been presented for base form reminiscence alloy (Cu + 13% Al + 3.8 % Ni) in instances austenitic and martensitic phase state. Furthermore, the effect of Fe additions as (0.4, 0.8 and 1.2 wt%) at the sliding wear and corrosion conduct of base alloy has additionally been studied. It is obvious that Cu Al Ni form reminiscence alloy in martensitic state has greater put on resistance than in austenitic shape . Also, corrosion resistances are higher than in martensitic shape due to the fact the alloy has corrosion current density as 336.45 μA/cm2 in martansitic wherein because the corrosion current density is 633.62 μA/cm2 in austenitic shape. Furthermore, whilst the iron content material increases, wear and corrosion price growth too.

In (2010), Zengin and Kayal [81] examined macroscopic, structural and morphological features of shape memory Cu-Zn-Al alloys Cu–24.98 Zn–4.43 Al and Cu–21.62 Zn–5.68 Al by elongation parameter measurement, X-ray diffraction and optical metallography. It has been seen that shape initiating temperature is greater than austenite start temperature (*A*s). According to the X-ray diffraction, it has been defined that transformation happened from austenite phase to martensite phase and martensite crystal lattice has been in monoclinic structure. In metallographic observations the grain structures were observed, then plate martensites, V-type martensite structures, twin-like bands, precipitation phases were found. In addition, it has been observed that -sediment phase has occurred in specimens with ageing at7h in the phase cause deterioration of the shape-memory capacity or life.

In (2014), Huda Abbas et al. [71] n this study , Cu-based shape memory alloys of Cu-25Zn-4Al alloy as master alloy have been prepared by powder metallurgy technique in different alloying elements. The addition of alloying elements such as manganese and titanium with (0.5%wt,0.7%wt and 1%wt respectively) of each element added to the master alloy. After mixing of powders ,compaction stresses of (450,550,650 and 750 Mpa) have been used to compact the master alloy to choose best compress . disc samples (13mm in diameter) and cylinder samples (10mm in diameter) have been prepared by using 650 Mpa as best compress . then sintering process in vacuum tube furnace has been achieved by three stages ,the first stage is at (350℃) for 2hr. ,second stage is at (550℃) for 1hr. and third stage is at (900℃) for 3hr. all samples are solution treatment by heating up to (850℃) for (1hr.) then rapid quenched in (ice water +salt) . The results obtained from this study have been presented .it found that at 650Mpa the green density is(6.84g/cm^3) and green porosity is 16.88% ,while apparent density and porosity of sintering master sample are (4.731 g/cm^3) and (25.95%) respectively . Corrosion results have been shown that corrosion rate decrease with addition Mn% and Ti% addition .The corrosion alloying where the (Cu-25Zn-4Al-1%Mn) alloy has (10.678 mpy) in sintering state while (Cu-25Zn-4Al-1Ti) alloy has (1.732 mpy) in quenchingstate.

In (2014), Sathish et al. [84] Studied The microstructure, martensitic transformation behavior and shape memory effect of Cu-Zn-Ni shape memory alloy have been studied by X-ray diffraction (XRD), optical microscopy (OM) and differential scanning calorimetry (DSC). The results show that the recrystallization occurs in the hot-rolled Cu-Zn-Ni alloy by annealing at 800˚C and alloy is primarily composed of martensite. A reverse martensite transformation temperature higher than

100˚C upon heating has been detected. The alloys exhibit good ductility and shape memory effect (SME).The results shown the transformation temperatures are highly sensitive to the variation in zinc concentrations of the alloy. As the content of zinc increases, the transformation temperatures decrease, whereas as the content of nickel increases, the transformation temperature increase.

In (2017),**Zorica. et al. [88]** studied Two Cu-Zn-Al alloys with variable content of Zn (25 and 30 wt%) and constant Al content (4wt%) prepared by induction melting of pure metals and hot rolled into strips of 0.5 mm thickness .Then thermally processed by using three different heat treatments: direct quenching, step-quenching and up quenching with boiling water and room temperature water as the quenchants. The effects of composition and different methods of heat treatment on the microstructure and transformation temperatures of the investigated Cu-Zn-Al alloys were investigated using SEM-EDS and DSC techniques .The results of microstructure and thermal analysis investigations following conclusions can be made: 1) Microstructure of the as-cast Cu-25%Zn-4%Al alloy consists of β phase in the base and a considerable amount of irregular dendritic α particles with an FCC structure distributed in the β matrix. Cu-30%Zn-4%Al alloy in the as-cast state has single phase microstructure which includes large polygonal grains of β phase. Direct quenching and up-quenching produce fully martensitic microstructure in the Cu-25%Zn-4%Al alloy. Martensite was also induced by step-quenching, but microstructure of thestep-quenched Cu-25%Zn-4%Al sample also includes small precipitate particles of α phase.

In (2017), Abdul Raheem K. Abid Ali et al. [76] studied (Cu-13Al-4Ni-xCr) shape memory alloys have been prepared by using Powder metallurgy technique with added Cr element (x=0.3,0.6,0.9) . After compacted , sintering process has been done in vacuum pressure (10^{-4}

torr) at (550°C for 120 minute) and (900°C for 60 minute) then cooling inside furnace .Quenching heat treatment carry out at (850o C for 60 minute) then cooling in cold water to (3-4°C) . The microstructure has been studied by optical microscope and scanning electron microscope (SEM) , porosity , compression behavior(stress-strain) for quenched specimens also have been studied . The results have been approached that the hardness increases with percent chrome while the porosity decreases . The compression stresses to fracture , have been increased with respect to (0.3% C) had porosity (27%) and decreased for (0.9%) with porosity (22%) . From the previous results , quenched alloy (Cu-13%Al-4%Ni-0.3%Cr) is the more compression strength.

In (2017), E.S. Al-Hassani and A.H. Ali et al. [99] Studied the alloy (Cu-(15-40) wt%Zn-6wt.%Al) has been prepared by powder metallurgy technique Zn element (15, 20, 25, 30, 35, 40 wt%Zn) and fixed percentage of Al content which is 6.wt%Al then aluminum replaced by (Si, Sn, Ni)element at fixed percentage of 6wt.%, in order to study the effect of these elements on SMA. After samples preparation examination were done by using XRD, SEM technique, DSC, Vickers hardness, Archimedes method to measure the porosity percentage and corrosion . X-ray diffraction showed that all samples alloys consist mainly of two phases (α+β) biphasic structure; the martensitic phase (α-phase) orthorhombic structure and the austenitic phase (β-phase) BCC structure ,the centered cubic intermetallic phase β of binary alloy Cu-Zn exhibit a martensitic transformation but the transformation temperature that can be obtained by varying the composition are extremely low(practically lower than -50°C) the addition third element such as (Al, Si, Sn) to the binary alloy (Cu-Zn) enables to obtained the martensitic transformation , the temperature for which can be adjusted by the composition , over a wide range .The goal of quenching for Cu based shape memory alloys it is enough that the quenching process be sufficiently quick to prevent diffusion reactions. In certain cases, even air quenching may suffice .From the results of corrosion test can be show the addition element nikel lead to improve the corrosion resistance. Finally, from the results shown the addition of element Ni lead to raise the transformation temperature and the corrosion rate decreases with increase the element Ni in the alloy (Cu-25%Zn-4%Al) .

In (2018), Hussain and ali [78 In this study Cu-11.9%Al-4.5%Ni based alloy has been prepared. The alloying element additions such as Titanium and Silver with (0.4, 0.7, 1, 1.5%wt) and germanium with (1, 2, 3%wt) have been added to the base alloy so that the number of alloys equal to 12 alloys. All the samples are solution treated by heating the samples up to (900C) for (60 min) followed by rapid quenching in iced water at 3~4C. X-ray diffraction test for sintered, quenched and aged samples , apparent density of elemental powders and blended powders, green density and green porosity for compacted specimen and true porosity of aged samples have been studied. The highest shape memory effect in Ti addition was (9.85%)when the addition was (1.5%wt) . Corrosion results have showed that the highest corrosion resistance in NaCl solution was found in alloy contain silver with addition amount (1.5%wt) which give the lowest corrosion rate (0.07mpy) .

In (2018), Deepjyoti Basak. [86] studied the options and substitute of few Copper based shape memory alloys such as Cu-Zn-Al, Cu-Al-Mn, and Cu-Al-Be over the other conventional shape memory alloys used as a reinforcement in metal matrix composite. Results shows that the grain size is fine which develops a strong bonding between atoms that directly conclude that its strength requirement can be varied by changing the composition as per the requirement of application. Corrosion resistance is also another important factor which makes it useful in moisture condition.

Addition of Mn and Zr as other alloying material in Cu-Zn-Al shows good mechanical behavior, with high tensile strength and high ductility. Boron addition increases the elongation up to 50 % and tensile strength up to 130%, it also reduce the grain size.

In (2018), Kenneth et al . [89] Cu Zn Al shape memory alloy, and added (0.1– 0.4) wt% Ni added in order to enhance characterizations of Cu Zn Al shape memory alloy. Optical microscopy, scanning electron-microscopy and X-ray diffraction analysis were utilized for structural characterization of the alloys, while hardness measurement was used to assess the mechanical properties. The results show that, all the alloy compositions consisted of β (CuZn) phase. Sharp edged elongated grain structures were observed in the unmodified of Cu Zn Al alloys, while the 0.1, 0.2 and 0.4 %Ni modified Cu Zn Al alloy compositions, had more of granular/smaller/round grain edges and smaller grain widths. So the results showed that the grains size decreased from 7.9 ± 0.04 µm to 3.8 ± 0.02 µm. Also noticed that, the hardness of the unmodified Cu Zn Al alloy (194.5 ± 2 VHN) was lower than that of the Ni modified Cu Zn Al ones with an increase in hardness ranging between 23.5 and 38.4% .

In (2018) , P. Heresi et al . [90] investigated the fabrication Cu-Zn-Al shape memory alloy and studied effect of the Boron addition on behavior of shape memory Cu-Zn-Al alloy. Differential Scanning Calorimeter (DSC) analysis and optical metallography were performed to samples of Cu-Zn-Al SMAs to establish the phase transformation temperatures A_s & A_f , and measure average grain sizes. The results of study showed that, average grain size was around 0.5 µm and the transformation temperatures was about (258 to 280) ^{0}C for A_s and from (384 to 393) ^{0}C for A_f . Also noted that, Addition of boron contribution in an increase of phase transformation temperatures about 8 % and it has an effective role in reducing the granular size.

In (2019) Duong Nam Nguyen et al. [85] Microstructure and phase transformation in shape memory alloy Cu-Al (Fe addition: 9% Al, 4 % Fe) were investigated in this study. It is a material capable of restoring its original shape when impacted by a reasonable temperature or cyclic stress and production cost is not too expensive. In many years, shape memory alloys (SMA) based on Cu - Fe is considered to be very attractive to industrial and biomedical applications such as cardiovascular, orthopedic, surgery and production of spare parts and jigs. Shape memory rate obtained 6%-24% corresponding to each deformation angle before the experiment. Phase transformation between these two phases during deformation as well as the heating cooling process which create the basis for the unique properties of the alloy.This results observed analyzed and explained the mechanism of SME of the alloy system based on the transformation of the martensite phase of this alloy system. When heated and quenching, this alloy was created a martensite microstructure, but when it was heated again, the martensite structure decomposed into the forms: β '; vitmantet and finally return to the initial state with α and γ2 phases.The initial restoration of the structure will show the ability to remember the shape of this alloy system.

In (2020) Linrong Z. et al. [98] Cu-based shape memory alloys are promising materials for functional or intelligent applications because of its good shape memory properties and low cost. As an additive manufacturing technique, selective laser melting (SLM) is easy to produce such complex intelligent components, moreover, the rapid solidification rate can obtain fine microstructure and get good properties. In this study, CuZnAl shape memory alloys were prepared by SLM for the first time to study the effect of the process parameters on the relative density, phase constitution, microstructure, phase transformation behavior, microhardness and superelastic response. Results show that the intrinsic reason for the differences in the microstructure and the macroscopic properties is the different Zn content in samples fabricated with different energy densities. The lower energy densities lead to the lower amount of Zn evaporation and thus the higher remained Zn content in the fabricated samples. In terms of phase constitution, samples with higher Zn content mainly consist of martensite (β') and present needle-like shape microstructure morphology. On the contrary, samples with lower Zn content are predominated by α phase and have rod-like or even equiaxed shape microstructure. In addition, higher amount of martensite in the samples results in the higher peak intensity in the DSC curves, the higher microhardness and the lower irrecoverable strain.

2.12. Summary of Literature Review

The following statements summarize the important point of previous literature review :

1- Shape Memory Alloys is one of the most important and famous alloys is used in the manufacture of structures that are characterized by high corrosion resistance .

2- A literature review shows the powder technique method is one of the most used in manufacturing of shape memory alloys .

3- Many researchers studied the effect of different alloy elements on properties such as mechanical, chemical, shape memory effect and other properties.

4- Some researchers have studied the effects of adding element nickel on the properties of Cu-Zn-Al alloy .

5- Few researchers have studied the effect element boron on the properties of Cu-Zn-Al alloy .

6-Few of the published studies have improved hardness, wear resistance and general mechanical properties by adding boron oxide.

Chapter Three
Experimental Part

Chapter Three

Experimental Part

3.1. Introduction

In this chapter, materials and equipment used in this study are presented. Experimental procedure used to prepare samples from the elementals powders by powders mixing , compaction and finally sintering based onto standard steps of powder metallurgy technique. Several tests such as apparent density, porosity, hardness, shape memory effect,and transformation temperature measurement using differential scanning DSC calorimeter are also explained .Microstructure investigation using optical microscopy , scanning electron microscopy SEM and X-Ray diffraction are presented . Corrosion and wear tests are also presented in this chapter .

3.2. Materials and It's Tests

Powders of copper , aluminum , zinc, nickel , boron and boron oxide were used to prepare the alloys. The source of all these powders was Lemandou Ltd. co. China. Basic materials were tested as listed below:

A. Chemical composition analysis for the copper , aluminum zinc , nikel , Boron and boron oxide powders in order to insure their purity. The tests were carried out at General Company for Inspection and Engineering Rehabilitation-Baghdad via spectro analyzer model (SPECTROMAXx) shown in Figure (3.1).The purity of the powders used are listed in Table (3.1).

Figure (3.1): The Spectro Analyzer Type (SPECTROMAXx) .

B. Particle size analysis was carried out to all powders using via laser particle size analyzer type: Bettersize 2000 shown in Figure (3.2). The tests were carried out at the University of Babylon/College of Materials Eng. /Ceramics and Building Materials Labs. The average particle size for each used powders is listed in Table (3.1). The test report of particle size analysis is shown in Figure (3.2) .

Table (3.1): The Purity and the Average Particle Size of the Powders Used

Powder	Purity (%)	Average Particles Size (μ m)
Copper	99.87	30.62
Zinc	99.75	25.18
Aluminum	99.52	27.8
Nikel	99. 63	31.0
Boron	96.53	35.12
Boron Oxide	98.34	32.43

Figure (3.2.): Laser particle size analyzer.

3.3. Apparatuses and Program of Present Study

Figure (3.3) shows the summary of the overall program used in the present work.

The preparation of mixed powders with different chemical compositions requires many equipments and instruments which are used not only in preparation of powder mixture but also in compaction and sintering stages. These equipments and instruments use in this study include the following:

1. Polyethylene zip-lock bags
2. Electric tube furnace up to 1200°C with alumina tube and type K thermocouple and digital thermostat controller with accuracy ±2.0°C .
3. Quartz type (2cm in diameter with 30cm length).
4. - Electric hydraulic press ,model CARVER . made in USA with 120-ton capacity
5. Graphite lubricant
6. Cube and cylinder compression machines , type CT340-CT440 manufactured by china, max load 1800 KN.
7. Balance with 0.0001g accuracy
8. Ethyl alcohol 95%.
9. Alumina balls.
10. Diamond paste, size 6 quantity 5 gr. (soluble in every lubricants).

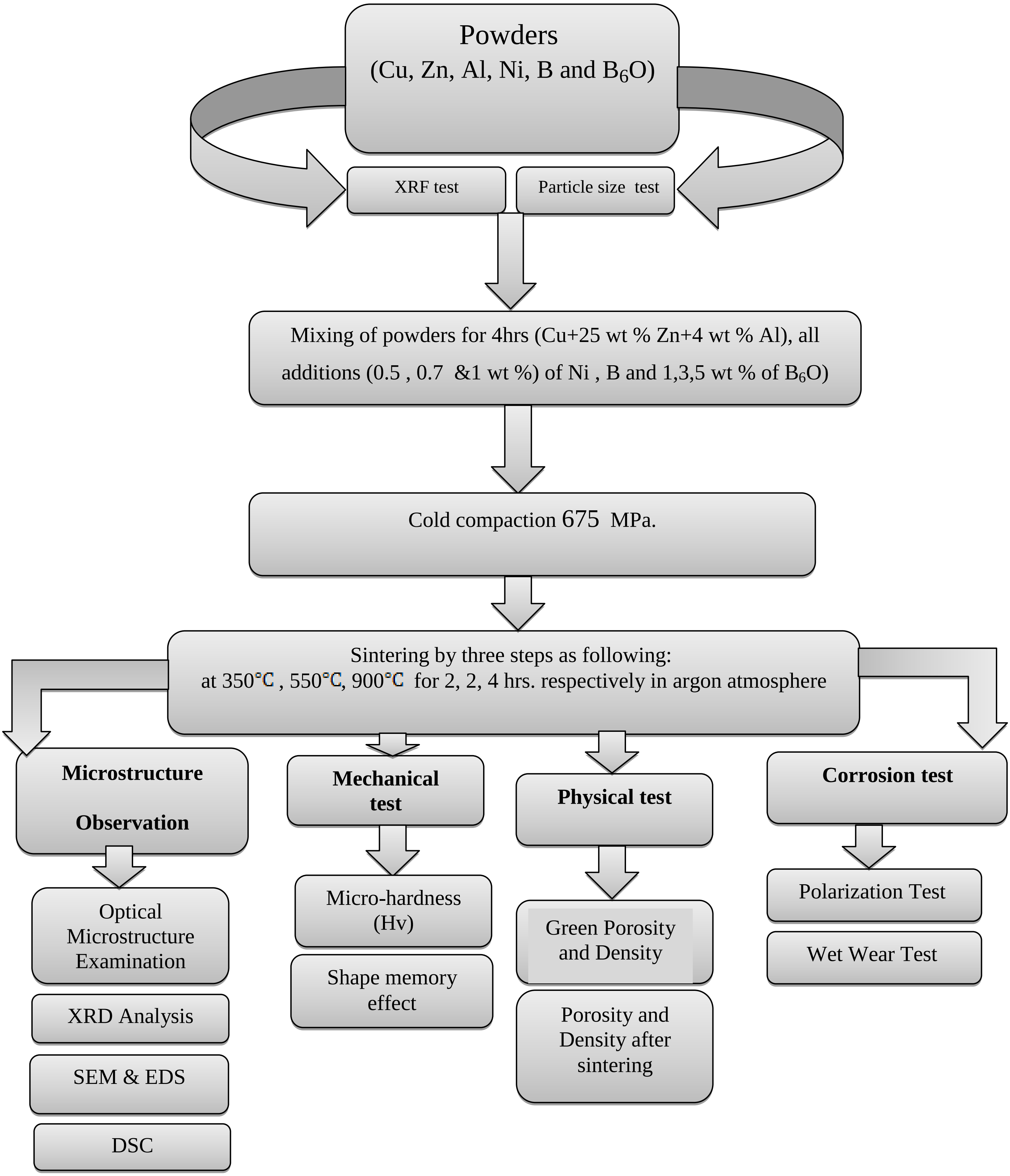

Figure (3.3): Program of the Present Study.

3.4. Samples Preparation

All samples were prepared at the laboratories of Metallurgical Engineering Department / college of Materials Engineering / University of Babylon. Samples are made using powder metallurgy method. The procedure involved mixing, compacting and sintering practices.

3.4.1. Mixing of Powders

Wet mixing for constituents of the mixtures has been done by using a ball mill, original Local. the mixing process was achieved by ball mill, type STGQM-15 / -2 for 4 hours in order to get the perfect and homogenous distribution of powder particles. Medical alcohol (ethyl alcohol 96%) has been used in wet mixing. The mixture was dried at 60 ^{o}C for 30 min. Chemical Compositions of prepared alloys from elemental powders used in this study have been listed in Table (3.2).

Table (3.2) : Mixtures and their Compositions Prepared in this Study

Alloys	Sample Coding	Alloy Compositions wt .%					
		%Cu	%Zn	%Al	%Ni	%B	%B_6O
A	Alloy A	Bal.	25	4	----	----	----
B	Alloy B1	Bal.	25	4	----	0.5	----
	Alloy B2	Bal.	25	4	----	0.7	----
	Alloy B3	Bal.	25	4	----	1.0	----
C	Alloy C1	Bal.	25	4	0.5	----	----
	Alloy C2	Bal.	25	4	0.7	----	----
	Alloy C3	Bal.	25	4	1.0	----	----
D	Alloy D1	Bal.	25	4	1.0	----	1
	Alloy D2	Bal.	25	4	1.0	----	3
	Alloy D3	Bal.	25	4	1.0	----	5
E	Alloy E1	Bal.	25	4	----	1.0	1
	Alloy E2	Bal.	25	4	----	1.0	3
	Alloy E3	Bal.	25	4	----	1.0	5

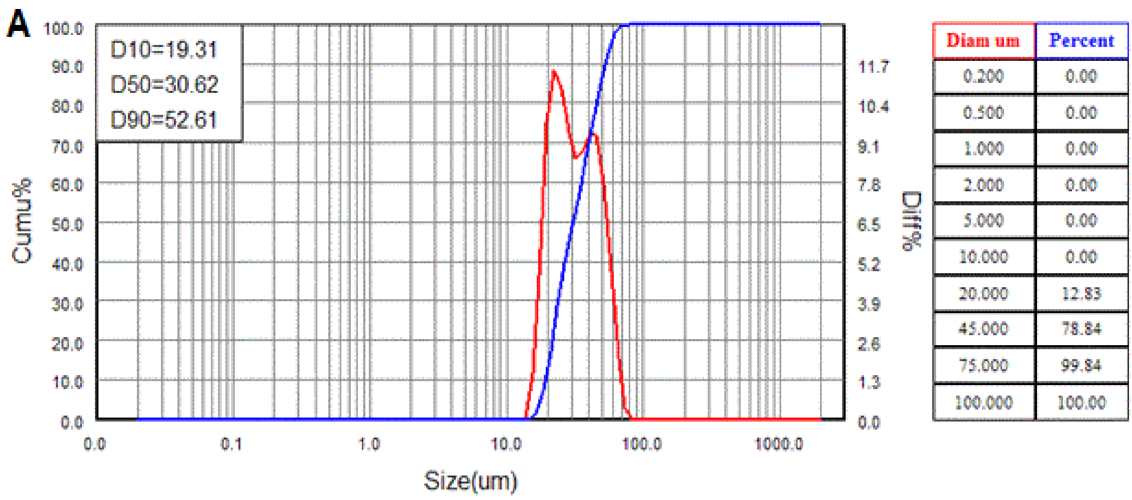

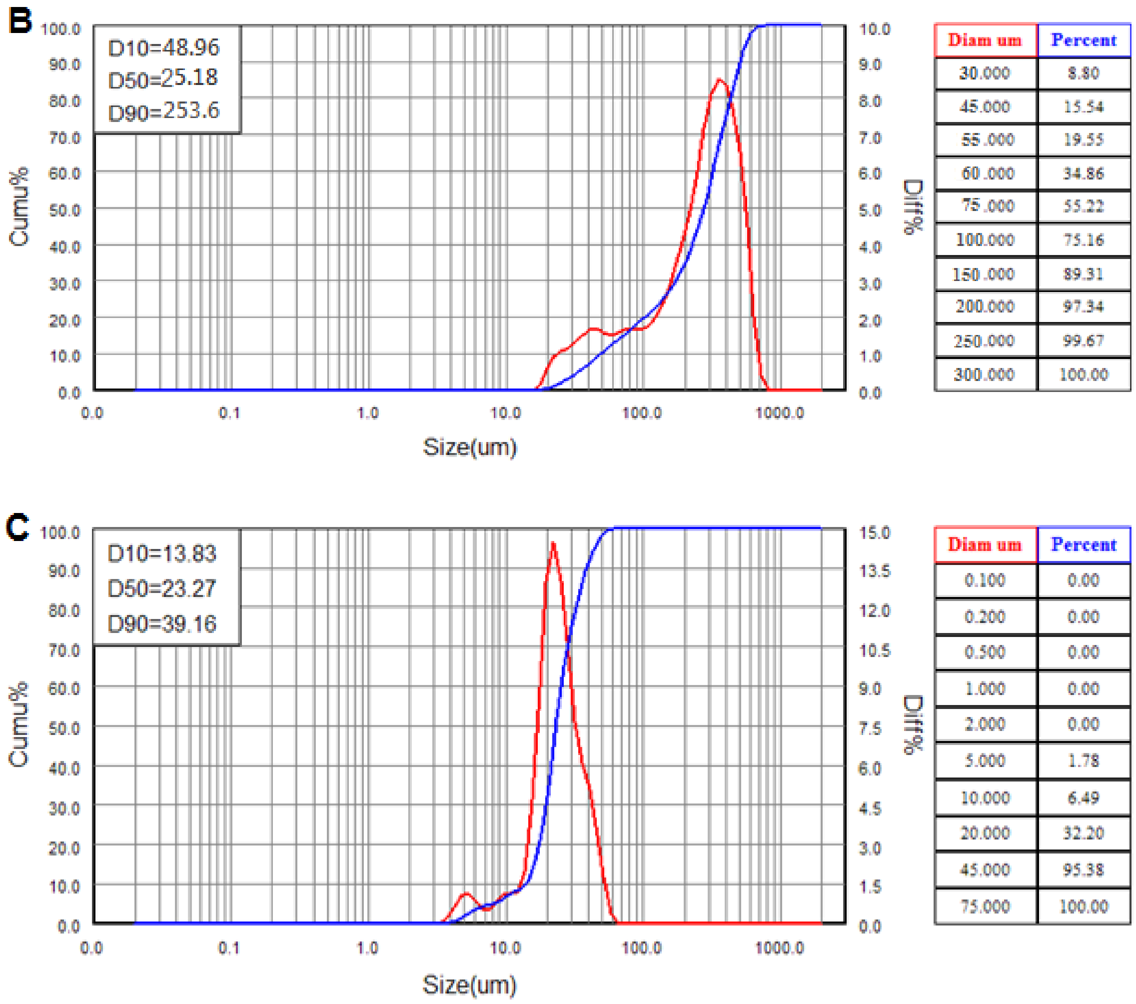

Figure (3.4): Test Report of Particle Size Analysis; (A) Copper; (B) Zn ; (C) Al .

3.4.2. Compaction of Powders

In this stage, cold uniaxial pressing dies has been used. Compression machines with uniaxial pressing is used Various compacting pressure stresses from(450, 550, 650 and 750 Mpa) to compact green disc samples ,finally used compacting pressure 675 Mpa using cold uniaxial pressing in the compression machines with 1800 KN capacity.

Steel die type CT340-CT440,was used for the present study as shown in Figure (3.5) and Figure (3.6) also shown scheck displays dimensions of Steel Die .

Disc samples with (12.8 mm) in diameter and (6mm) in height shown in Figure (3.7) used for density, porosity, hardness , optical microscopy , X-Ray diffraction , SEM , shape memory effect, DSC , electrochemical and wet-wear and EDS tests. The inside walls of the steel die were lubricated by graphite .

Figure (3.5): Steel Die Uesed at Present Study.

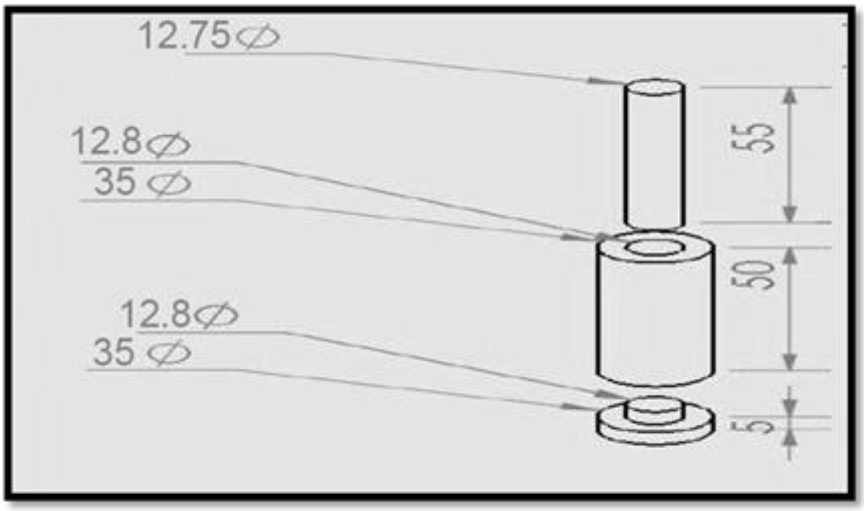

Figure (3.6): Dimensions of Steel Die.

Figure (3. 7): Prepared Samples

3.4.3. Sintering Process

The sintering process of the green compacts was achieved by high temperature tube furnace under “controlled atmosphere of argon type GSL 1600X shown in Figure (3.8) .The sintering process included the following as shown in Figure (3.9) [87] :

1. Heating green compact from room temperature to 350°C.
2. Soaking time 2hr in 350°C.
3. Raising the temperature to 550°C.
4. Soaking time for 2hr at 550°C.
5. Raising the temperature to 900°C with heating rate 6.6°C/ min .
6. Soaking time for 4hr at 900°C.
7. cooling under argon .

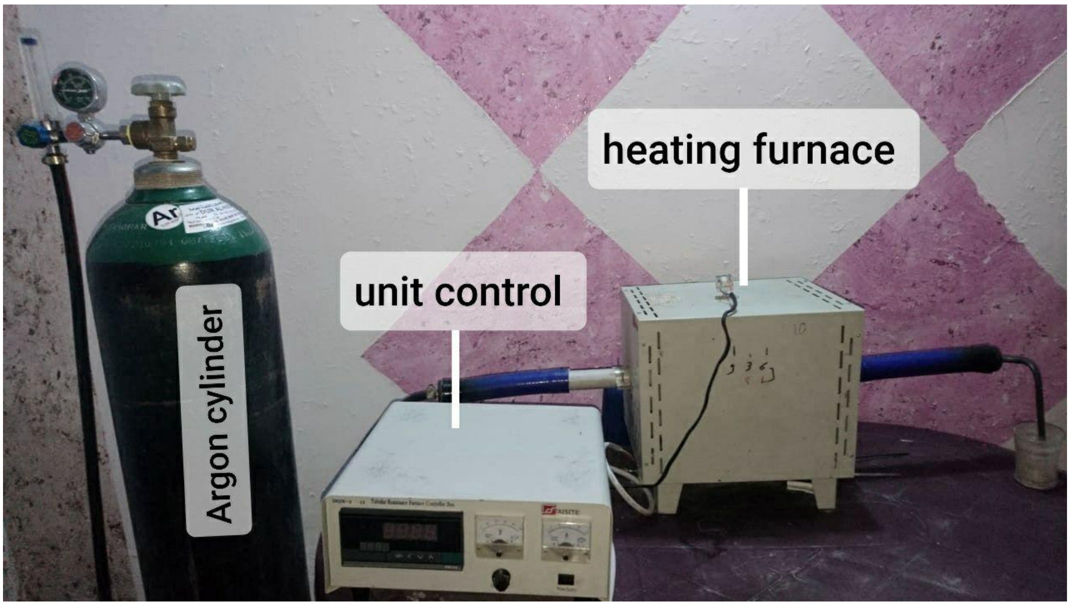

Figure (3.8): Tube Furnace under argon

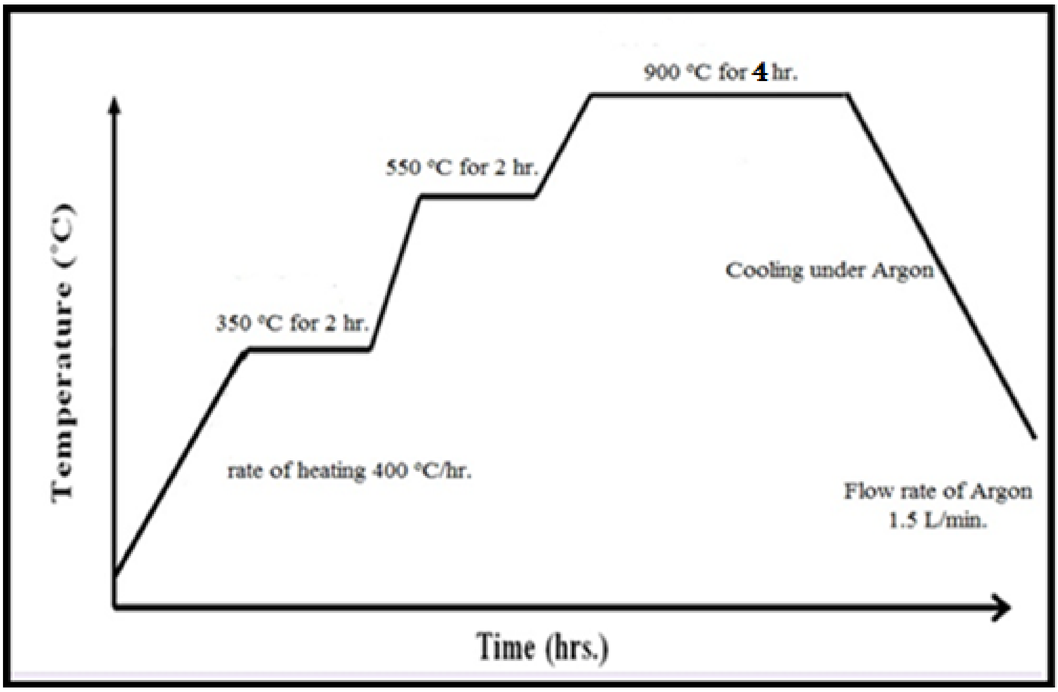

Figure (3.9): The Sintering Program of The Green Samples

3.5. Experimental Tests

Most tests were carried out at the Materials Eng. Labs. / University of Babylon .

3.5.1. Sample Preparation

Prior to the microscopy investigation, shape memory properties , electrochemical and wear tests sintered .samples were prepared using grinding , polishing and etching. Sintered were ground using SiC paper grits as(180, 400, 800, 1000 ,1200 and 2000), then polished using diamond solution.The specimens were etched by(10mLHCl+5g $FeCl_3$+H_2O) at room temperature agreement with [97]. After etching, the samples were washed with distilled water and dried by using an electric drier .

3.5.2. X-ray Diffraction Analysis (XRD)

The samples were prepared for X-ray Diffraction Analysis(see 3.5.1). Sintered samples were tested using XRD instrument type a SHIMADZU Lab XRD-6000, Japan. X-ray diffraction tests are carried out at Faculty of Materials Engineering,department ceramic and building materials .The measure conditions are: Target: Cu, wave length of 1.54060 A°, voltage and current are 30 KV and 15 mA respectively, Scanning speed 2deg/min, the scanning range 30^o-80^o. The X ray diffraction was used in order to determine the phases produced after the sintering and compare it with standard charts.

3.5.3. Optical Microscope Analysis

The samples were prepared for optical microscopy analysis(see 3.5.1). An optical microscope type 1280 XEQMM300TUSB shown in Figure (3.10) with suitable magnification was used to capture the microstructure of the specimens .

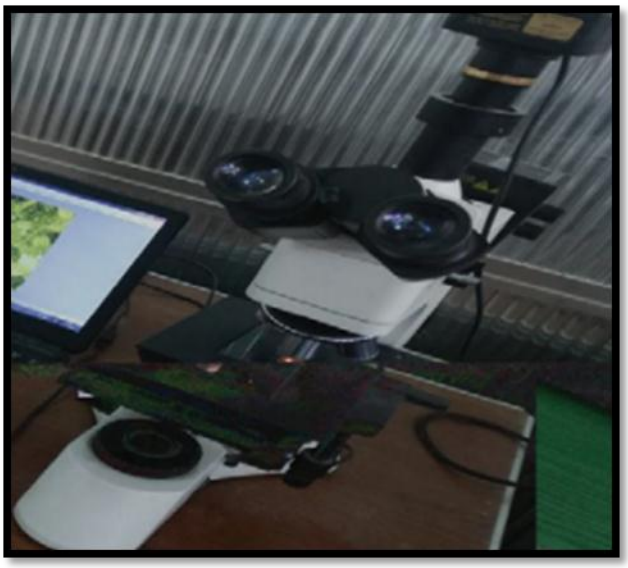

Figure(3.10): A light optical microscope (LOM).

3.5.4. Scanning Electron Microscopy (SEM) analysis

The samples were prepared for Scanning Electron Microscopy analysis(see 3.5.1). In this study, SEM images were captured in order to investigate the microstructure clearly with high accuracy , characterize the morphology of the surface , porosity, and size of pores. This test was carried out at University of Babylon/Pharmacy College Labs. using scanning electron microscope device shown in Figure (3.11) .

Figure (3.11) :The Scanning Electron Microscopy (FEI, Quanta 450) Analyzer.

3.5.5. Energy Dispersive X-ray Spectroscopy (EDX)

The samples were preparedfor Energy Dispersive X-ray Spectroscopy analysis (see 3.5.1).Energy dispersive analysis have been done for corroded surface of samples in order to estimate the chemical composition of the corroded film and to see the distribution of alloying elements in the samples .Two areas have been taken for each sample. the test has been done in Babylon University/collage of pharmacy.

Figure (3.12) : Scanning Electron Microscope

3.5.6. Micro-Hardness Measurements

The samples were prepared Micro-Hardness Measurements (see 3.5.1). The test was carried out using at micro Vickers hardness device type (Digital Micro Vickers Hardness Tester TH 717) using a load of 300g for 10 sec with a square base diamond pyramid. The hardness was recorded as an average of five readings for each specimen.

3.5.7. Porosity and Density Measurement

Green density is the weight of unit volume of compacted blended powder in gram per cubic centimeter .It is calculated from green mass of the compact and volume of the compact as follows[23]:

$$\rho_g = \frac{m_g}{V_g} \tag{3.1}$$

Where:

ρ_g = green density (g/ cm^3). , m_g = green mass of the compact (g).

V_g = volume of the compact (cm^3).

Green porosity is determined from the knowledge of the theoretical density of mixture which is calculated by the weight percent of elemental powder multiply by its theoretical density as follows[23]:

$$\rho_{tB} = \sum_{i=1}^{n} Wt_1 * \rho_1 + Wt_2 * \rho_2 + Wt_3 * \rho_3 + ... + Wt_n * \rho_n \tag{3.2}$$

Where:

ρ_{tB} = theoretical density of mixture (g/cm^3). , n = No. of elemental powders. W_t = weight percent (%). , $\rho_{1,2,3,...n}$ = density of elemental powder (g/cm^3). So the green porosity is calculated from the equation [23]:

$$P_g = \left(1 - \frac{\rho_g}{\rho_{tB}}\right) \times 100\% \tag{3.3}$$

Where:

P_g = green porosity (%). , ρ_g = green density (g/ cm^3).

ρ_{tB} = theoretical density of blended mixture (g/cm^3).

3.5.8 True density and Porosity of sintering compacts

These samples were used after sintering process to study the compression effect on the porosity and density. Density and Porosity are determined from equations(3-4) and(3-5) [57].According to ASTM B328 [101] .

$$P = \left(\frac{B-A}{(B-C+E)\times D_o} \times 100\right) \mathrm{Dw} \qquad (3\text{-}4)$$

$$D = \left(\frac{B}{B-C+E}\right) \mathrm{Dw} \qquad (3\text{-}5)$$

where:

- ❖ After drying at 100 °C for 5 hours in vacuum furnace at a pressure of (10^{-4} torr) the sample was weighted ,and the weight represent mass A .
- ❖ At room temperature, the sample is completely immersed in oil with a density of 0.8 g/cm³ for 30 min.
- ❖ Weighting the fully impregnated sample in air, to get the mass B.
- ❖ Weighting the fully impregnated specimen in water, to get the mass C .

Where:

D_o = density of oil (0.8 g/cm³) .

D_W = density of water (1 g/cm³) .

3.5.9 Shape memory properties

3.5.9.1DifferentialScanningCalorimeter(DSC) Analysis

Differential Scanning Calorimeter (DSC) analysis has been done in order to estimate the transformation temperatures for samples for the forward transformations to determine the A_s (austenite start temp.) and A_f (austenite finish temp.) and use these temperatures for shape memory effect test.DSC tests are carried out at Faculty of Materials Engineering, department polymer . The test has been done using DSC type Series shown in Figure (3.13) for all samples. The range used for the DSC test is form the range 20 - 360 °C and heating rate 5 °C/min.

Figure (3.13) : Differential Scanning Calorimeter (DSC) Type I Series.

3.5.9.2 Shape Memory Effect

The samples were prepared for the Shape Memory Effect (see 3.5.1). Shape memory effect can be determined form the brinell impression by using brinell macrohardness test with load of 31.25kg and holding time of 10 sec, the test has been done for all samples , the heat treatment temperature was done depending the results from DSC test of all samples. After the heat treatment completed ,carried out the cooling process for samples inside the furnace under control argon gas carried out . The diameter of the ball impression before and after the heat treatment has been measurement using light optical microscope with X100 as magnification then the shape memory effect can be calculated from the equation below[53].

$$\text{Shape memory effect (SME\%)} = \frac{d_b - d_a}{d_b} \times 100 \ldots\ldots\ldots\ldots\ldots\ldots\ldots\ldots \quad (3\text{-}4)$$

Where: d_b= diameter of impression in μm before heat treatment.
d_a= diameter of impression in μm after heat treatment.

3.5.10 Corrosion Test

The samples were prepared for corrosion test (see 3.5.1). Corrosion behavior was conducted using the Tafel-Extrapolation .The test was carried out in solution of (3.5gm NaCl +96.5ml distillated water) at room temperature. A platinum wire was used as counter-electrode, the working electrodes were made of cylindrical pieces fastened with appropriate nut and reference electrode. The process has been programmed in computer to draw potential (mv) and log current (µAm) to obtain corrosion current by intersection of the tangents to the two curves. The corrosion behavior of all alloys has been investigated by Tafel potentiostatic type WENKING M lap shown in figure (3.14) that is used to estimate corrosion current and corrosion potential. Corrosion rate may be determined by (mdd) and give the value expressed in (mpy) according to the equation (4.1) [57] :

Figure (3.14) : Tafel Instrument for Polarization Test.

3.5.11 Wet Sliding Wear Test

The samples were prepared for wet sliding wear test (see 3.5.1).Wet sliding wear was investigated using pin on disk concept using the wet sliding wear device (250 rpm) and constant sliding distance(5mm) with (2,5,10 N) normal load . The lubricants used in the wet-sliding wear tests was tap water . Shown in Figure (3.15) the sample is weight before the test using digital electronic balance with four digits . After a period of sliding time (5,10,15, 20, 25 min) , The samples were weight again and the weight loss during sliding wear was measured according toG99-04 **ASTM**. The relation between weight loss and time is plotted for all alloy to compare the wear behaviour of alloys.

Figure(3. 15): The Wet Sliding Wear device.

Chapter Four
Result & Discussion

Chapter Six
Reference

Chapter Four

Results and Discussion

4.1. Introduction

Chapter four records all results of experimental tests that carried out in this study. In this chapter discussed green density and porosity , X–Ray Diffraction (XRD) and Microstructure Observation such as Optical Microstructure and Scanning Electron Microscopy(SEM) , (EDS). These results are scientifically discussed the affecting of elements addition (Ni) ,(B) for Cu +25 wt.% Zn+4 wt.% Al alloy for results differential scanning calorimeter test , shape memory effect and corrosion test . Also discussed the affecting of element (B_6O) for Cu +25 wt.% Zn + 4 wt.% Al-1% wt Ni alloy and Cu +25 wt.% Zn + 4 wt.% Al-1% wt B alloy for hardness and wet-sliding wear test.

4.2. Green Density and Green Porosity of Compacts

Figure(4.1) illustrates the effect of compacting pressure on the green density of the prepared samples. As it is obvious there is an increase in the green density with the increase of the compacting pressure applied for unmodified Cu-25Zn-4Al alloy prepared. The increase in density gradient decreases with increase of compacting pressure till the density reaches a constant value of (6.8 g/cm^3) and up on these results the pressure (675 MPa) is used as a favorable pressure and used to prepare all of the specimens .

The reason for that was first, the green density is progressively increased with the increase of compacting pressure because in compacting stage powder particles joined together and rearranged themself , therefore when the compacting pressure increases this will cause an increase in plastic deformation for the particles and eventually increase in green density.

Figure (4.2) shows the effect of compacting pressure on green porosity. The results indicate that the green porosity decreases with the increase of compacting pressure. This is due to an increase in deformation resulting from the contact between particles which reduces the voids between the particles [93].

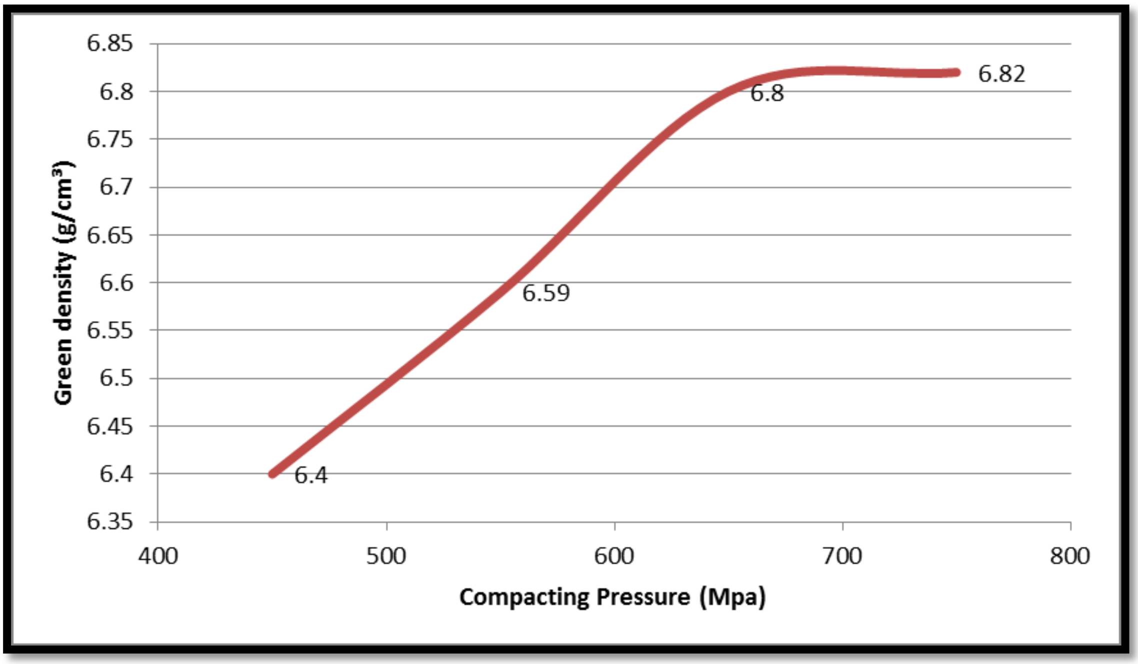

Figure (4.1) the green density with compacting pressure for unmodified Cu-25Zn-4Al alloy

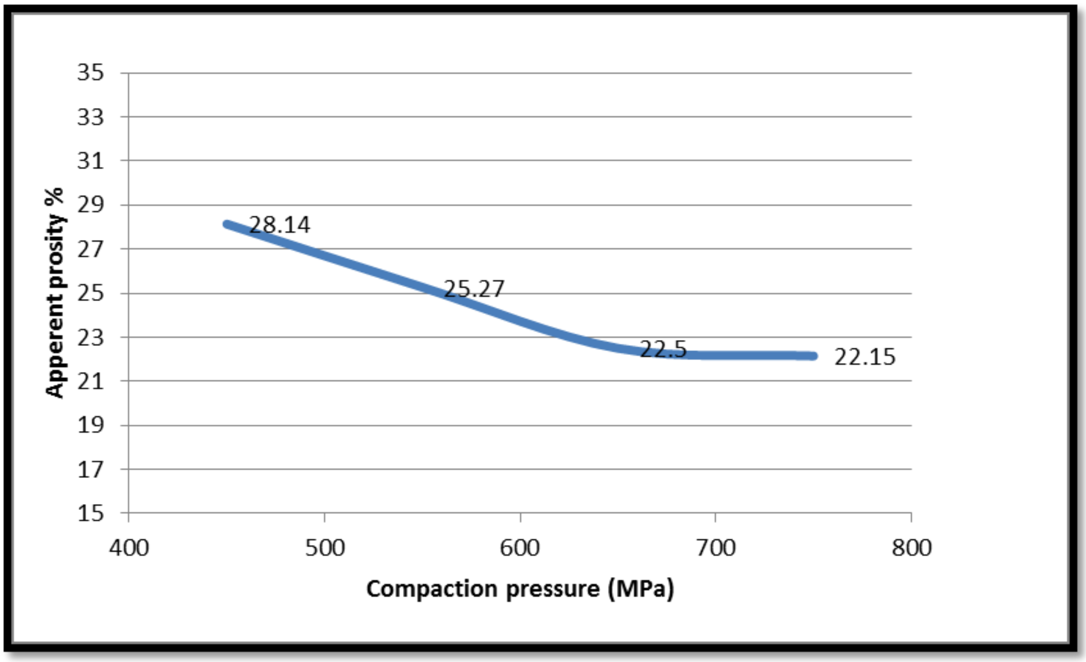

Figure (4.2) : Porosity with compacting pressure for unmodified Cu-25Zn-4Al alloy

4.3 Density and Porosity of Sintered Sample

Density has been decided after the samples of reference alloy with distinct compacting stress had been sintered .It increase whilst compacting stress will increase as proven in Figure (4.3) . that was due to the distance among particles fills with small particles because of the difference withinside the granular size used for the powders, it found that the small-sized particles take a seat down among the large-sized particles and that leads increase the density and reduce the porosity .Apparent density depends on factors such as particles size and distribution , surface area and particle shape [42]. Apparent porosity of sintered unmodified alloy is determined after alloy compressed under different pressures as shown in Figure (4.4).

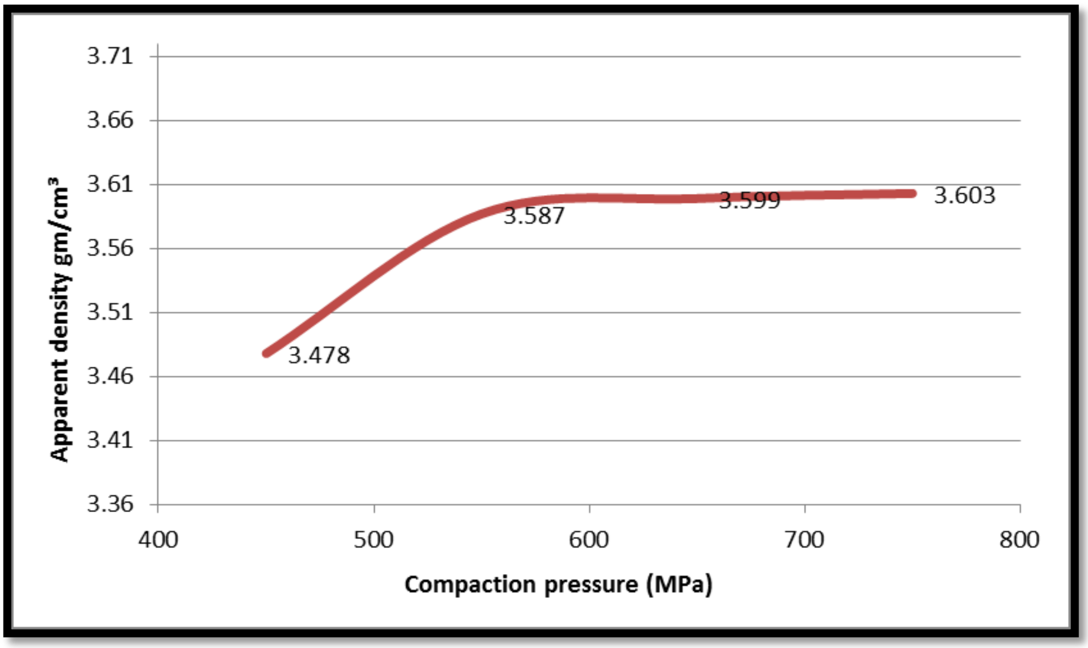

Figure (4.3) Density after sintering for unmodified Cu-25Zn-4Al alloy vs. compact pressure.

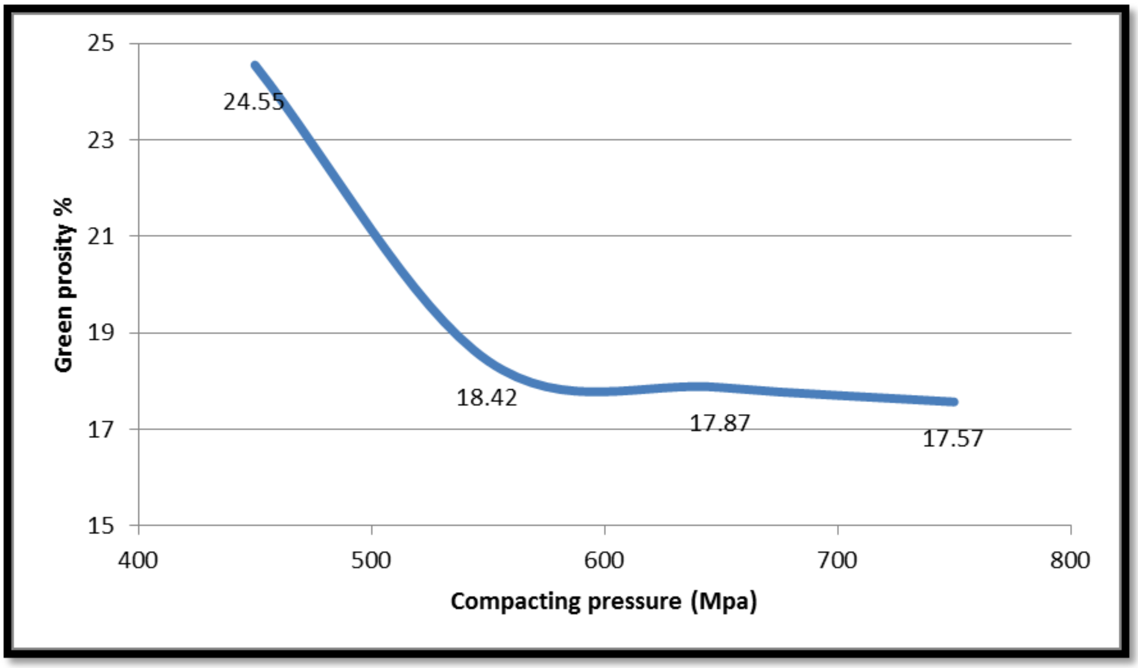

Figure (4.4) Porosity after sintering against compact pressure for unmodified Cu-25Zn-4Al alloy.

4.4 X-Ray Diffraction (XRD)

X-ray diffraction tests were done for samples after the sintering process. Figure (4.5) shows the XRD pattern of the reference alloy after sintering , were the phases that established because of sintering process could be distinguished . The phase analysis of (Cu-Zn-Al) alloys with and without addition was carried out by X-ray diffraction (XRD). At this attempt the resulting peaks which indicated after comparing it with standard charts in appendix A .

It has been shown that the initial stages of sintering process (low temperatures (350 ^{o}C and 550 ^{o}C) first and two stages of sintering) proceed by forming the complete range of compositions from copper and zinc. This is the appearance of the initial interdiffusion across the copper-zinc interparticle boundaries. At later stage of sintering process (high temperature 900 ^{o}C for 4 hours is the third stage of sintering) result in (β Cu_5Zn_8) internetallic compound.X-ray diffraction showed that all samples alloys consist mainly of two phases (α+β) biphasic structure; the martensitic phase (α-phase) orthorhombic structure and the austenitic phase (β-phase) BCC structure.

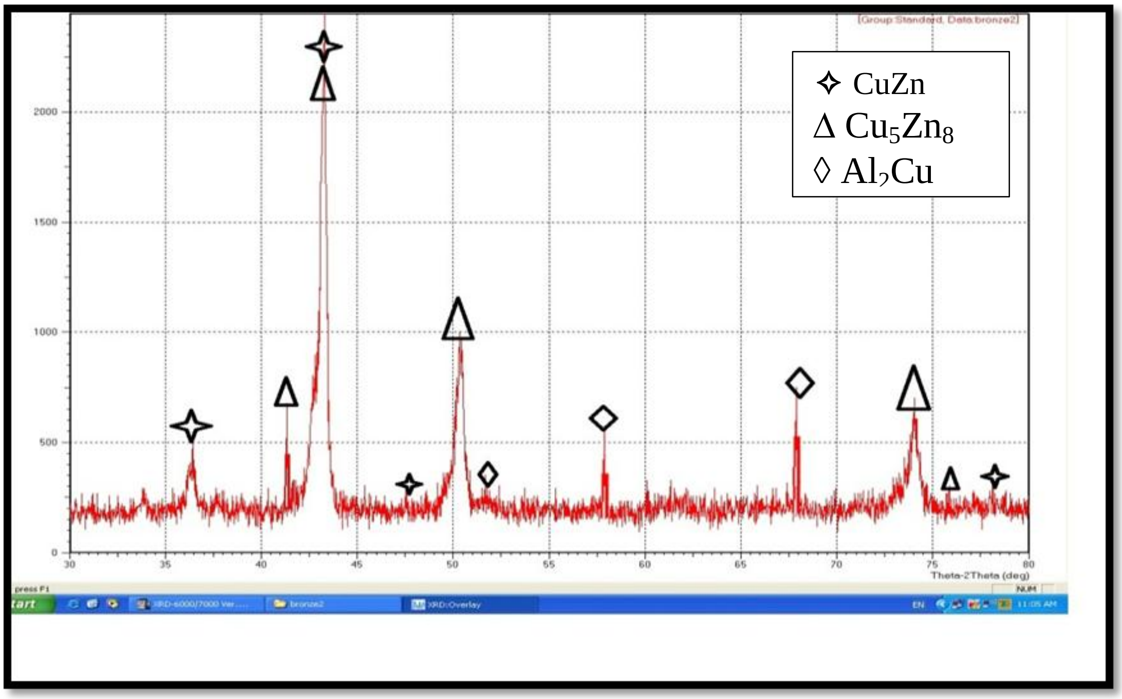

Figure(4.5) XRD Pattern for Sintered unmodified Cu-25Zn-4Al alloy.

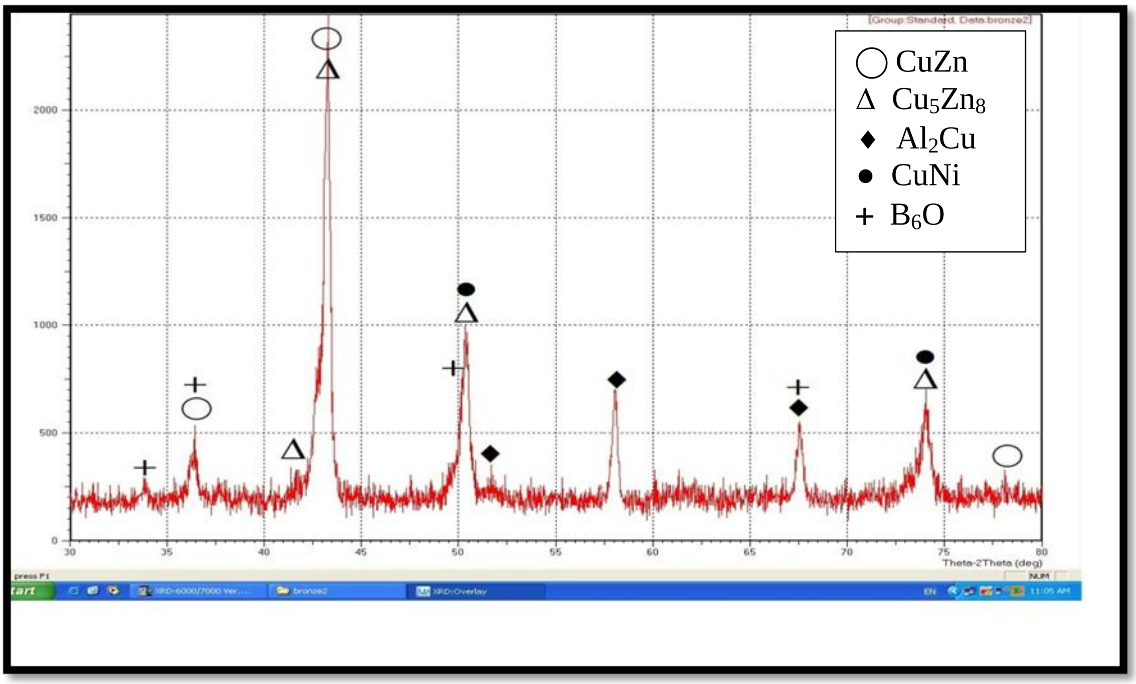

Figure(4.6) XRD Pattern for 1wt. % Ni modified Cu-25Zn-4Al alloy and 5 wt. % B_6O .

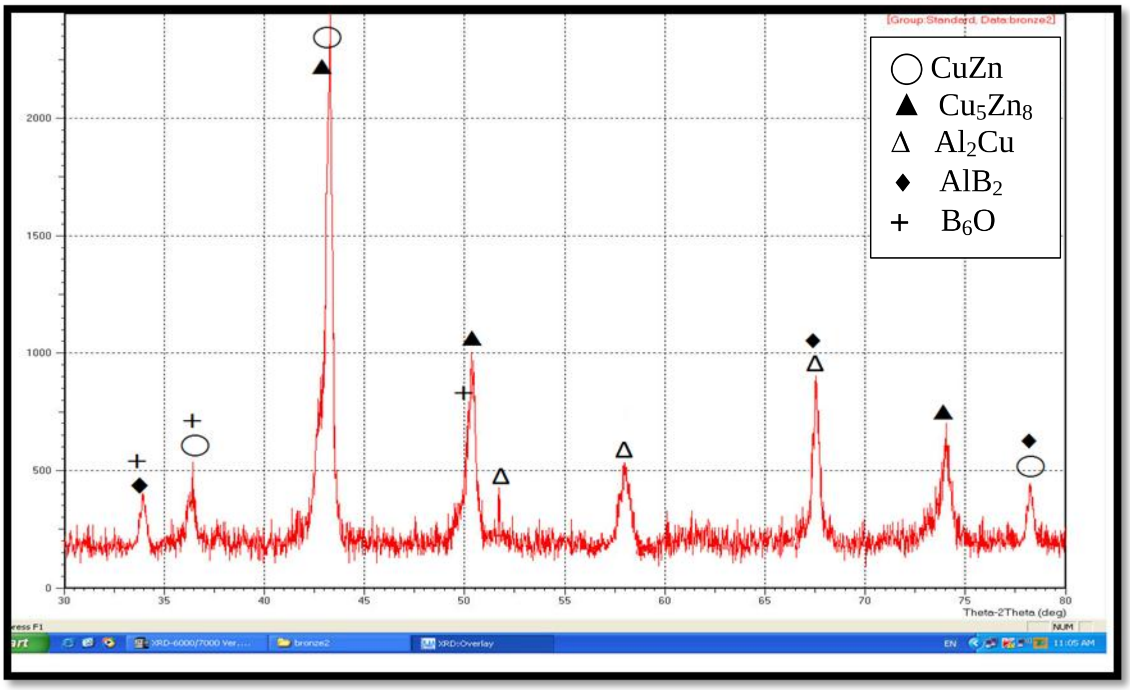

Figure(4.7) XRD Pattern for 1wt. % B modified Cu-25Zn-4Al alloy and 5 wt. % B_6O .

4.5. Microstructure Observation

4.5.1. Optical Microstructure

Optical microstructures image of the (Cu-Zn-Al) alloy with and without addition are shown in Figure (4.8) though to (4.14) . Figure(4.8) shows the optical microstructures image of the base alloy . Observed from images that, the samples after sintering process have a microstructure composed of two regions, light (bright) which represents α-phase represent martensite structure, and the other region is dark which refers to β-phase the austenite structure. So, the composition of the Cu-25%Zn-4%Al alloy has α phase + β two-phase region. Also, it is seen in Figure (4.9) though to (4.14) show optical microstructures image present in samples the grain size is small with Ni addition because this alloying element has been great contribution on finest size grain structure. This improved the mechanical properties. The microstructure results are in good agreement with X-ray data chart in this present study and specifically matches the structural features reported in [99] [100] .

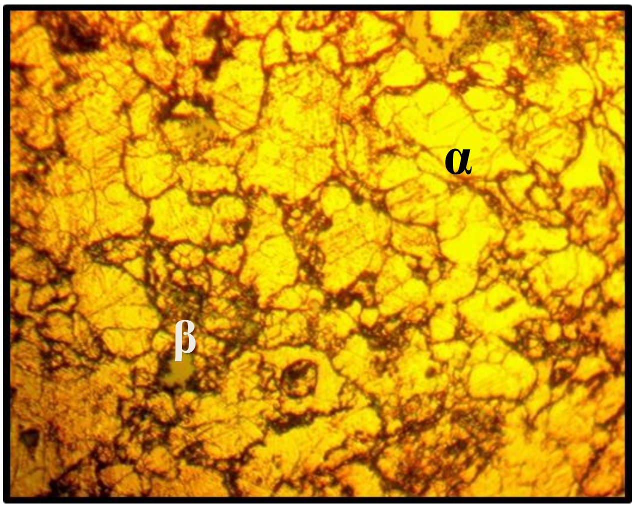

Figure(4.8) : Optical Microscope Image (600 X): for Sintered unmodified Cu-25Zn-4Al alloy

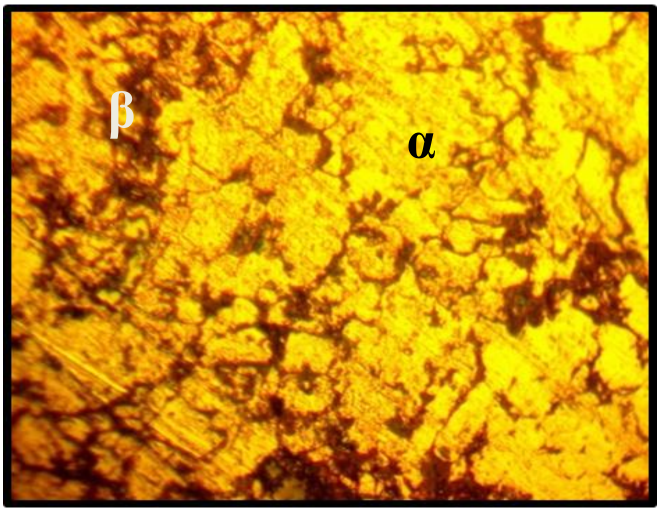

Figure(4.9) : Optical Microscope Image (600 X): For 0.5 w % Ni modified Cu-25Zn-4Al alloy .

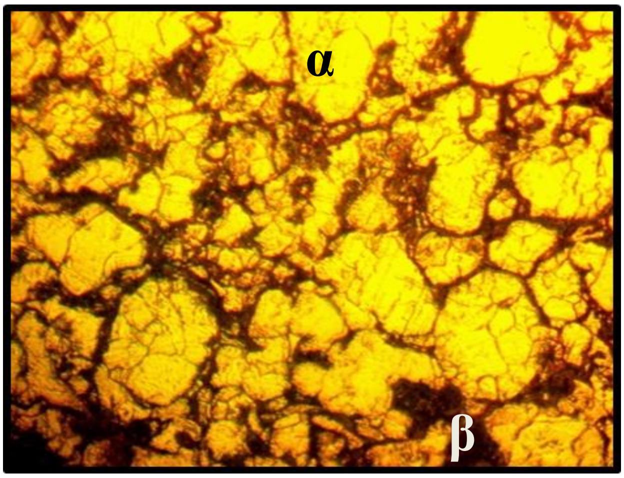

Fig(4.10) : Optical Microscope Image (600 X) For 0.7 wt. % Ni modified Cu-25Zn-4Al alloy .

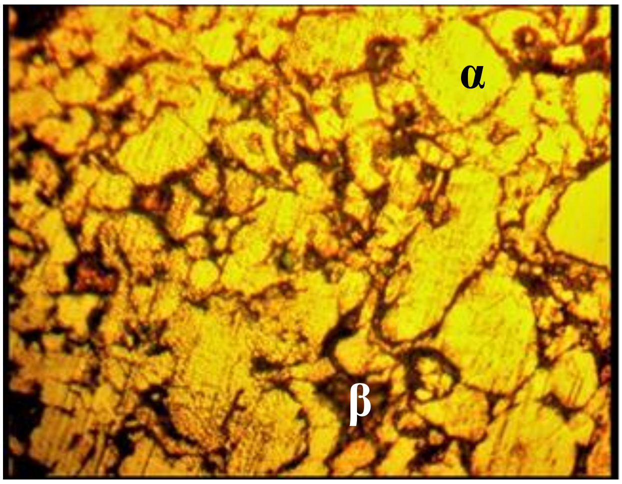

Figure (4.11) : Optical Microscope Image (600 X): For 1wt. % Ni modified Cu-25Zn-4Al alloy.

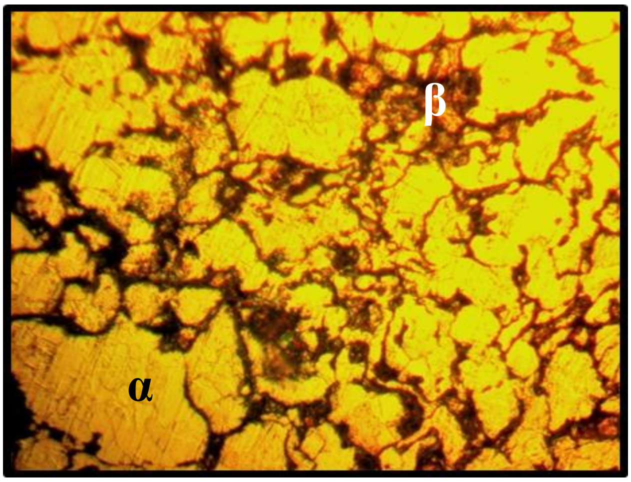

Figure (4.12) : Optical Microscope Image (600 X): For 0.5 wt. % B modified Cu-25Zn-4Al alloy .

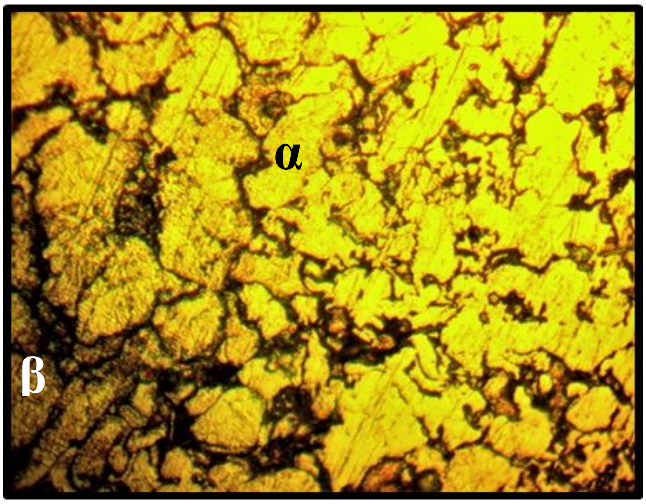

Figure (4.13) : Optical Microscope Image (600 X)For 0.7 wt. % B modified Cu-25Zn-4Al alloy .

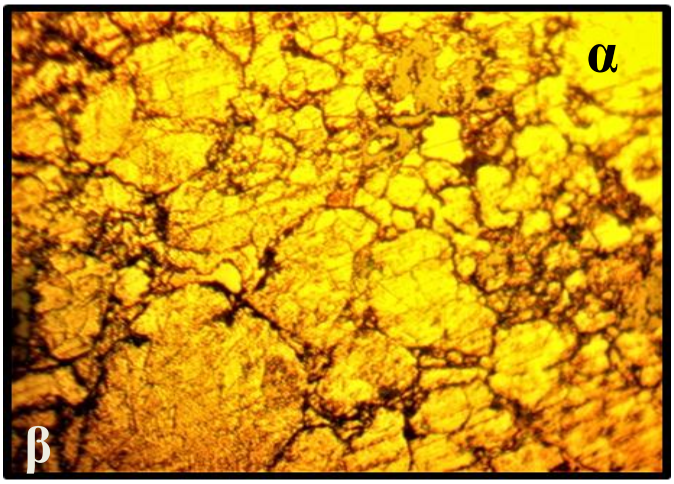

Figure (4.14) : Optical Microscope Image (600 X) For 1wt. % B modified Cu-25Zn-4Al alloy .

4.5.2 Scanning Electron Microscopy (SEM)and(EDS)

The characterizations of Cu-25Zn-4Al SMAs alloy are significantly affected by the microstructure. So, used Scanning electron microscope (SEM) and energy dispersive spectroscopy (EDS) in order to examined and identified the microstructures of reference sample (Cu-25Zn-4Al SMA) and samples with addition .

Scanning electron microscope images for etched sintering specimens of alloys are shown in Figure (4.15), (4.18) and (4.21). Etching reveal grain boundaries which are easily confused with the particle boundaries that also appear as thin gray or black lines.

Through the SEM images, these samples were polished with smooth cloth. It insures the success of the manufacturing process and appearance of martensite phases in the form layers of α alpha phase and beta phase β. It is worth noting that, the intermetallic compounds (some of which didn't appear in the X-ray due to their relatively small percentages) are responsible for an increase and improving of the mechanical properties such as micro-hardness and wear-resistance .

While results of Energy dispersive spectroscopy (EDS) that studied and analyzed used to illustrate the chemical composition of the phases of the reference specimen and the specimens with/without of addition elements show in the figure (4.16) to (4. 23).

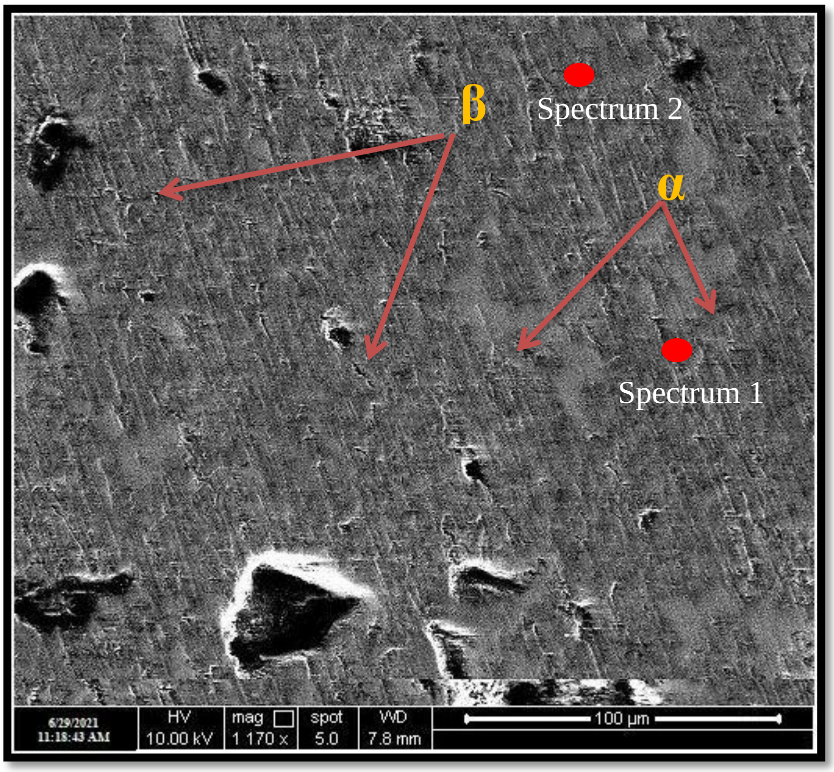

Figure (4.15) SEM Image for Etched unmodified Cu-25Zn-4Al alloy after Sintering Process.

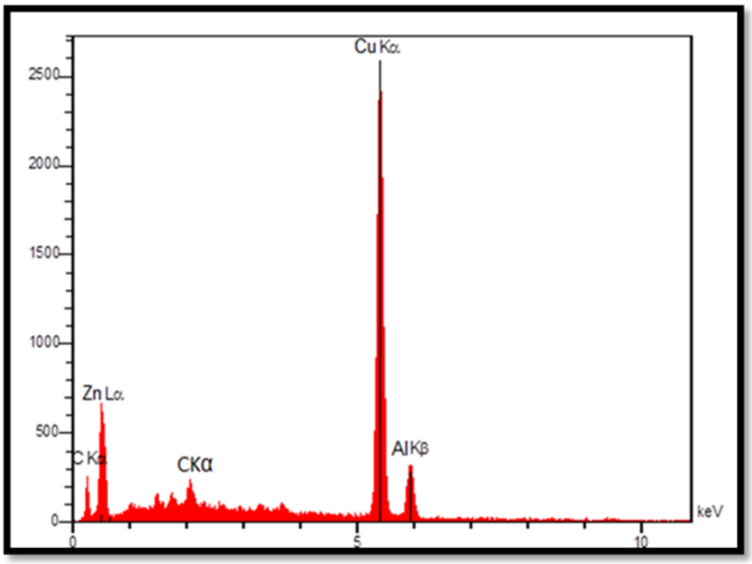

Elt	Int	Error	K	Kr	W%	A%
Cu	2711.5	1.6657	0.0852	0.0712	64.92	50.26
Zn	754.44	1.1102	0.9148	0.7641	31.08	49.74
Al	575.11	1.02	1.0000	0.8352	4.00	100.00
C	411.54	1.11	1.0000	0.9352	1.00	10.00

Figure (4. 16) EDS analysis for unmodified Cu-25Zn-4Al alloy for Spectrum 1 region.

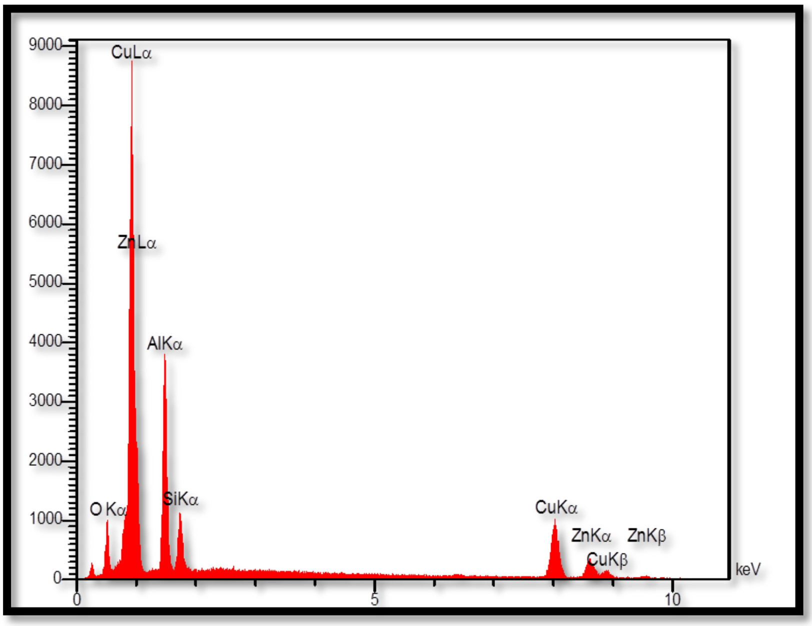

Elt	Int	Error	K	Kr	W%
Cu	2711.5	1.6657	0.0852	0.0712	64.92
Zn	754.44	1.1102	0.9148	0.7641	31.08
Al	575.11	1.02	1.0000	0.8352	4.00
C	411.54	1.11	1.0000	0.9352	1.00

Figure (4. 17) EDS analysis for unmodified Cu-25Zn-4Al alloy for Spectrum 2 region.

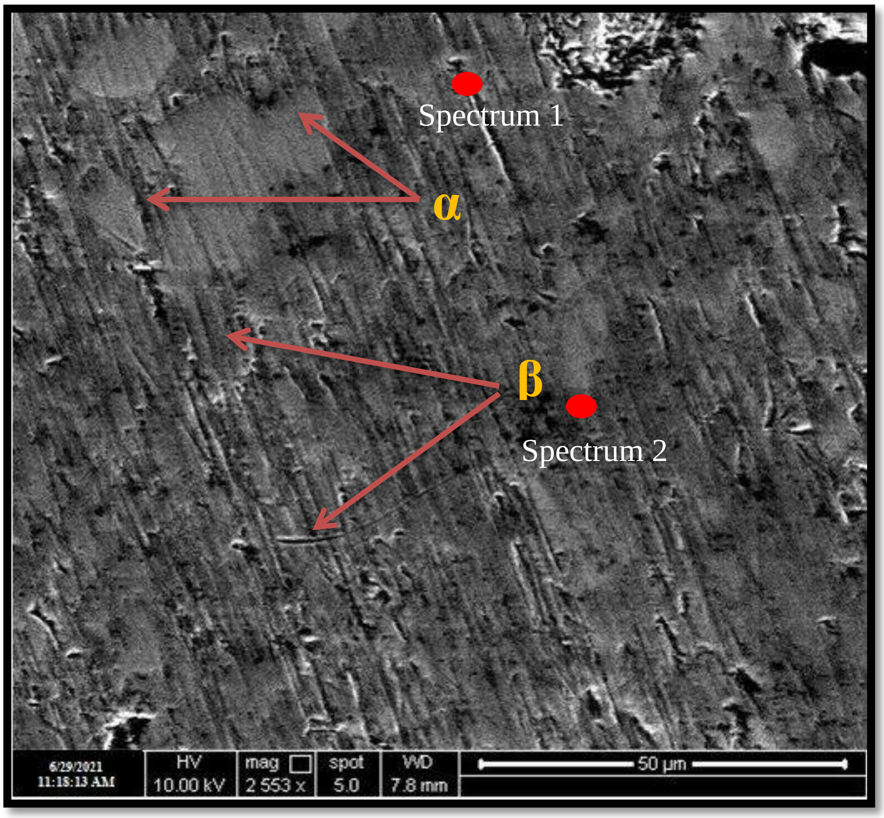

Figure (4.18): SEM image for 1%Ni modified Cu-25Zn-4Al alloy and 5 wt % wt B6O.

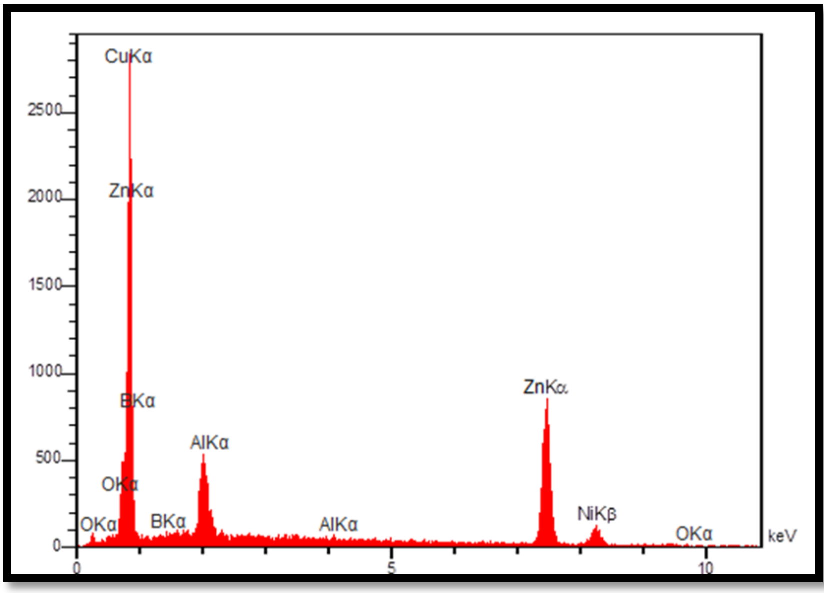

Elt	Int	Error	K	Kr	W%
Cu	2945.1	1.0006	0.0895	0.0820	51.63
Ni	173.1	8.5950	0.0265	0.0243	43.21
Zn	1287.6	0.7473	0.8442	0.7739	4.16
Al	723.8	0.7473	0.0398	0.0365	1.00

Figure (4.19) : EDS analysis for 1 wt % Ni modified Cu-25Zn-4Al alloy and 5%B_6O alloy for Spectrum 1 region .

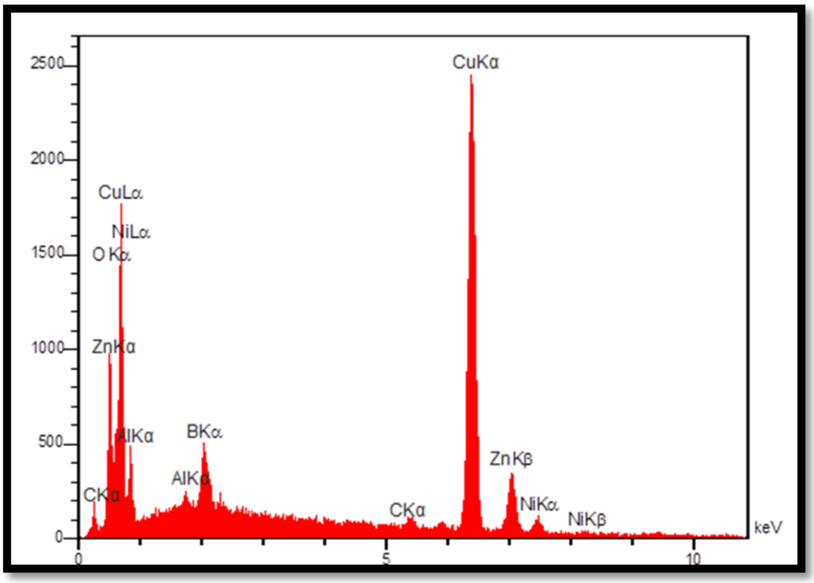

Elt	Int	Error	K	Kr	W%
Cu	2945.1	1.0006	0.0895	0.0820	51.63
Ni	173.1	8.5950	0.0265	0.0243	43.21
Zn	1287.6	0.7473	0.8442	0.7739	4.16
Al	723.8	0.7473	0.0398	0.0365	1.00
B	587.6	0.7473	0.8442	0.7739	4.16

Figure (4.20) : EDS analysis for 1 wt %Ni modified Cu-25Zn-4Al alloy and 5 wt %B6O alloy for Spectrum 2 region .

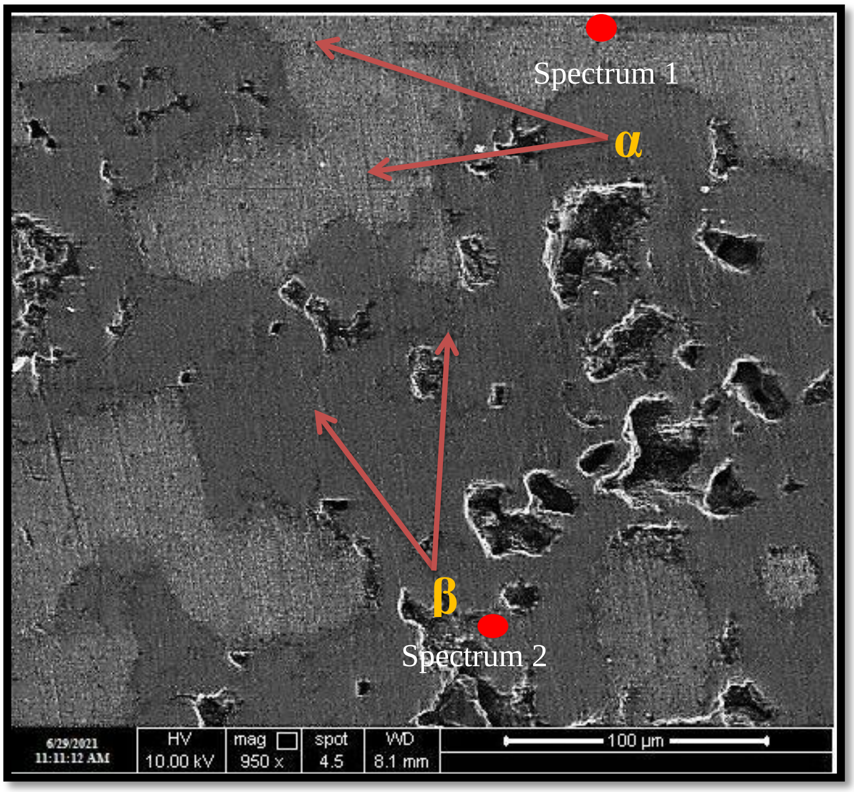

Figure. (4.21): SEM image for 1wt %B modified Cu-25Zn-4Al alloy and 5% wt B6O.

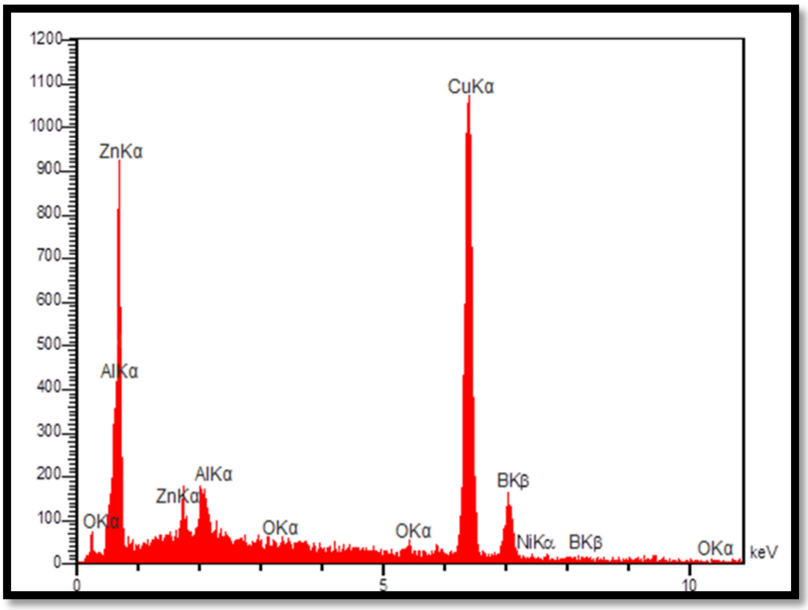

Elt	Int	Error	K	Kr	W%
Cu	1153.7	3.4513	0.0246	0.0243	51.20
Zn	951.5	0.5977	0.9719	0.9600	25.44
Al	422.1	0.875	0.0035	0.0034	9.37
B	214.9	0.1497	1.0000	0.745	11.00
Ni	91.98	0.734	1.0044	0.598	2.98
O	78.3	0.8741	1.0874	0.981	1.11

Figure. (4. 22) EDS analysis for 1 wt% B modified Cu-25Zn-4Al alloy and 5wt%B6O alloy for Spectrum 1 region .

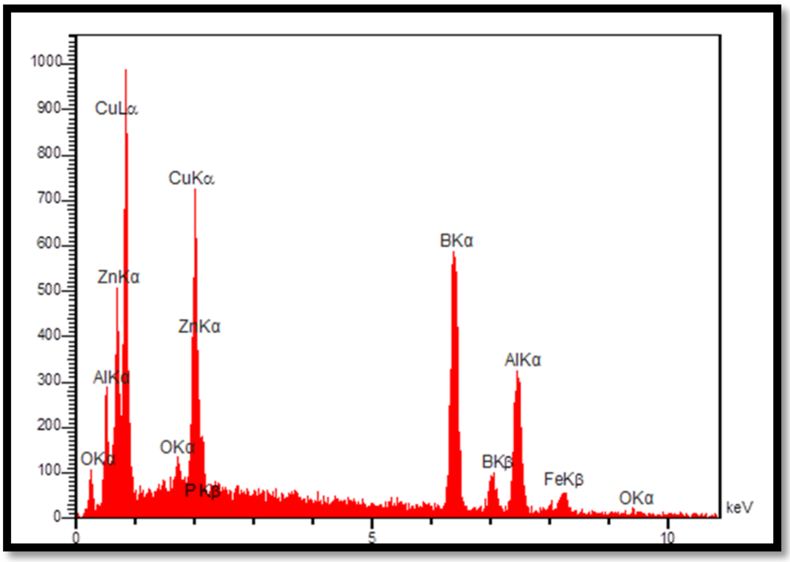

Elt	Int	Error	K	Kr	W%
Cu	908.2	1.0285	0.0914	0.0885	41.96
B	654.8	0.9698	0.4939	0.4783	33.01
Zn	551.1	0.9698	0.4147	0.4017	21.03
Al	314.5	1.0285	1.0000	0.9685	4.00
O	154.5	1.0784	1.1478	0.7894	0.587
Fe	117.5	1.9874	1.2874	0.5478	0.147
P	89.7	1.1457	1.9874	0.3154	0.375

Figure (4.23) EDS analysis for 1 wt% B modified Cu-25Zn-4Al alloy and 5 wt %B6O alloy for Spectrum 2 region .

4.6.Differential Scanning Calorimeter (DSC) Analysis

This test is done using DSC series at heating rate of 5 ^{o}C.min^{-1}, from 20^{o}C to 360 ^{o}C in order to calculate the A_S and A_f which is the austenite finish temperature that used in the shape memory effect test as heat treatment temperature. This test has been done for unmodified Cu-Zn-Al alloy and Ni,B modified Cu-Zn-Al alloy after sintering process as shown in the figures from (4.24) to (4.30) .It was found that the A_S (onset temp.) is 228.32 ºC and A_F(endset temp.) is 326.26 ºC for the base alloy(Cu-Zn-Al). When we add 0.5 and 0.7 wt % Ni note that,the transformation temperature is changes , but the maximum of transformation temperature at 1 wt % Ni where the beginning of the transformation temperature from A_S(onset temp.) is 274.64 ºC to A_F(endset temp.) is 335.38 ºC as shown in figure (4.27) .This results agreement with [84] [99].

Notice that, maximum increase of the transformation temperature at the addition of B in the amount 1%wt , so the A_S and A_F of (onset temp.) is 273.88 ºC and (endset temp.) is 343.68 ºC respectively as shown in Figure (4.30).

It was found that the addition of Ni and B in the amount 1%wt increase the A_S and A_F of the base alloy which make the alloy more stable at high temperatures. The type and amount of the precipitates and intermetallic compounds which are Cu_5Zn_8, Al_2Cu , CuNi , Al_2O_3 , B_2O_3 , NiO , CuO and might have influence on the transformation temperatures of the alloy. This results agreement with [90,100]. It was observed from the DSC curve for alloy from (A) to (C3) the sites for phase transformations depends upon the exothermic or endothermic reaction that shown in the Table (4.1) .

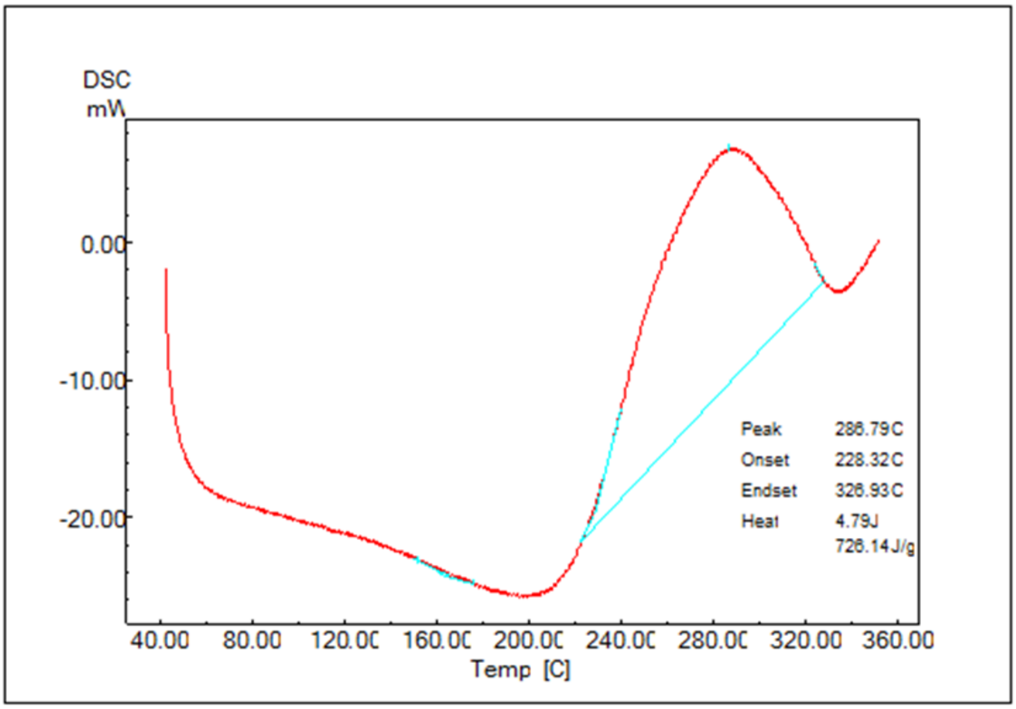

Figure (4.24) : DSC Analysis of unmodified Cu-25Zn-4Al alloy.

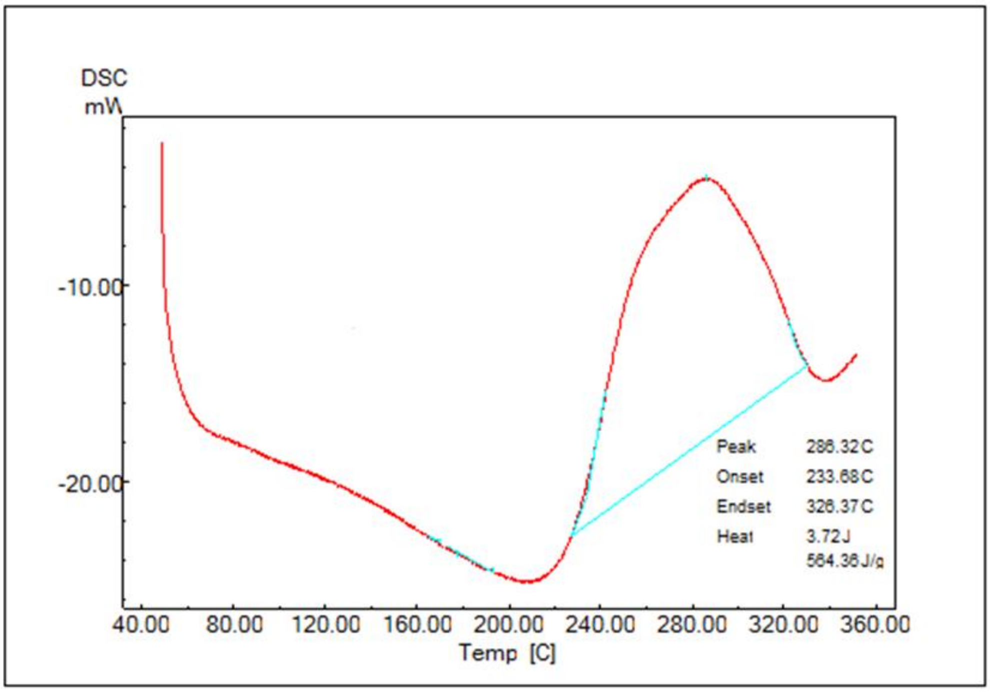

Figure (4.25) : DSC Analysis For 0.5 wt % Ni modifiedCu-25Zn-4Al alloy .

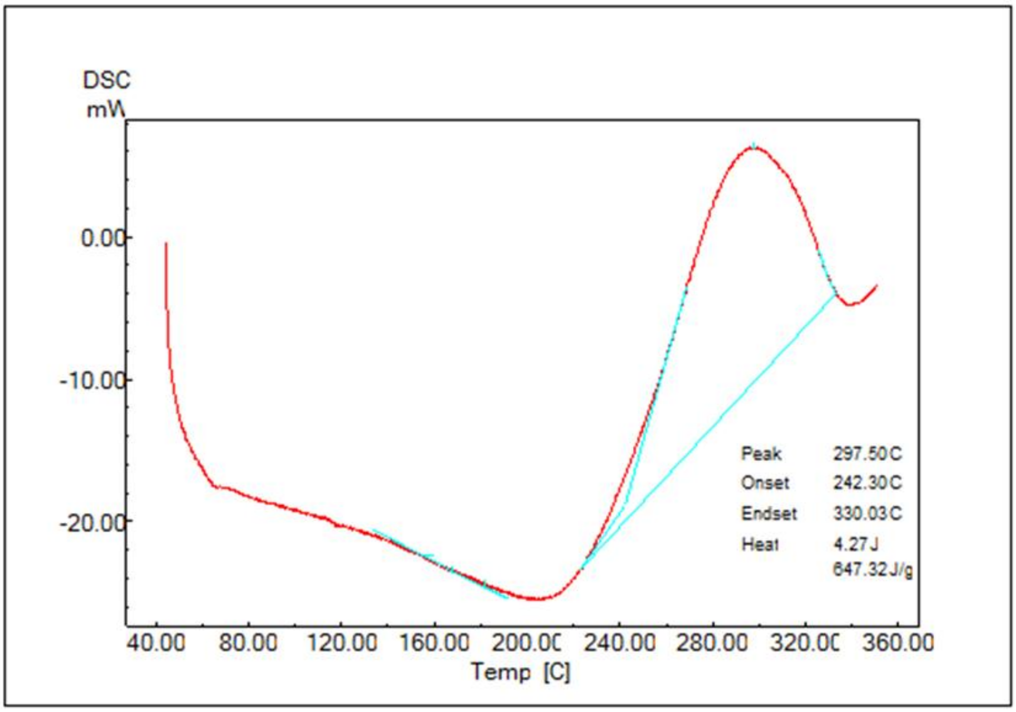

Figure (4. 26) : DSC Analysis For 0.7 wt % Ni modified Cu-25Zn-4Al alloy .

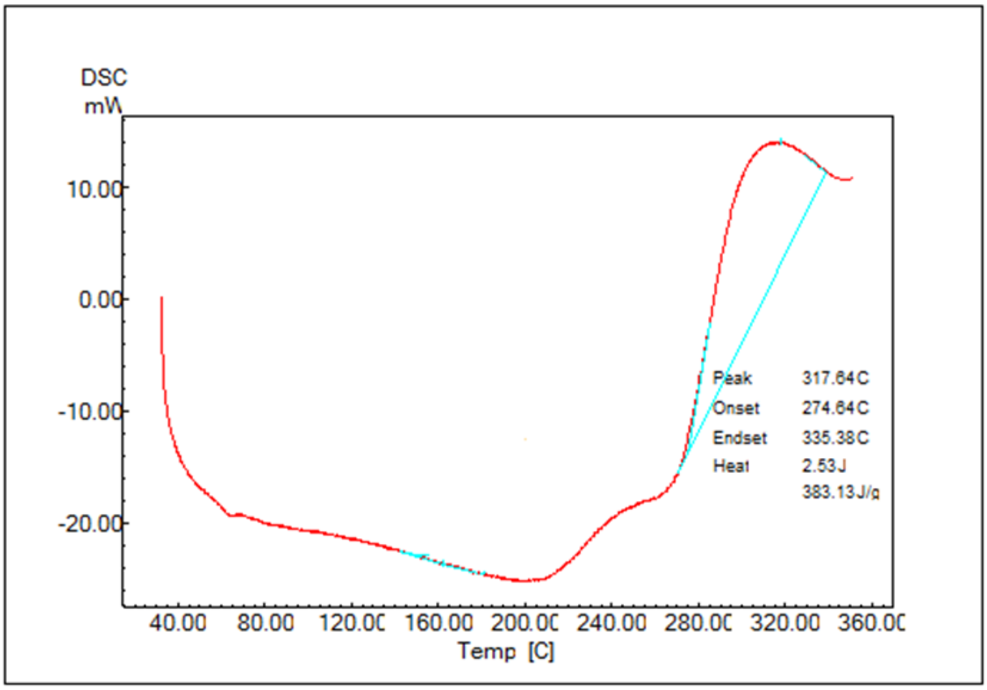

Figure (4.27) : DSC Analysis For 1 wt% Ni modifiedCu-25Zn-4Al alloy.

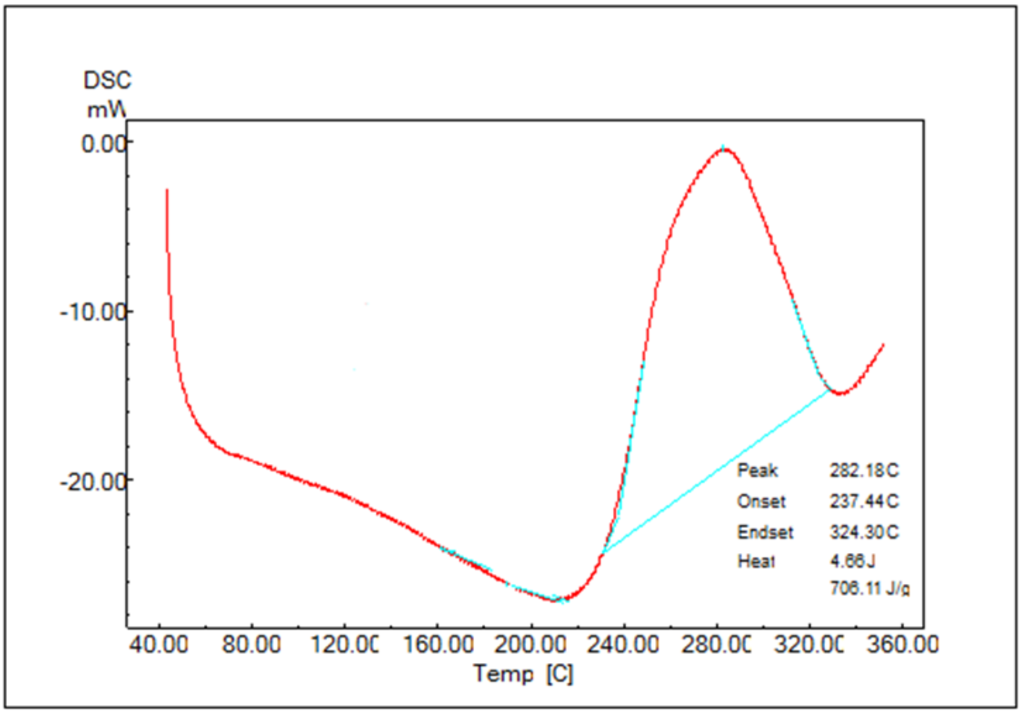

Figure (4.28): DSC Analysis For 0.5wt % B modifiedCu-25Zn-4Al alloy.

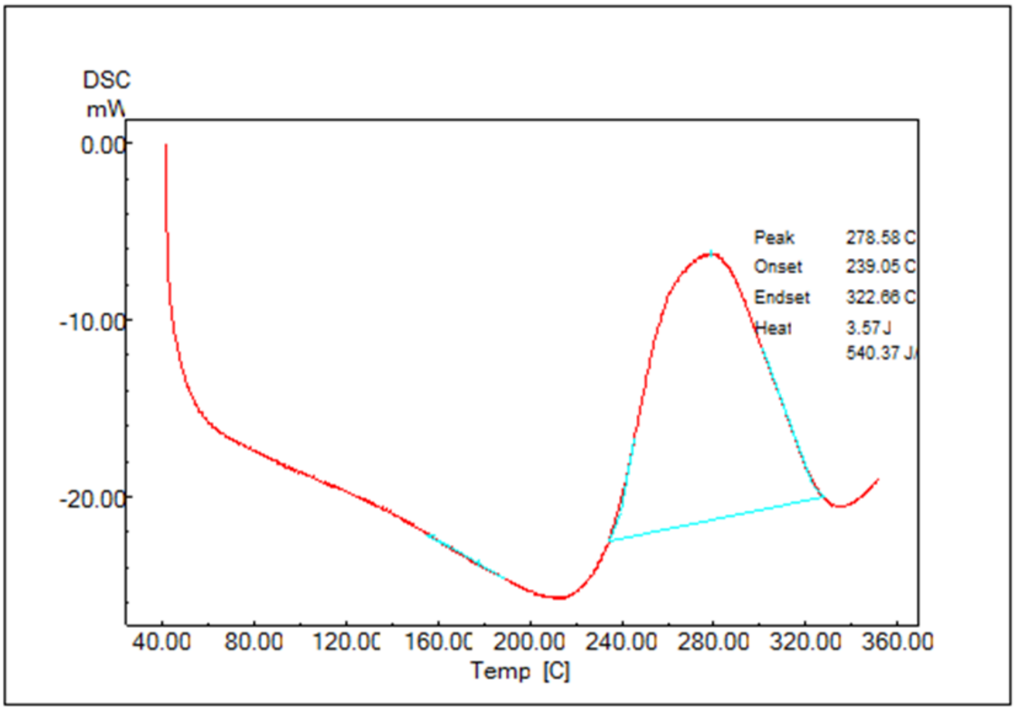

Figure (4.29) : DSC Analysis For 0.7 wt % B alloy modified Cu-25Zn-4Al alloy .

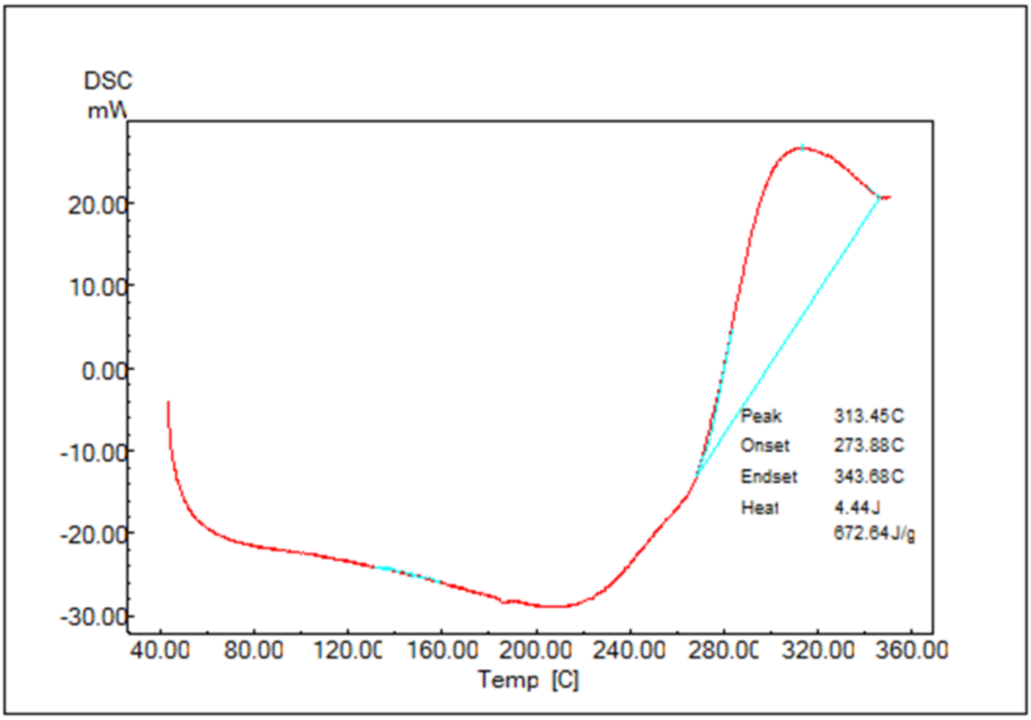

Figure (4.30) : DSC Analysis For 1 wt % B modifiedCu-25Zn-4Al alloy.

Table (4.1) Results from DSC experimental (Figure 4.26through to 4.32) Performed in this study .

Alloy No.	**Alloy composition**	**A_s** °C	**A_f** °C
A	Cu-25n-4Al	228.32	326.93
B1	Cu-25Zn-4Al-0.5 B	237.44	324.30
B2	Cu-25Zn-4Al-0.7 B	239.05	322.66
B3	Cu-25Zn-4Al-1 B	273.88	343.68
C1	Cu-25Zn-4Al-0.5 Ni	233.68	326.37
C2	Cu-25Zn-4Al- 0.7 Ni	242.30	330.03
C3	Cu-25Zn-4Al-1 Ni	274.64	335.38

4.7 Shape Memory Effect

The shape memory effect (SME%) all specimens after heat treatment in temperature at more than A_F (endset temp.) with 5 ^oC of all specimens. SME% was determined by using brinell hardness via measuring the diameter of ball indenter after d_a(µm) and before d_b(µm) the heat treatment.The highest shape memory effect by Ni and B was achieved when the addition was 1 wt% of Ni and B respectively .

The shape memory effect (SME%) of the alloys more than 1 wt% of Ni was slight-decrease in SME% because the changes in shape memory effect take place due to appearance the different types and the amount of the precipitates and intermetallic compounds . This results in good agreement with [84].

Table (4.2) Shape memory effect for alloys .

Alloy No.	Alloy composition	d_a(µm)	d_b (µm)	SME%
A	Cu-25n-4Al	485	538	9.85
B1	Cu-25Zn-4Al-0.5 B	549	627	12.44
B2	Cu-25Zn-4Al-0.7 B	425	514	18.25
B3	Cu-25Zn-4Al-1 B	390	510	23.65
C1	Cu-25Zn-4Al-0.5 Ni	430	515	16.41
C2	Cu-25Zn-4Al- 0.7 Ni	420	500	24.88
C3	Cu-25Zn-4Al-1 Ni	350	495	29.1

4.8 Potentiodynamic Polarization Test Results

The result of electrochemical curves for all specimens in 3.5%NaCl were shown in Figures (4.31) through to (4.37).Two areas has been observed . cathodic area, the current decreased reaction and corrosion potential increased , then the film tends to stable. In the anodic area ,the corrosion potential decreases and dissolve of the metals .

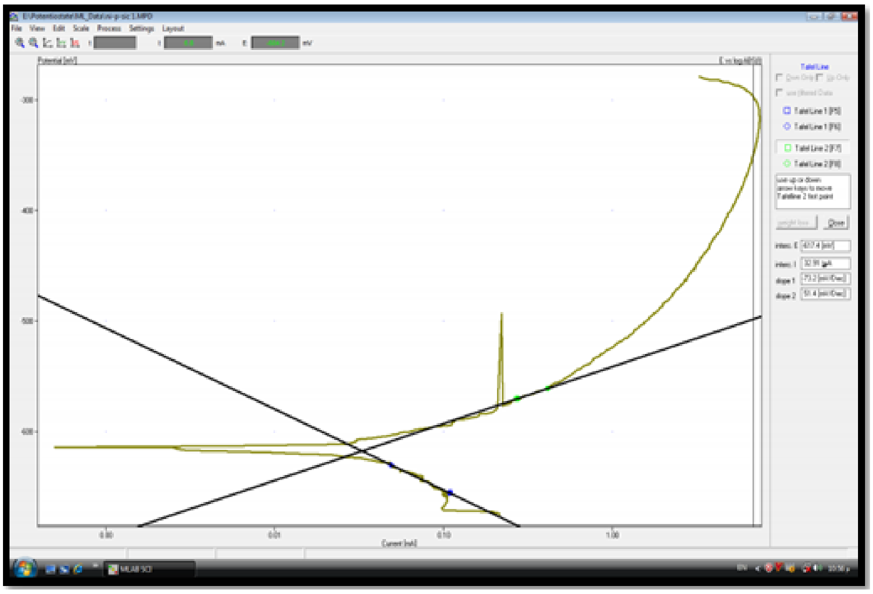

Figure (4.31) : Potentiodynamic Polarization curve for unmodified Cu-25Zn-4Al alloy

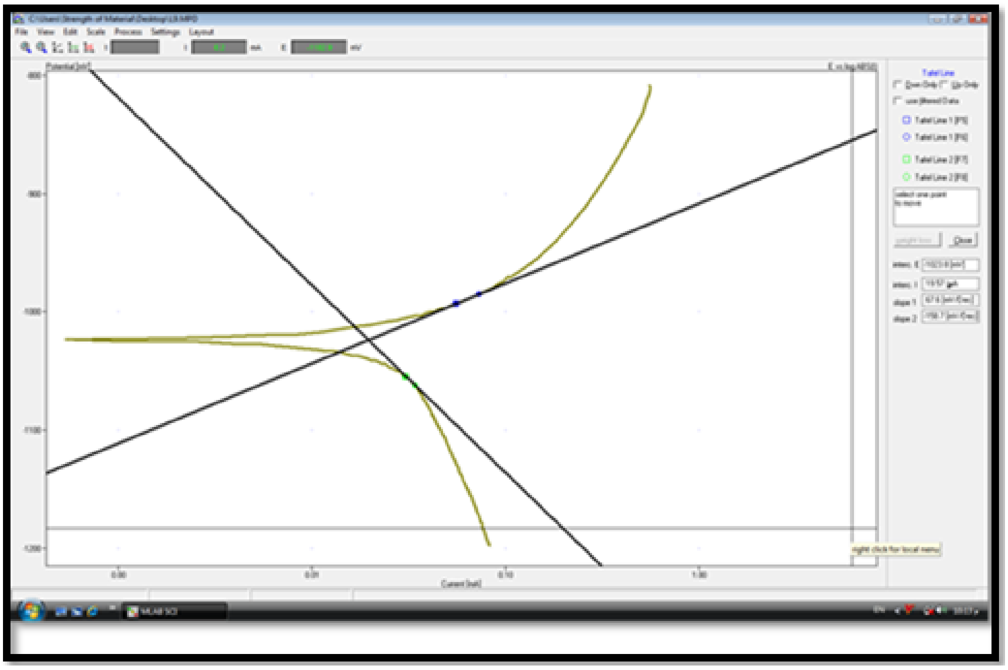

Figure(4.32) : Potentiodynamic Polarization curve For 0.5 wt % Ni modified Cu-25Zn-4Al alloy .

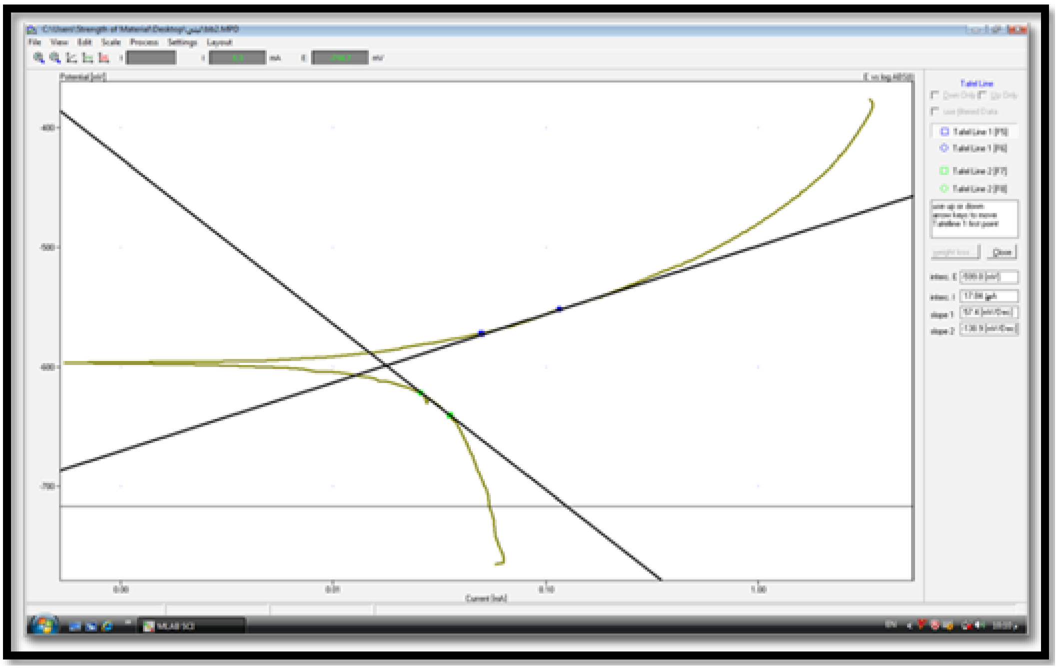

Figure (4.33) : Potentiodynamic Polarization curve For 0.7 wt % Ni modified Cu-25Zn-4Al alloy .

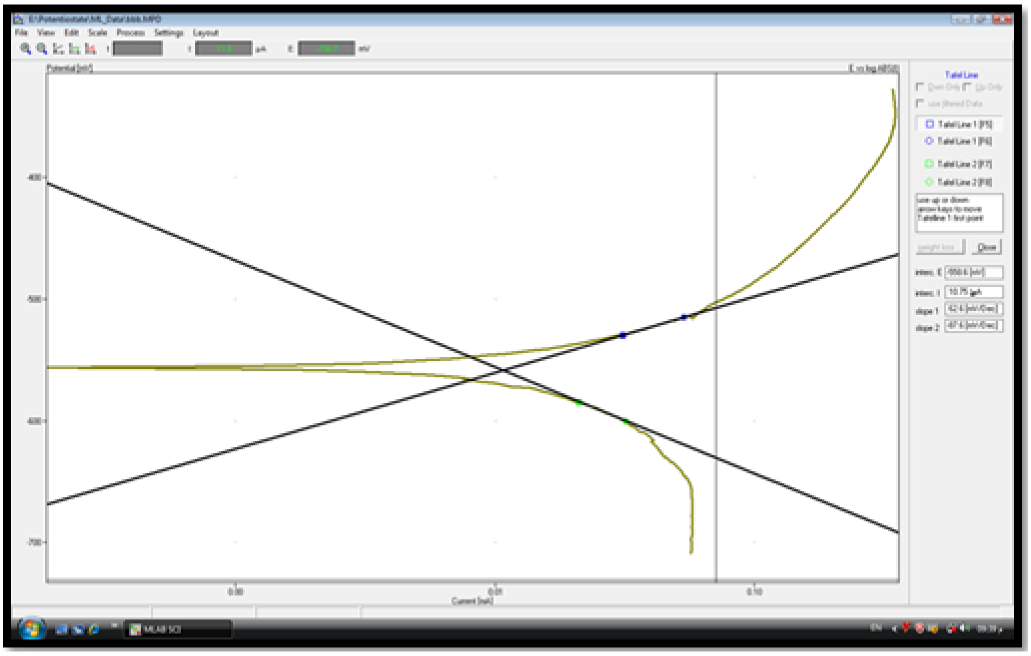

Figure(4.34) : Potentiodynamic Polarization curve For 1 wt % Ni modified Cu-25Zn-4Al alloy .

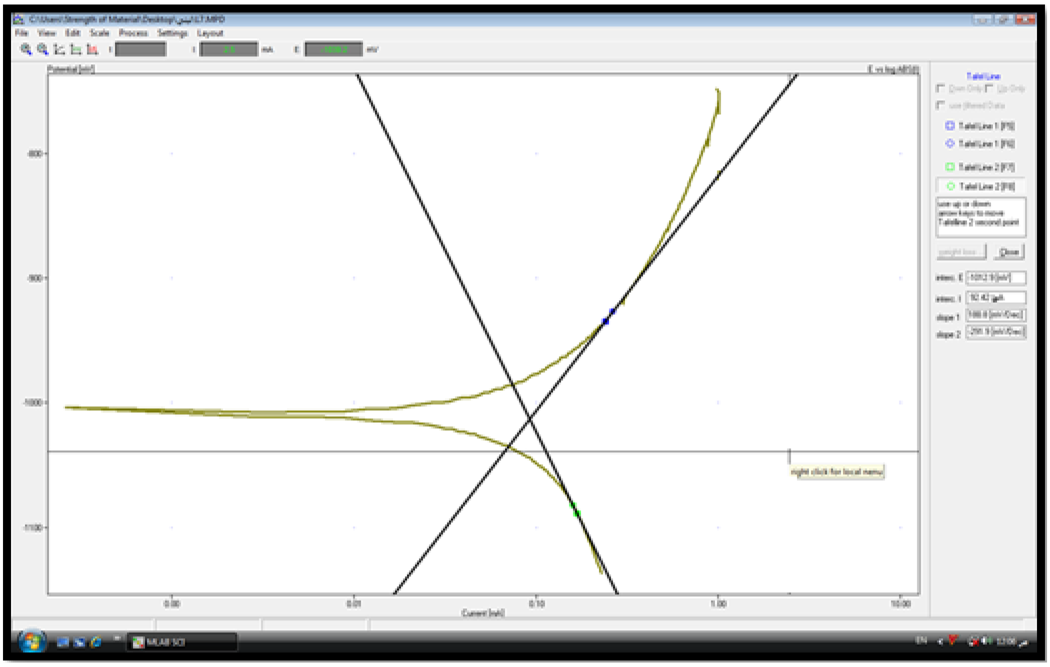

Figure(4.35) : Potentiodynamic Polarization curve For 0.5 wt % B modified Cu-25Zn-4Al alloy .

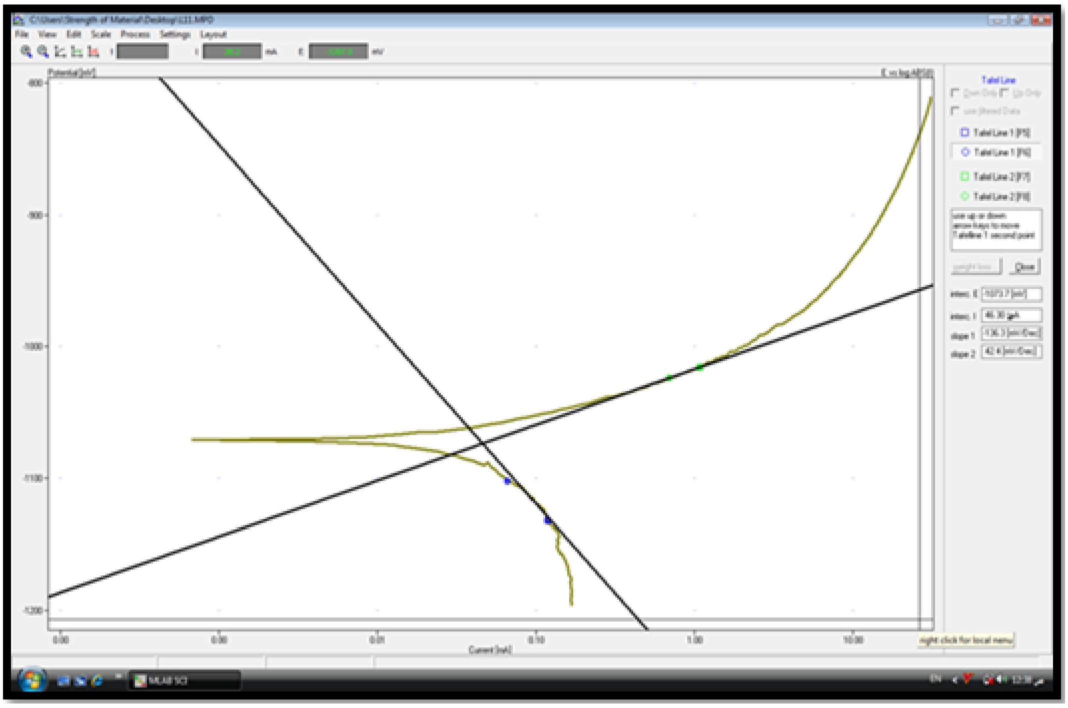

Figure(4.36) : Potentiodynamic Polarization curve For 0.7 wt % B modified Cu-25Zn-4Al alloy .

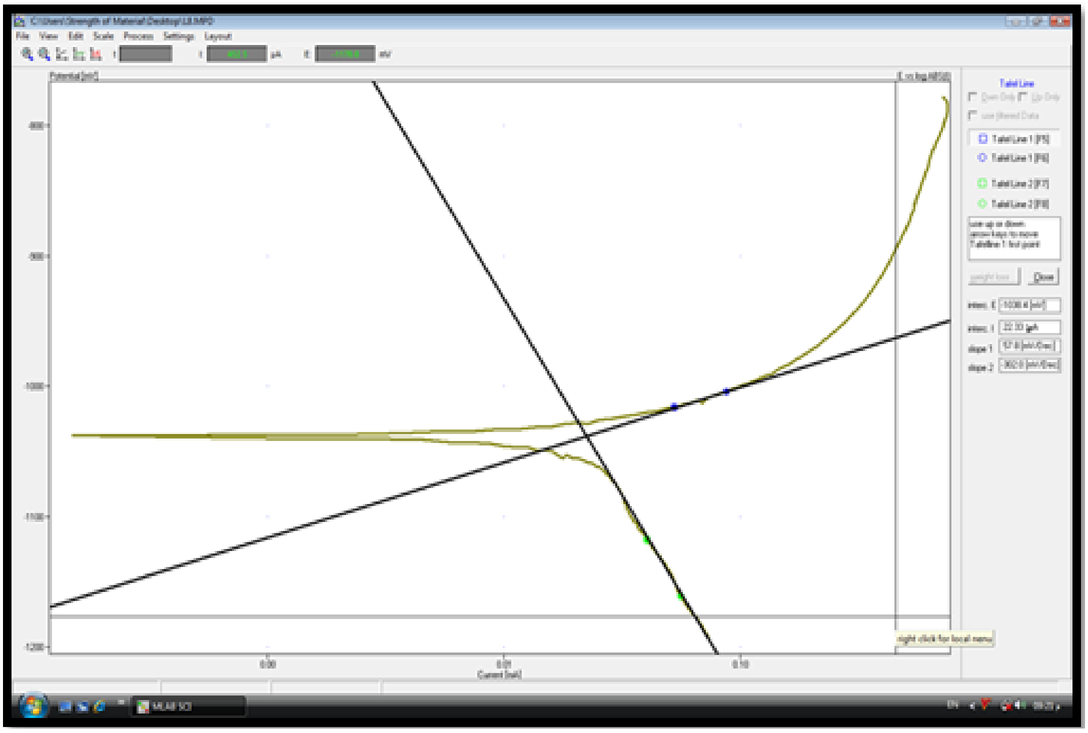

Figure(4.37) : Potentiodynamic Polarization curve For 1 wt % B modified Cu-25Zn-4Al alloy.

4.9 Corrosion Test Results

Electrochemical test for all specimens in 3.5 % NaCl has been done in order to estimate the corrosion rate (mpy) and to investigates the influence of Ni and B on the corrosion resistance of Cu-Zn-Al SMAs.

The corrosion rate (mpy) ,corrosion potential (E_{cor}) and corrosion current density (I_{cor}) of samples calculated from the polarizations curves presented in table (4.3). The corrosion current (I_{corr}) is associated with corrosions rate (mpy) through the following experiential equations [91].

$$C.R\ (mpy) = \frac{0.13 \times I_{corr} \times E.W}{A \times \rho} \qquad \text{…………….Eq. (4-1)}$$

Where :

mpy=mil inch per year.

A= area of the surface (cm^2).

ρ = density of the sample (g/cm^3).

I_{corr}= corrosion current density (μA/cm).

E.w = equivalent weight (g/eq.).

0.13 = metric and time conversion factor.

$$E.w = \text{weight equivalent} = \frac{1}{NEQ} \quad \text{……..……Eq.(4 - 2) [91].}$$

$$NEQ = \frac{\Sigma fi.\ n}{ai} \text{…………Eq.(4- 3)}$$

Where: fi= weight fraction for each element.

ni= electron exchange for each element.

ai= atomic weight for each element.

The corrosion routine starts with dissolution of copper to soluble cuprous chlorides ion complex's ($CuCl^{2-}$) and its diffusions to the bulk solutions. At more potentials the currents density reduced to some extents due to the formations of corrosions products on the electrodes surfaces, which have some protective effects and minimize the actives dissolutions. This decrease come from the decreases of electrode potential for oxidation and lowering in currents density is usually clarified by formations of cuprous chlorides (CuCl) , cuprous oxides (Cu_2O)and aluminum oxides.

Notice from the table(4.3) that, the corrosion rate decreases with increases the percentage weight content of the nickel additions to the base alloy from 0. 052 to 0. 03 mpy. So the addition of nickel from 0. 5 to 1 % wt has developed and improved the corrosion resistance of Cu-25Zn-4Al alloy by 36% . The reason for that the nickel element addition greatly contributed to the reduction of the grain size .This lead to the grain boundaries area. which in turn-act as fast passages for the transfer of aluminum ions, which made to form the protective oxides layers and isolates the alloy from the corrosive medium and this decrease in the corrosion rate is attributed to the formation of aluminum oxide (Al_2O_3), cuprous oxides (Cu_2O) and nikel oxides (NiO) layers (as shown in the XRD patterns after corrosion) which act as protective layers on the surface .This agreement with [78].

Also from the Table (4.3) notes that, the effect of boron-addition on the corrosion resistance of the base alloy, as the corrosion resistance improved by 25% percentage. While the corrosion resistance of the base alloy has improved significantly, but at a lower rate than in the case of adding nickel. Also note that the highest corrosion resistance was at 1 wt of boron because of boron element has effective contributions in reducing the grains size too, so the grains boundaries increase and act as passages for aluminum ions that form a protective oxide layer efficiently but less than state of nickel addition. Finally, concluded from the results that the Nickel element addition at 1 wt considered very effective in improving corrosion resistance .Figure (4.38) Show the Corrosion rate (mpy) of Cu–Zn– Al SMA After and Before the Alloying Element Additions in 3.5% NaCl Solution .

Table (4.3) : Show the Polarization Parameters of Cu–Zn– Al SMA After and Before the Alloying Element Additions in 3.5% NaCl Solution

Alloy No.	Alloy composition	Corrosion rate C.R (mpy)	Current density I_{corr} (μA/cm2)	Corrosion potential E_{corr} (mV)	Corrosion resistance Percentage
A	Cu-25Zn-4Al	0. 0 52	9. 629	-617.4	-----
B1	Cu-25Zn-4Al-0.5 B	0.047	8.324	-1023.8	%9
B2	Cu-25Zn-4Al-0.7 B	0. 043	7.592	-599. 0	%17
B3	Cu-25Zn-4Al-1 B	0.039	7.213	-558. 6	25%
C1	Cu-25Zn-4Al-0.5 Ni	0. 045	8.703	-1012.9	13%
C2	Cu-25Zn-4Al- 0.7 Ni	0. 041	7.962	-1073	21%
C3	Cu-25Zn-4Al-1 Ni	0. 033	6.157	-1038.4	36%

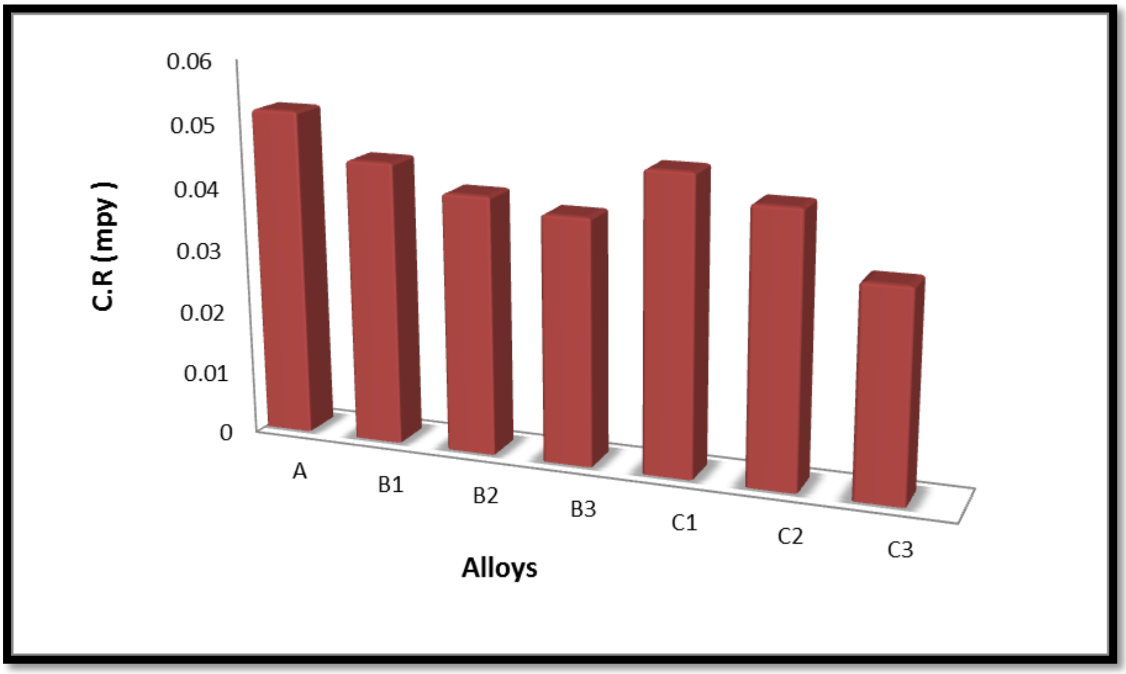

Figure (4.38): Show the Corrosion rate (mpy) of Cu–Zn– Al alloy After and Before the Alloying Element Additions in 3.5% NaCl Solution.

4.9.1. X-Ray Diffraction After Corrosion

In this test X-Ray diffraction for specimens after corrosion test in 3.5% NaCl solution has been done for alloy B3,C3. In Figure (4.39) is the XRD result of alloy B3 , showed that the formation of corrosion products on the specimens surface in 3.5% NaCl solution , the corrosion products were Al_2O_3 , NiO , CuO , ZnO and CuCl. While in the figure (4.4 0) which is for alloy C3 ,the corrosion products were Al_2O_3 , CuO , ZnO , CuCl and B_2O_3.

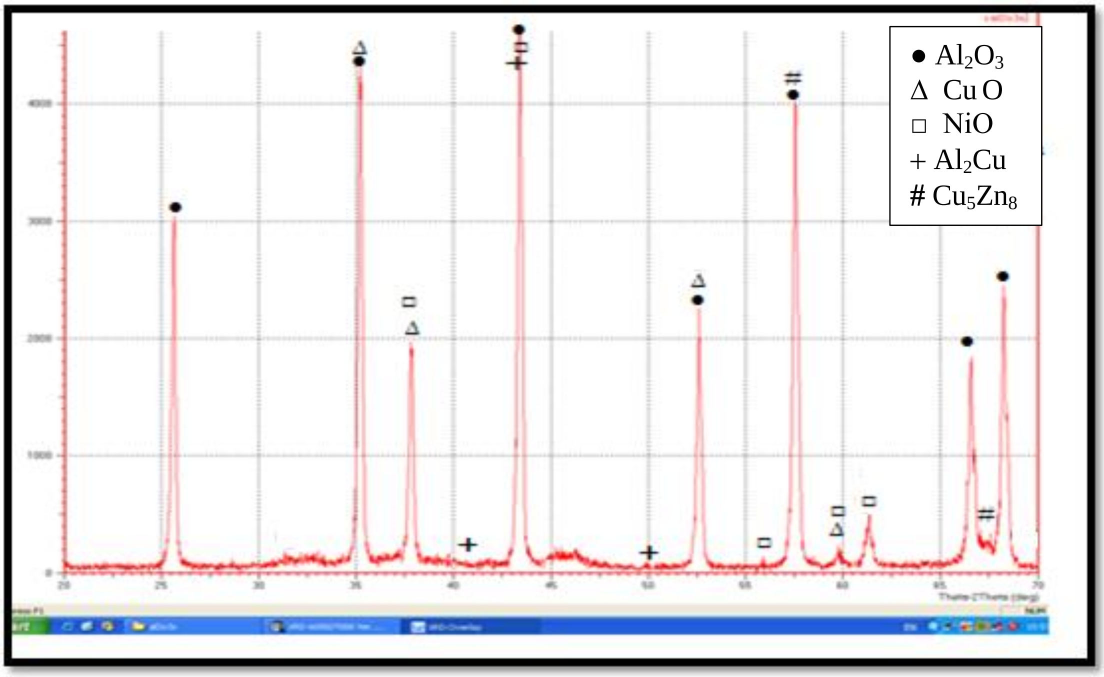

Figure (4.39) : XRD Analysis For 1 wt % Ni modified Cu-25Zn-4Al alloy in 3.5%NaCl solution.

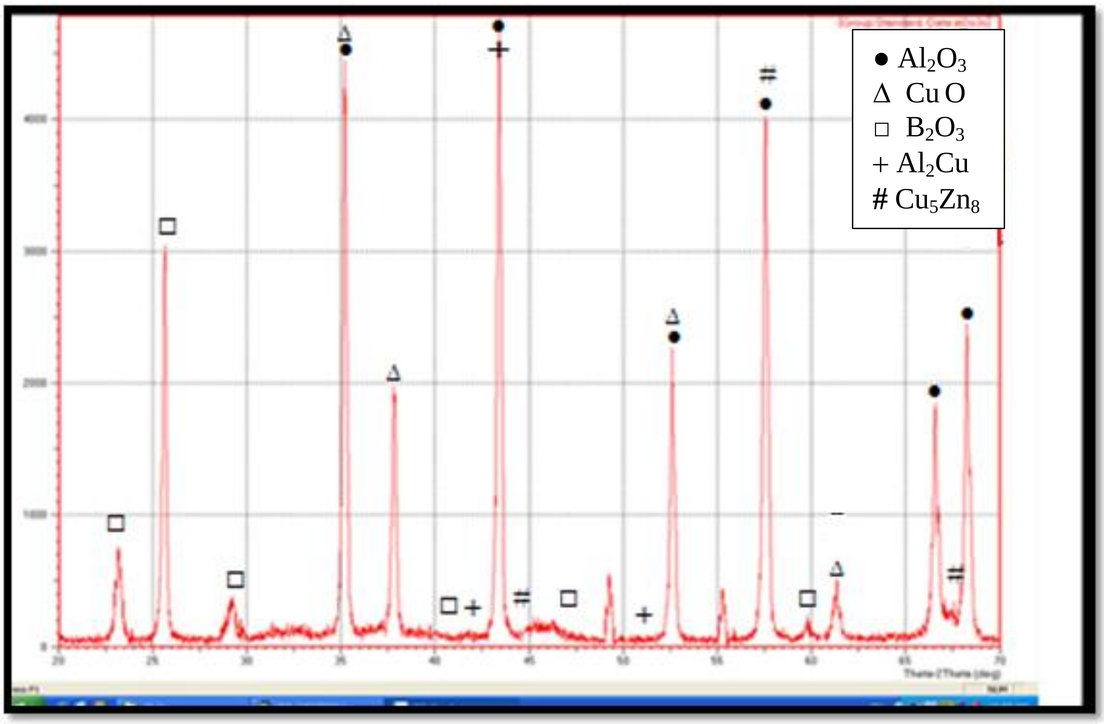

Figure (4.40) : XRD Analysis For 1 wt % B modified Cu-25Zn-4Al alloy in 3.5%NaCl solution.

4.10 Vickers of Micro-Hardness Results

The micro-hardness values for unmodified Cu-Zn-Al alloy and boron oxide modified Cu-Zn-Al alloy are presented in Figure (4.41). It is observed that the hardness values of the unmodified Cu-Zn-Al alloy are basically increase with increase the boron oxide additions .However, the value of micro hardness slightly decrease with increase the amount of boron oxide up to 5% of both type spacemens with Ni and B .This could be related to the increases in boron oxide addition cause decreases on efficiently of sintering processe.

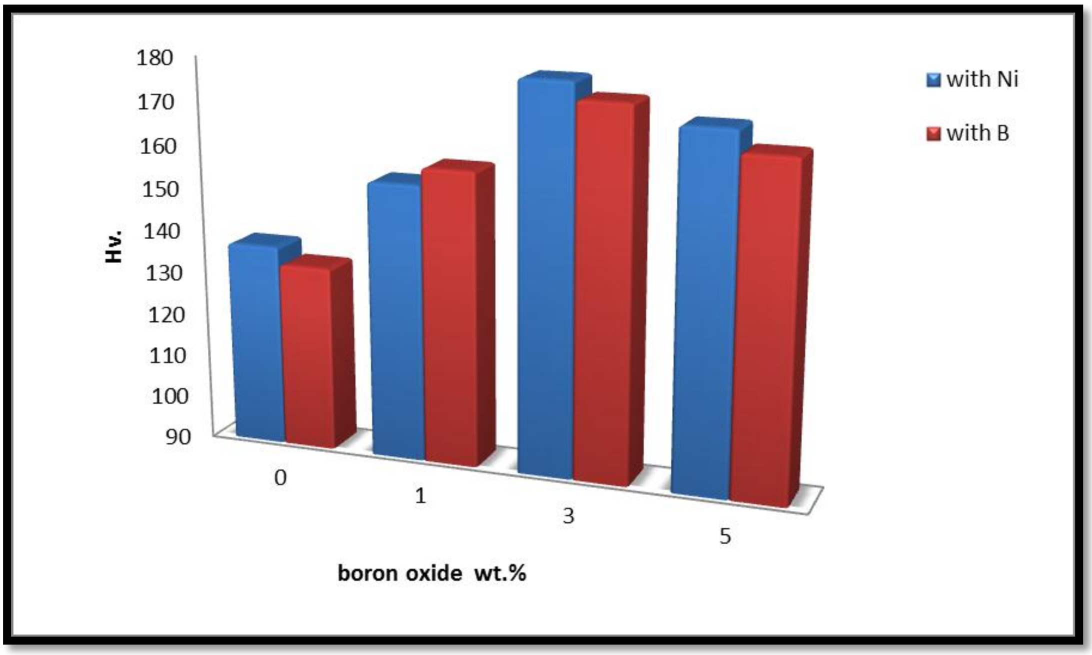

Figure (4.41) : Hardness for all samples after sintering

Also, it is seen in Figure (4.41) most value of the micro-hardness present in samples with Ni addition because this alloying element has been great contribution on finest size grain structure .This improved hardness due to inhibit of motion dislocations.

4.11. Wet-Sliding Wear Test Results

Disk specimens with (12.8 mm) in diameter and (6 mm) in height have been performed on the spacemens of Cu +25 wt% Zn+ 4 wt% Al alloy with and without elements-additions for wet-sliding wear test. The actual mechanisms include material removal due to rubbing action at the interfaces.Loss amount of martial removal identified of the effect alloying elements in improvement material resistance. The curve of volume loss against time for unmodified Cu-Zn-Al alloy and boron oxide modified Cu-Zn-Al alloy under (2N, 5N and 10N) loads have been presented in Figures (4.42), through to (4.48).

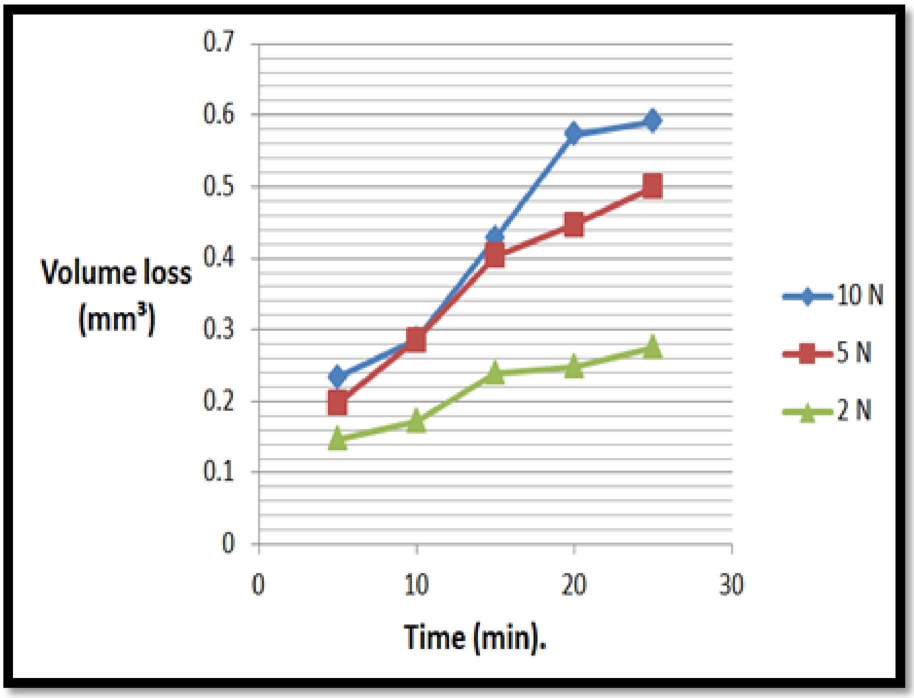

Figure (4.42) : Volume Loss Vs. Sliding Time of the unmodified Cu-25Zn-4Al alloy.

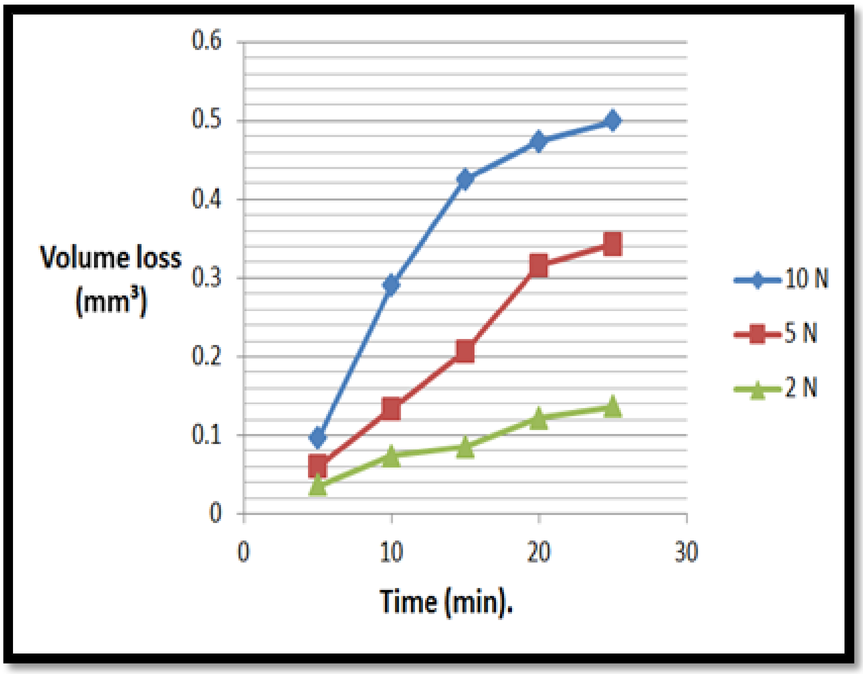

Figure (4.43) : Volume Loss Vs. Sliding Time For1 wt.% Ni modified Cu-25Zn-4Al alloy and 1wt.% B6O

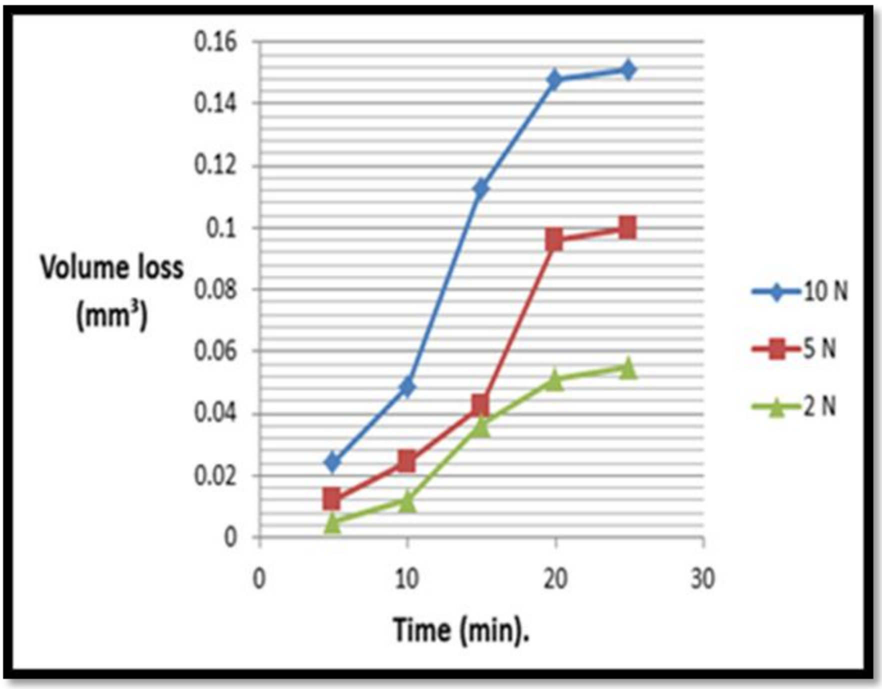

Figure (4.44) : Volume Loss Vs. Sliding Time For1 wt.% Ni modified Cu-25Zn-4Al alloy and 3wt.% B6O

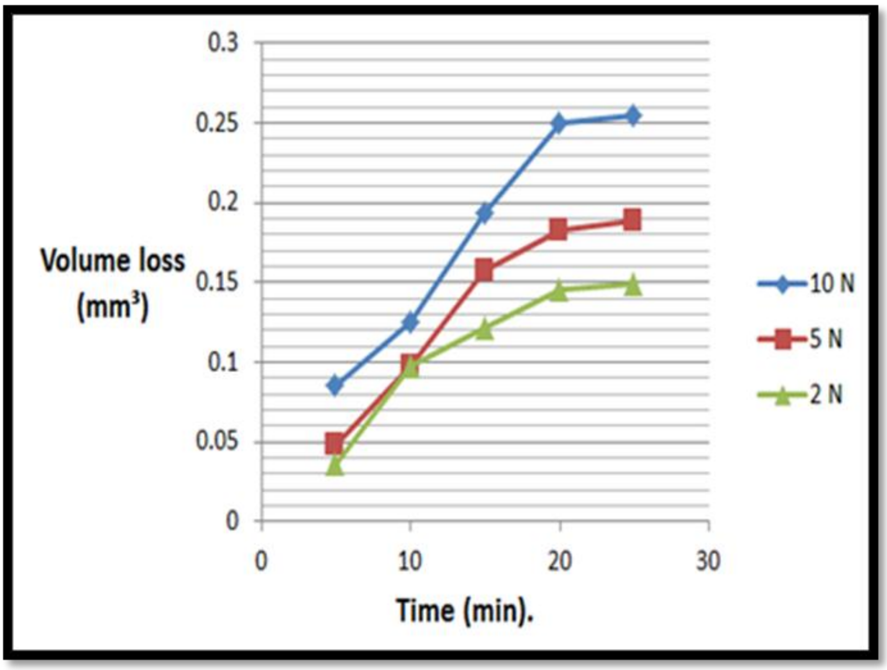

Figure (4.45) : Volume Loss Vs. Sliding Time For1 wt.% Ni modified Cu-25Zn-4Al alloy and 5wt.% B6O

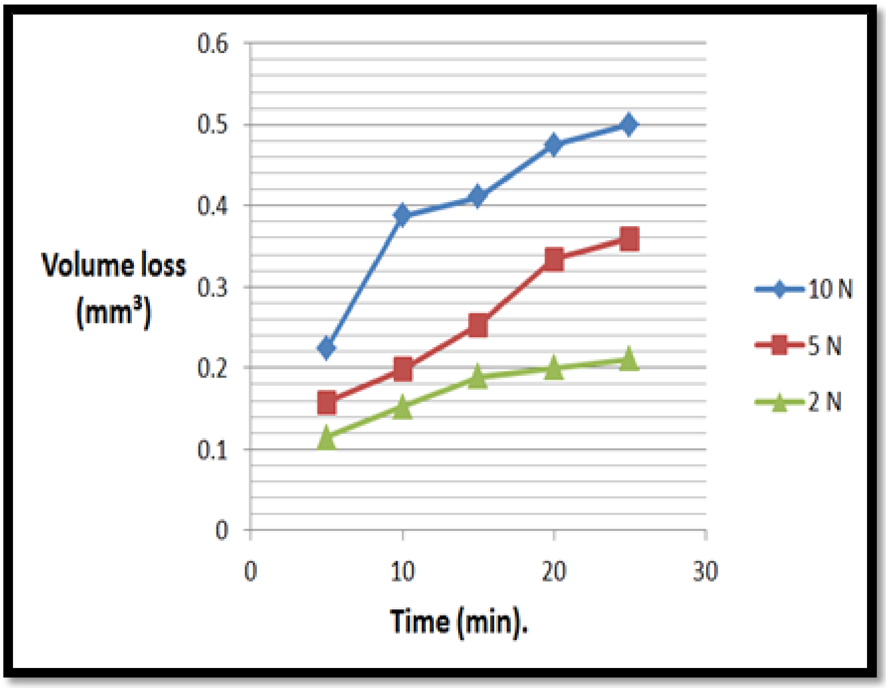

Figure (4.46) Volume Loss Vs. Sliding Time For 1 wt.% B modified Cu-25Zn-4Al alloy and 1wt.% B6O

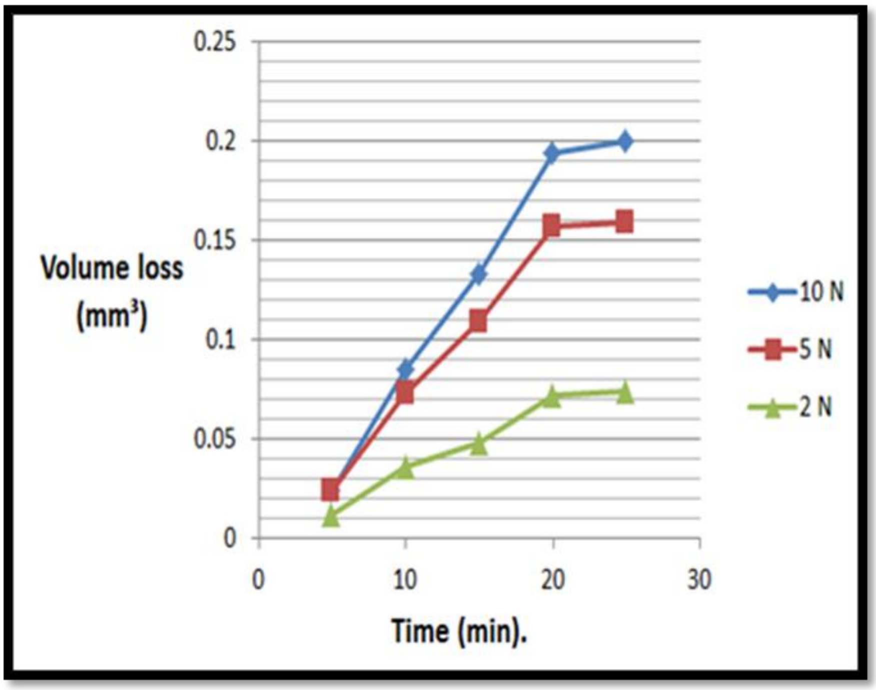

Figure (4.47) : Volume Loss Vs. Sliding Time For 1wt.% B modified Cu-25Zn-4Al alloy and 3wt.% B6O

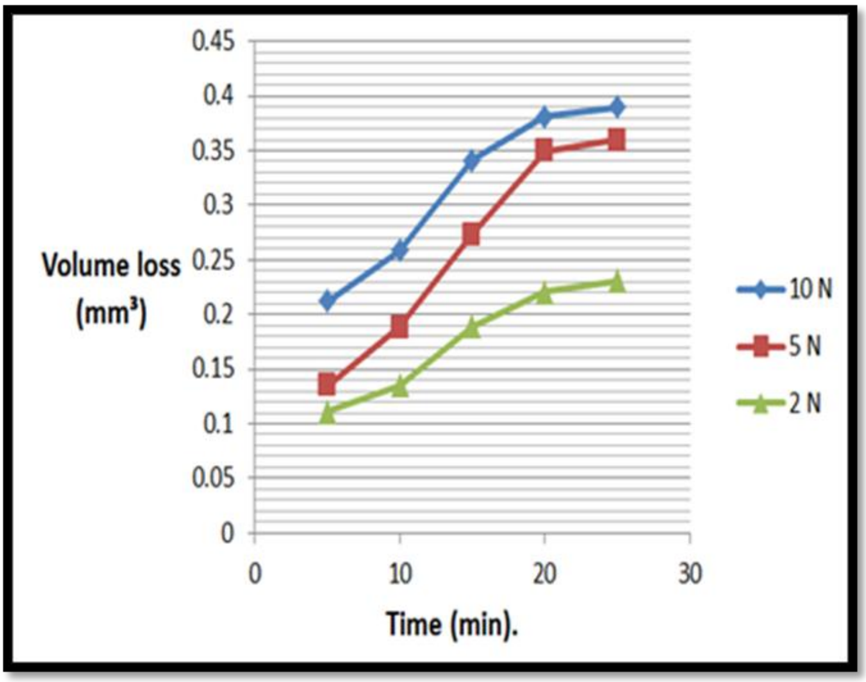

Figure (4.48) : Volume Loss Vs. Sliding Time For 1wt.% B modified Cu-25Zn-4Al alloy and 5wt.% B6O .

It is clear from the Figures that, the values of volume loss increased with an increasing the time for all normal loads . The reason is due to the increase in the plastic deformation on the surface of sample exposed to wear , then the removal of material from the surface of this sample. This occurs as a result of overcoming the forces of cohesion and crystalline bonds subjected to friction force between surface of the disc and surface of the specimen caused increased temperature due to an increase in the period of time of the dominated applied load.

Furthermore, from the curves, it is identified that wear rate decreases with an increase of the boron oxide content and above 3%(B_6O) decrease wear rate . This could be related to the boron oxide act as the handle and holder of the network-structure of substrate specimens [69].

However wear rate slightly increased at 5 wt.% boron oxide (B_6O) .Thus might be related to may be when increase of the oxide content made decreases in efficiency of the sintering process . So, the additive of boron-oxide (3 wt.%) gives the alloy structure more resistance to volume loss due to friction and sliding effect and more protected and adhered with substrate of the alloy surface. The curves of wet wear rate against sliding time for modified Cu-Zn-Al alloy with 1 wt.% Ni , B and boron oxide under (5N) loads have been presented in Figures (4.49) through to (4.50)

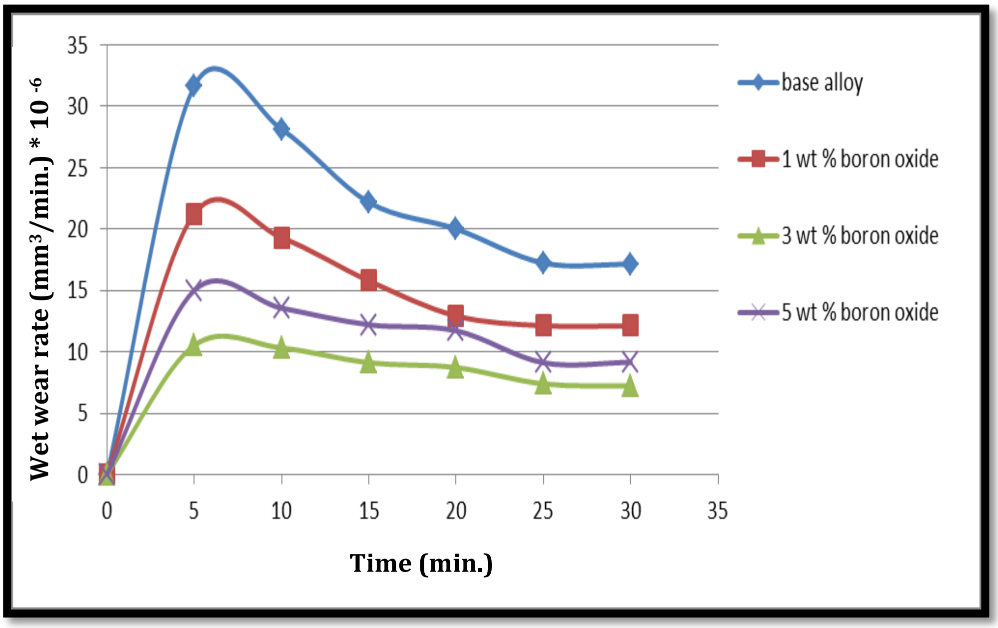

Figure (4.49) : Wet wear rate with Sliding Time For 1wt.%Ni modified Cu-25Zn-4Al alloy and all addition of boron oxide under 5KN normal load.

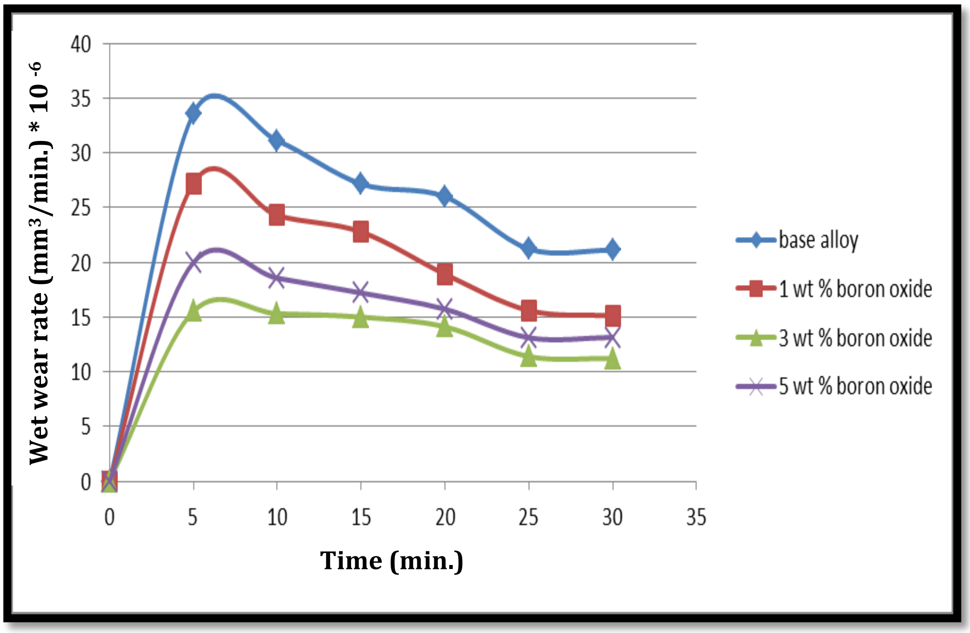

Figure (4.50) : Wet wear rate with Sliding Time For 1wt.% B modified Cu-25Zn-4Al alloy and all addition of boron oxide under 5KN normal load .

4.11.1 Topography Examination after Wear Test

Microstructure examination has been investigated by light optical microscope for worn surface of unmodified Cu-Zn-Al alloy and boron oxide modified Cu-Zn-Al alloy as shown in Figure 4.51 through to 4.53 .

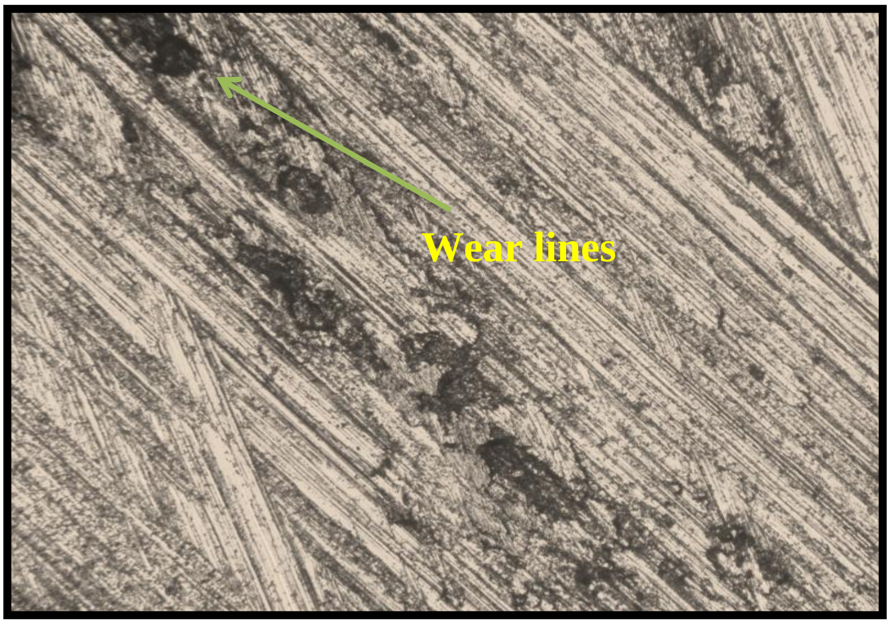

Figure (4.51) : Optical Microscope Image of Sample Surface (100 X) for unmodified Cu-25Zn-4Al alloy.

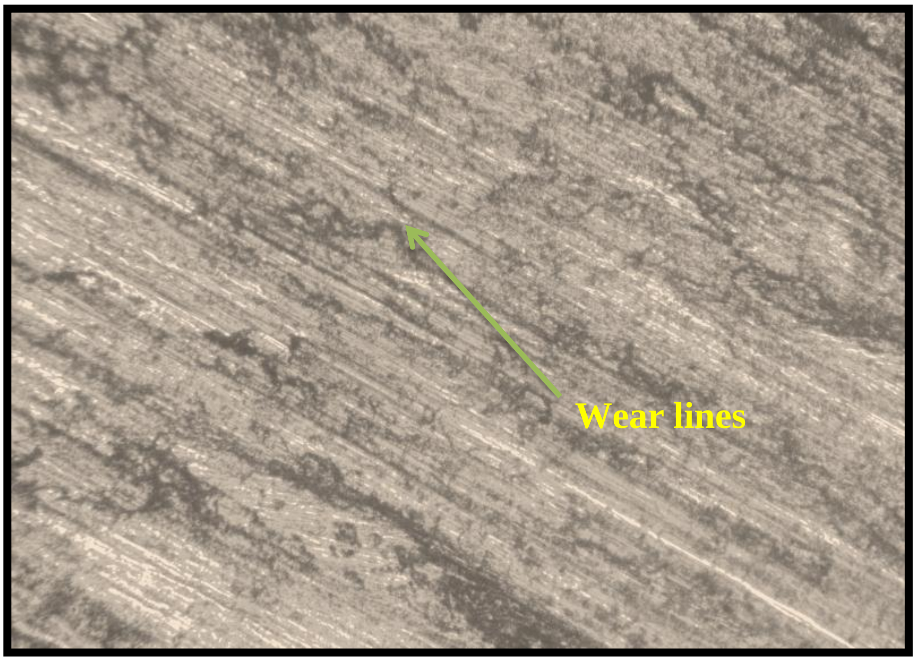

Figure (4.52) : Optical Microscope Image of Sample Surface (100 X) for 1% wt Ni modified Cu-25Zn-4Al alloy and 3wt% B_6O .

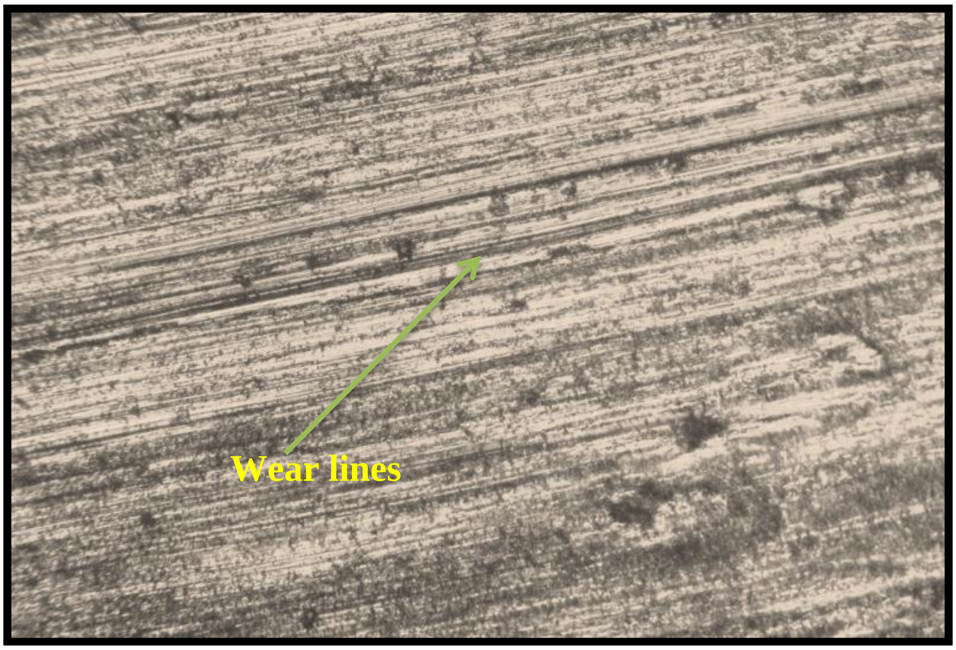

Figure (4.53) : Optical Microscope Image of Sample Surface (100 X) for 1% wt B modified Cu-25Zn-4Al alloy and 3wt% B_6O .

As shown in the figures it is observed that wear lines on worn surface and cavity are in the direction of line wear, and debris has been observed. The Figure (4.51) for 250 rpm and load 10N reveals cavities and debris of reference alloy .In addition that, as time and load are gradually increased, initially small scratches are formed on the surface.

Chapter Five

Conclusions & Recommendations

Chapter five
Conclusions and Suggestions
For Future Works.

5.1. Conclusions

The main conclusions from the experimental study of the examined Cu-25Zn-4Al SMA in this research are included as follows :

1- All the samples with and without additives consist of the two main phases (β-phase and(α-phase) , this is obtained from XRD and microstructure observation.

2- The Ni and B with modified Cu-25Zn-4Al alloy had austenite transformation temperature value higher than that of the unmodified Cu-25Zn-4Al alloy.

3- Addition of 1wt% B to the unmodified Cu-25Zn-4Al alloy reduce the corrosion rate by 25% with respect to reference sample in the 3.5 NaCl .

4- Addition of 1wt% Ni to the unmodified Cu-25Zn-4Al alloy reduce the corrosion rate by 36% with respect to reference sample in the 3.5 NaCl .

5- The XRD results of the corrosion products on the structure of Ni and B modified Cu-25Zn-4Al alloy indicate the position contribution of the Ni and B addition that lead to a denser thicker passive layer of NiO , B_2O_2 , Al_2o_3 ,CuO , ZnO .

6- The 3wt.% boron-oxide modified Cu-25Zn-4Al-1Ni or Cu-25Zn-4Al-1B alloy had an average hardness value higher than that of unmodified Cu-25Zn-4Al alloy and to other amount of boron oxide used in this study .

7- The 3wt.% boron-oxide modified Cu-25Zn-4Al-1Ni or Cu-25Zn-4Al-1B alloy show relatively lower volume loss in wet wear test compared that of unmodified Cu-25Zn-4Al alloy and to other amount of boron oxide used in this study .

5.2. Suggestions For Future Work

The following suggestions should be taken into consideration for future work of copper-based shape memory alloys prepared by powder metallurgy technique.

1- Investigate the effects of element such as Al , Ni and B to the binary alloy (CuZn) on the martensite transformation temperatures .

2- Transmission electron microscopy (TEM) should be used to reveal the structure of another intermetallic compound.

3- To obtain of mechanical properties good recommended used double action press or hot isostatic pressing should be used.

4- Study the resistance for Cu-Zn-Al alloy with Ti ,Ag and Ge against erosion corrosion.

5- Study the corrosion resistance of Cu-Zn-Al prepared by casting with rare earth metals as alloying element additions.

6- Study the properties for Cu-Zn-Al alloy after performing the quenching process with the same element additions .

Chapter Six

Reference

Chapter Six
Reference

[1] V. J. Mathai1, S. Kumar, H. K. Dave and K.P. Desai," Machining/Processing of Shape Memory Alloys – A Review" , 5th National Conference , Recent Advances in Manufacturing,pp.160-165,2015

[2] M. Follon, , & Aernoudt, E. Powder-metallurgically processed shape memory alloys, Proceedings of the 5th European Symposium on Powder Metallurgy, Stockholm (pp. 275-281).

[3] H. J.Van, & Cederstrom J. The present state of shape memory materials and barriers still to be overcome. Proceedings of the first international conference on shape memory and superelastic technologies, (1–6), March 1994.

[4] T. W. Duerig, J. Albrecht, and G. H. Gessinger," A Shape Memory Alloy for High-Temperature Applications", Journal of Metals , pp.14-20,1982 technologies, (1–6), March 1994

[5] ASM Handbook, "Shape Memory Alloys", Properties and Selection: Nonferrous Alloys and Special-Purpose Materials, pp. 897-902, Vol. 2, 1990.

[6] A. C. Kneissl, E. Unterweger, M. Bruncko, G. Lojen, K. Mehrabi and H. Scherngeell," Microstructure and Properties of NiTi and CuAlNi Shape Memory Alloys"Metallurgija – Journal of Metallurgy,Vol.14,pp. 90-100, 2008.

[7] A. Eshghinejad, "Finite Element Study of a Shape Memory Alloy Bone Implant", M.Sc. Thesis, The University of Toledo Digital Repository, (2012).

[8] D.J. Inman, Smart Structure and Materials (2001), Damping and Isolation, (Eds.), 4331, 324-332.

[9] D. E.Hodgson, , Wu M. H., Biermann, R. J., Shape Memory Applications, Inc., Memory Technologies,

andHarrisonAlloys,Inc.,http://web.archive.org/web/2000605085 042/http://www.smainc.com/SMAPa per.html (2011)

[10] M. Granito," A Cooling System for S.M.A (Shape Memory Alloy) Based on The use of Peltier Cells ",PH.D. Thesis, University of Naples “Federico II” – Italy ,Industrial Engineering (XXIII Cycle) ,2010

[11] S. Xenos, " The Unique Properties, Manufacturing Processes and Applications of Near Equatomic Ni-Ti Alloys", M.Sc. Thesis, University of Thessaly Department of Mechanical Engineering Laboratory of Materials, (2016).

[12] X. Liu, Paul K. Chu and C. Ding, "Surface Modification of Titanium, Titanium Alloys, and Related Materials for Biomedical Applications", Materials Science and Engineering R 47,pp. 49–121, (2004) .

[13] D. Tarnita, D. Tarnita and D. Bolcu.,"Orthopaedic Modular Implants Based on Shape Memory Alloys", Biomedical Engineering– From Theory to Applications, pp.431-469, (2011).

[14] M. H. Wu and L. Mc. Schetky , Industrial application for shape memory alloys : A tutorial review ,proc. Technolgies, Pacific Grove, California, 2000 , 171-182.

[15] K. Otsuka and X. Ren, ReviewRecent developments in the research of shape memory alloys, Intermetallics, 7 ,1999, 511-528.

[16] A. Eshghinejad, "Finite Element Study of a Shape Memory Alloy Bone Implant", M.Sc. Thesis, The University of Toledo Digital Repository, (2012).Skočovsk, P. (2000) Designing materials, 1st edition, (ISBN 80-7100- 608-4), Žilina, Slovak republic .

[17] C. Dimities and Lagoudas,"Shape memory alloys modeling and engineering application", Texas AZM University, USA, 2008.

[18] S.L. Angionic , M. Meo and A. Foreman ,"Impact damage resistance and damage suppression properties of shape memory alloys in hybrid composites - a previous" smart Mater . Strut. , Vol 20, 2011, PP. 1 – 24.

[19] T. Yoneygma and S. Miyazaki, " Shape memory alloys for biomedical application" Cam Bridge, England, 2009.

[20] A. Biscarini, G. Mazola and A. Tuissi," Enhanced Nitinol Properties for Biomedical application", Biomedical Engineering, Vol. 1, No. 3, 2008, PP. 180 - 196.

[21] E. Zanaboni, " One way and two way–shape memory effects: thermomechanical characterization of Ni–Ti wires" M.Sc. Thesis, biomedical engineering department, Pavia University, 2008.

[22] ASM Hand book,"Properties and selection nonferrous alloy and Special purpose Materials", 5th edition, Vol. 2, 1998, PP. 897 - 9010.

[23] E . patoor , D . C. Lagoudas and P. B. Entcheve , " Shape memory alloys , part I : General properties and modeling of single crystals " , Mechanics of Materials , Vol . 38, 2006, PP. 391 - 429.

[24] F. Cristina," Iron based shape memory alloys', mechanical and microstructural properties", Chapter 5, http: // creative Commons. Org / licenses / by / 3.0 /, 2013 Borges, pp. 115 - 128.

[25] A. Baruj, T. Kikuchi and S. Kajiwara," Effect of pre - deformation of austenite on shape memory properties in Fe -

Mn - Si - based alloys containing Nb and C ", materials transactions, Vol. 43, No. 3, 2002, pp. 585 - 588.

[26] G. Rondelli and B. vicentini, " Effect of copper on localized corrosion resistance of Ni -Ti shape memory alloy ", Biomaterials, Vol. 23, 2002, pp. 639 - 644.

[27] C .Cismasiu, " shape memory alloys",Janeza Trdine, Croatia, 2010.

[28] A. Nespoli and S. Besseghini, " A complete Thermo - mechanical study of NiTiCu shape memory alloy wire ", J. Thermal Anal Calorim, Vol. 03, 2011, pp. 821 - 826.

[29] S. Kujala, J. Ryhänen and T. Jämsä, " Bone modeling controlled by a nickel - titanium shape memory alloy intra medullary nail ", Biomaterials, Vol. 23 , 2002 , PP . 2535 - 2543.

[30] Q. Li, Y. Zeng and X. tang, " The application and research progresses of Nickel - titanium shape memory alloy in reconstructive surgery ", Australia's phys. Eng. Sci. Med., Vol. 33 2010, PP. 129 - 136.

[31] A. K. Abid Ali ,Effect of aging and step –quenched heat treatment on the Martensitic transformation of CuZnAl shape memory alloy , The Iraqi Journal For Mechanical And Material Engineering, 10(1), 2010 .

[32] A. k. Abid Ali , Preparation of copper zinc Aluminum shape shape memory alloy by using powder metallurgy technique , Babylon University journal , 17(1) , 2008.

[33] B. M. Rabeeh , M.M EL Batanouny and A. E. EL Ashram , microstructural characterization and solid state processing of Cu-Zn-Al shape memory alloy in a matrix composite , Canadian Journal on Mechanical Sciences and Engineering , 2 (2) , 2011.

[34] S. Pourkhorshidi, M. Naeimi , N. Parvin, S. Mohammad , M.Zamani, H. Ebrahimnia ,Manufacturing and evaluating cu-based shape memory alloy by hot extrusion of PM samples made by mechanical alloying , Brno, Czech Republic, EU. , 5, 2012, 23 – 25

[35] V. Torra, A. Isalgue, C. Auguet, G. Carreras, F. C. Lovey, P. Terriault, Damping in civil engineering using SMA Part 2 - particular properties of NiTi for damping of stayed cables in bridges, Canadian Metallurgical Quarterly 52 (2013) 81–89.

[36] Y. Bellouard,‟ Shape memory alloys for micro system: A review from a material research perspective ”, Materials science and engineering, A 481 - 482, 2008, pp. 582 - 589.

[37] D. R. Walker,‟ Fabrication and design of Hybrid monolithic shape memory alloy actuator ”, M. Sc. thesis, university of Water Loo, 2008.

[38] J. F. Wakjita‟ The VT1 shape memory alloy heat Engine Design”, M. SC. thesis ,,Virginia university , Blacksburg , 2001

[39] D. Stoeckel , The Shape Memory Effect - Phenomenon, Alloys and Applications , Proc.Shape Memory Alloys for Power Systems EPRI , NDC . Nitinol Devices & Components, Inc., Fremont, CA, , 1995,1-13 .

[40] J.S. Cory, and J.C. McNchols, , Society of Automotive Engineers, Inc., 1978, pages 1998-2004..

[41] J. Arghavani , Thermo-mechanical behavior of shape memory alloys under multiaxial loadings: constitutive modeling and numerical implementation at small and finite strain , doctoral diss., Sharif University of Technology, Tehran, Iran ,2010.

[42] L.E. Penrod, , Fabrication and characterization of porous shape memory alloys , Master diss., Texas A& M university , 2003.

[43] C. Bouvet Calloch, S. Lexcellent,: Mechanical behavior of a Cu-Al-Be shape memory alloy under multiaxial proportional and nonproportional loadings. J. Eng. Mater. Technol. 124, 112–124 (2002).

[44] W. Huang , shape memory alloys and their application to actuators for deployable structure , doctoral diss. , university of Cambridge department of engineering ,1998.

[45] J. A. Harvey ,Smart materials ,Handbook of Materials Selection, Edited by Myer Kutz , John Wiley & Sons, Inc., New York ,2002.

[46] A. Bekker, , L.C. Brinson,: Temperature-induced phase transformation in a shape memory alloy: Phase diagram based kinetics approach. J. Mech. Phys. Solids 45(6), 949–988 (1987)

[47] K.Yamauchi , I. Ohkata , k. Tsuchiya and S. Miyazaki , Shape memory and super elastic alloy: technologies and application (Published by Woodhead Publishing Limited , Sawston , Cambridge CB22 3HJ, UK,2011).

[48] S. Suranen , Microwave Assisted Reactive Sintering of TiNi Shape Memory Alloy, Master thesis Submitted to the Graduate Faculty of Science Degree in Bioengineering , 2011.

[49] M. Ahlers , " The martensitic transformation mechanisms and crystallography", philosophical magazine , Vol.82, No.6, PP.1039 , 2002.

[50] T.J.Lim, , Mc Dowell, D.L.: Mechanical behavior of an Ni-Ti shape memory alloy under axial-torsional proportional and

[51] Y. F. Zheng, B. L. Wang, J. G. Wang, C. Li and L. C. Zhao, “Corrosion Behavior of Ti-Nb-Sn Shape Memory Alloys in Different Simulated Body Solutions,” Materials Science and Engineering A, Vol. 438-440, 2006, pp. 891- 895.

[52] C. M. Wayman and T.W Duerig , An introduction to martensite and shape memory , on Engineering Aspects of shape memory alloys, Duerig ,T.W, Metton , K.N, Stockel ,D. and Wayman , C.M. (eds) ,1990,P.3.

[53] M. H. Wu, T.W Duerig , K.N. Melton , D. Stockel and C. M. Wayman , Cu-based shape memory alloys , In Engineering Aspects of shape memory alloys , 1990 ,P.96.

[54] J. Malarria, F.C. Lovey and M. Sade ,Two way shape memory effect in CuZnAl single crystals after pseudoelastic cycling at low temperatures , Materials Science and Engineering Journal A ,517, 2009, 118–124.

[55] D. E Hodgson , H. Wu Ming and R.J. Biermann , shape memory alloys , ASM Handbook , 2(Properties and Selection: Nonferrous Alloys and Special-Purpose Materials ASM Handbook Committee ,1990) 897-902.

[56] A.C. Souza, , Mamiya, E.N., Zouain, N.: Three-dimensional model for solids undergoing stress-induced phase transformations. Eur. J. Mech. A/Solids 17(5), 789–806 (1998).

[57] R. Z. Jameel , manufacturing and properties studying of Cu-Al-Ni shape memory alloys , Master diss. , Alnahrain university in mechanical engineering , 2013

[58] V. Asanovic , , Delijic , K. and Jaukovic , N." Isothermal decomposition of the β phase in CuZnAl shape memory alloys " J.Materialin in Technologije , Vol.40 , pp.4, 2006.

[59] A . K. Abid Ali, & Z. T. Khulief.Al-Tai , The Effect of Iron Addition on the Dry Sliding Wear and Corrosion Behavior of Cu Al Ni Shape Memory Alloy ,Eng. & Tech. Journal, 28 (24) , 2010 .

[60] A. Lendlein, and S. KelchAngew , Shape-Memory Polymers , Angew.Chem. Int. Ed. , 41 ,2002 ,2034 – 2057

[61] Duerig, T.W., Melton, K.N., Stoekel, D., Wayman, C.M.: Engineering Aspects of Shape Memory Alloys. ButterworthHeinemann, London (1990)

[62] D. Golberg, Xu Ya, Murakami Y, Otsuka K, Ueki T, Shape memory and super elastic alloy Horikawa H. Mater Lett 1994;22:241.,: technologies and application (Published by Woodhead Publishing Limited , Sawston , Cambridge CB22 3HJ, UK,2011).

[63] A. Vanja , D. Kemal and J. Nada , Isothermal decomposition of the β′ phase in Cu-Zn-Al shape memory alloys , original scientific article / Izvirni znanstveni clanek ,Mtaec 9 , 40(4) , 2006 ,153-157 .

[64] V. Recarte and R.B. Perez-Saez ,Ordering kinetics in Cu-Al-Ni shape memory alloys, Journal of applied physics , 86(10) ,1999,5467-5473.

[65] Z. Xu, Q. Min and Y. Dazhi , (α + β) Dual phase CuZnAl shape memory alloy , Chin J. Met. Sci. Technology , 6, 1990, 427-430.

[66] G. Scarsbrook , and stobbs , W.M." The martensitic transformation behaviour and stabilization of rapidly quenched CuZnAl ribbons " J.Act Metall. Vol.35 ,No.l , pp.47 , 1987 .

[67] Z. G. Wez, R. Sandstrom and S. Miyazaki, “Review Shape Memory Materials and Hybrid Composites for Smart Systems,” Journal of Materials Science, Vol. 33, No. 15, 1998, pp.

[68] M. H. Wu, T.W Duerig , K.N. Melton , D. Stockel and C. M. Wayman , Cu-based shape memory alloys , In Engineering Aspects of shape memory alloys , 1990 ,P.96.

[69] J. Pena , F.J. Gil and T.M. Guilemany , Effect of microstructure on dry sliding wear behavior in CuZnAl shape memory alloys , Acta Mat., 50 , 2002 , 3115.

[70] C. Zhang and Z.N. Farhat , sliding wear of superelastic TiNi alloy, wear Journal ,267, 2009, 394-400.

[71] A.Huda Khairallah , Studying the Effect of Mn and Ti on some Properties of Cu-25Zn-4Al Shape Memory Alloy, Thesis of Master Degree of the Collage of Materials Engineering ,2014.

[72] Y. F. Zheng , B.L. Wang , J.G. Wang , C. Lia and L.C. Zhao , Corrosion behaviour of Ti–Nb–Sn shape memory alloys in different simulated body solutions , Materials Science and Engineering Journal A 438–440, 2006 ,891–895

[73] P. Rocher, L. El Medawar, J. C. Hornez , M. Traisnel, J. Breme and H.F. Hildebrand , Biocorrosion and cytocompatibility assessment of NiTi shape memory alloys, Scripta Materialia Journal , 50 ,2004,255–260.

[74] D. J. Puranen , Biocompatibility Evaluation of nickel titanium shape memory metal alloy , Academic diss. , Department of Surgery, Oulu University , Jorma Ryhanen , 1999 .

[75] H. wang , W. wu and F. yand , dry sliding wear behavior in CuZnAl shape memory alloys , Acta Mat., 50 , 2002 , 21117.

[76] R. K. Abdul Abid Ali and Aseel S. h , Study of Compression Behaviour of a Cu-13Al-4Ni-xCr Shape Memory Alloys Prepared by powder metallurgy process, Journal of Babylon University/Engineering Sciences/ No.(1)/ Vol.(25): 2017V.

[77] F. Sampath , effect of Zr on microstructure and transformation temperatures of Cu-Al-Ni shape memory alloys, proceedings of ISSS , 2005.

[78] H. ali , A . Hubio , Investigate The Effect of titanium addition on the microstructure , sliding wear resistance and shape memory effect of Cu-Al-Ni SMA, Journal of Engineering ans applied sciences , 13(16) 6910- 6914,2018.

[79] H. H. Kuo , W.H. Wang , Y.F. Hsu and C.A. Huang , The corrosion behavior of Cu–Al and Cu–Al–Be shape-memory alloys in 0.5 M H2SO4 solution , Corrosion Science ,48 ,2006,.4352–4364.

[80] U. S. Mallik , V. Sampath , Effect of alloying on microstructure and shape memory characteristics of Cu–Al–Mn shape memory alloys, A 481–482 , 2008, 680–683.

[81] R. Zengin and N. Kayal , Structural and Morphological Investigations on Shape Memory CuZnAl Alloys , 2010.

[82] B. Y. Chen, C. H. Liang, D. J. Fu and D. M. Ren, “Corrosion Behavior of Cu and Cu-Zn-Al Shape Memory Alloy in Simulated Uterine Fluid,” Contraception, Vol. 72, No. 3, 2005, pp. 221-224.

[83] M. Ahlers , " The martensitic transformation mechanisms and crystallography", philosophical magazine , Vol.82, No.6, PP.1039 , 2002.

[84] S1. Sathish , U. S. Mallik2, T. N. Raju1, Microstructure and Shape Memory Effect of Cu-Zn-Ni Shape Memory Alloys, Journal of Minerals and Materials Characterization and Engineering, 2014, 2, 71-77

[85] D. Nam Nguyen , P. Khanh , A Study Of Phase Transformation In Shape Memory Alloy Cual9fe4 , Journal For Mechanical And Engineering Research and Development , 42(2),72-75 , 2019

[86] S. Deepjyoti Basak " Investigation of Cu based shape memory alloy as a reinforcement for metal matrix composite" , Journal of Advancements in Material Engineering Vol, 3 , Iss.3 , pp. 19-29 ..

[87] S Jassim M.. , Abdul R. K.Abid AliȦ , Huda A. , (2014). Corrosion study of CuAlZn Shape Memory Alloys in 3.5 NaCl Solution, International Journal of Current Engineering and Technology E-ISSN 2277 – 4106, P-ISSN 2347 - 5161

[88] Zorica Stošića, Dragan Manasijevića. (2017). Effects of Composition and Thermal Treatment of Cu-Al-Zn Alloys with Low Content of Al on their Shape-memory Properties, 20(5): 1425-1431

[89] K. Kenneth Alaneme* , U. Shaibu " Mechanical behaviour and damping properties of Ni modified CueZneAl shape memory alloysy ,Journal of Science: Advanced Materials and Devices 3 (2018) 371-379.

[90] P. Heresi, R. Herrera, M. O. Moroni, Behavior of Shape Memory Cu-Zn-Al Alloy Plates for Use in Energy Dissipators, Universidad de Chile, Santiago, Chile , 2018, 1-11.

[91] A. S. Hamza , study of corrosion and dry sliding wear of Cu-Al-Ni shape memory alloys , Master diss. ,university of Babylon of the collage of materials engineering ,2013.

[92] R. Elst , J. V. Humbeek and L. Delaey , Grain Refinement of Cu-Zn-Al and Cu-Al-Ni by Ti addition , Mat. Sci. Tech., 4, 1988,644-648.

[93] T. Inaba , N. Shozo , I. Osamu , N.Norihiko and S. Toshihiko, The making of Cu-Zn-Al sintered shape memory alloys , Journal of the Japan Society of Powder and Powder Metallurgy, 36 (2) , 1989, 149-152.

[94] K.K. Alaneme, E.A. Okotete, M.O. Bodunrin Microstructural analysis and corrosion behaviour of B modified Cu-Zn-Al shape memory alloys Cor. Rev., 35 (1) (2017), pp. 3-12, 10.1515/corrrev-2016-0053.

[95] W.D.Callister , Materials Science and engineering , 5 th ed .,United States of Amerca ,2000.

[96] M. Gojic , L. Vrsalovi , S. Kozuh , A. Kneissl , L. Anzel , S Gudi , B. kosec , and M. kliski , Electrochemical and microstructure study of Cu-Al-Ni shape memory alloy , adopted from Journal of alloy and compound , 2011, 9782-9790.

[97] ASTM E407 − 07 (2011) " Standard Practice for Micro-etching Metals and Alloys" ASTM international .

[98] Z. Linrong , S. Ruidi L. , Qingsong W. , Chunze Y. , Effect of element evaporation on the microstructure and properties of CuZnAl shape memory alloys prepared by selective laser melting. journal homepage:127 (2020)106164.

[99] E.S. Al-Hassani , A.H. Ali , S.T. Hatem, Investigation of Corrosion Behavior for Copper-Based Shape Memory Alloys in

different Media, Engineering and Technology Journal, Vol. 35, Part A, No. 6, pp. 578-586, 2017.

[100] L. Christian, “Shape-Memory Alloys Handbook”, Apr 8, pp.61-108, 2013.

[101] ASTM B-328 (2003) "Standard Test Method for Density, Oil Content, and Interconnected Porosity of Sintered Metal Structural Part and Oil – Impregnated Bearing "ASTM international.

Appendixes

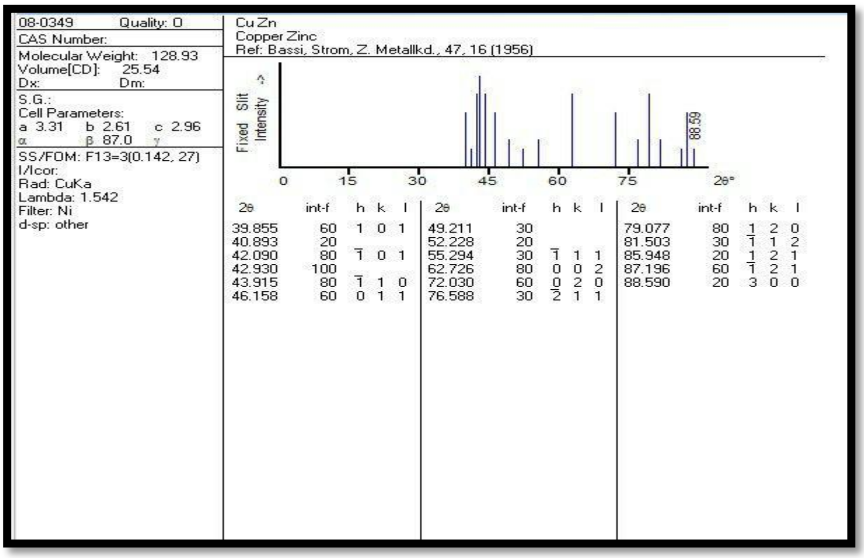

Figure (A-1): XRD Card for Compound (CuZn) .

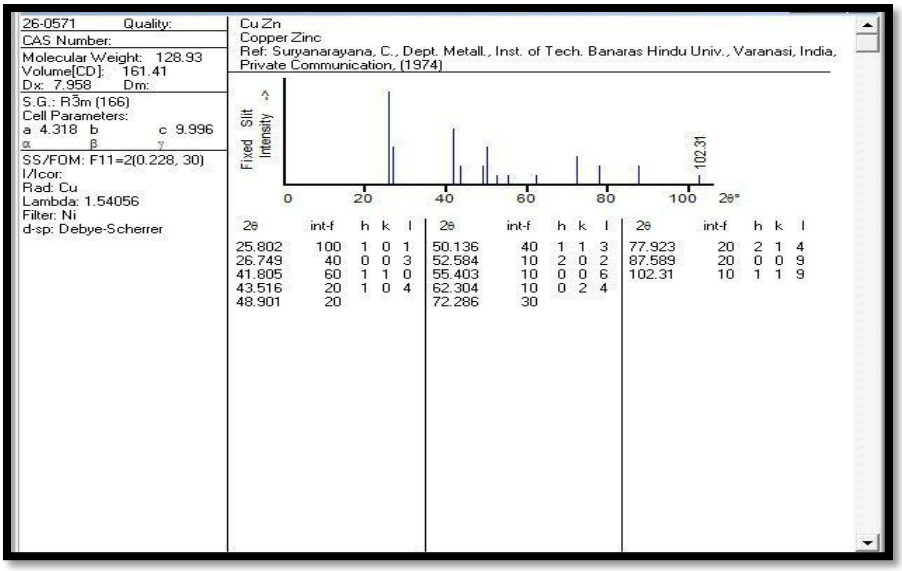

Figure (A-2): XRD Card for Compound (CuZn) .

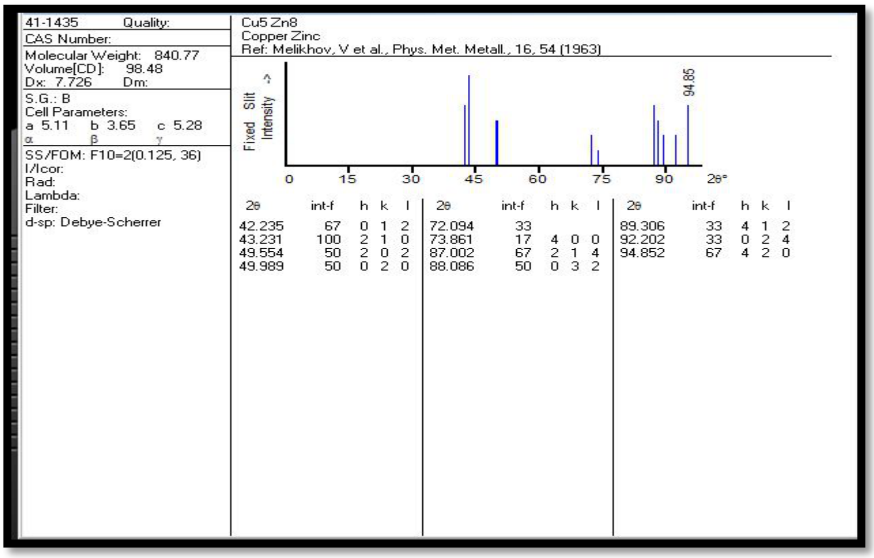

41-1435 Quality:
CAS Number:
Molecular Weight: 840.77
Volume[CD]: 98.48
Dx: 7.726 Dm:
S.G.: B
Cell Parameters:
a 5.11 b 3.65 c 5.28
α β γ
SS/FOM: F10=2(0.125, 36)
I/Icor:
Rad:
Lambda:
Filter:
d-sp: Debye-Scherrer

Cu5 Zn8
Copper Zinc
Ref: Melikhov, V et al., Phys. Met. Metall., 16, 54 (1963)

2θ	int-f	h	k	l	2θ	int-f	h	k	l	2θ	int-f	h	k	l
42.235	67	0	1	2	72.094	33				89.306	33	4	1	2
43.231	100	2	1	0	73.861	17	4	0	0	92.202	33	0	2	4
49.554	50	2	0	2	87.002	67	2	1	4	94.852	67	4	2	0
49.989	50	0	2	0	88.086	50	0	3	2					

Figure (A-3): XRD Card for Compound (Cu_5Zn_8) .

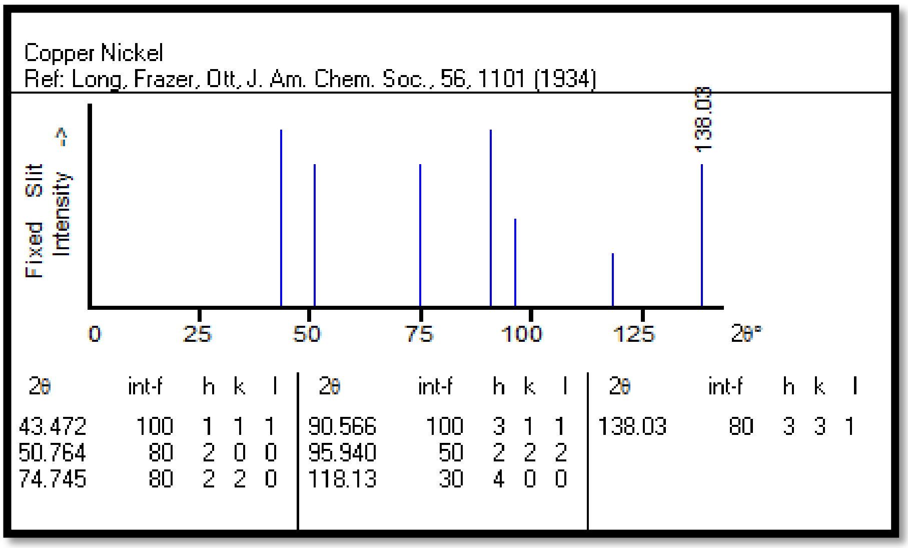

Copper Nickel
Ref: Long, Frazer, Ott, J. Am. Chem. Soc., 56, 1101 (1934)

2θ	int-f	h	k	l	2θ	int-f	h	k	l	2θ	int-f	h	k	l
43.472	100	1	1	1	90.566	100	3	1	1	138.03	80	3	3	1
50.764	80	2	0	0	95.940	50	2	2	2					
74.745	80	2	2	0	118.13	30	4	0	0					

Figure (A-4): XRD Card for Compound (CuNi) .

Al B2
Aluminum Boron
Ref: Wong-Ng, W., McMurdie, H., Paretzkin, B., Hubbard, C., Dragoo, A., NBS (USA), ICDD Grant-in-Aid, (1988)

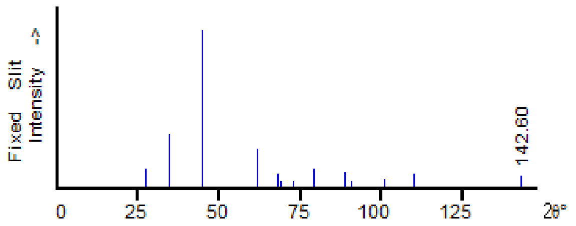

2θ	int-f	h	k	l	2θ	int-f	h	k	l	2θ	int-f	h	k	l
27.417	12	0	0	1	68.768	4	1	1	1	100.63	5	1	0	3
34.413	34	1	0	0	72.558	4	2	0	0	109.77	8	2	1	1
44.541	100	1	0	1	79.217	12	2	0	1	135.24	<1	2	0	3
61.693	24	1	1	0	88.512	10	1	1	2	142.60	7	0	0	4
67.905	8	1	0	2	90.557	4	0	0	3					

Figure (A-5): XRD Card for Compound (AlB_2) .

Al2 O3
Aluminum Oxide
Ref: Grier, D., McCarthy, G., North Dakota State University, Fargo, North Dakota, USA, ICDD Grant-in-Aid, (1991)

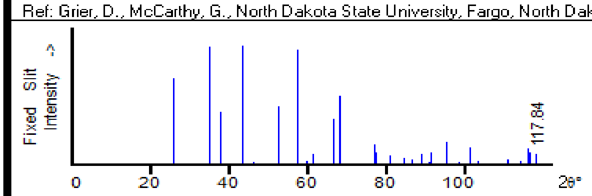

2θ	int-f	h	k	l	2θ	int-f	h	k	l	2θ	int-f	h	k	l
25.576	72	0	1	2	74.300	1	2	0	8	95.236	19	2	2	6
35.150	98	1	0	4	76.873	17	1	0	10	98.380	2	0	4	2
37.767	44	1	1	0	77.234	10	1	1	9	101.06	14	2	1	10
41.683	1	0	0	6	80.415	1	2	1	7	102.81	<1	1	1	12
43.340	100	1	1	3	80.692	7	2	2	0	103.30	3	4	0	4
46.175	2	2	0	2	83.208	1	3	0	6	104.63	<1	1	3	7
52.548	48	0	2	4	84.348	5	2	2	3	109.52	1	3	2	1
57.498	96	1	1	6	85.135	<1	1	3	1	109.85	<1	1	2	11
59.738	3	2	1	1	86.347	4	3	1	2	110.81	<1	2	3	2
61.124	4	1	2	2	86.500	4	1	2	8	110.97	4	3	1	8
61.303	9	0	1	8	88.997	8	0	2	10	114.06	3	2	2	9
66.514	38	2	1	4	90.705	2	0	0	12	116.08	13	3	2	4
68.202	57	3	0	0	91.179	10	1	3	4	116.61	10	0	1	14
70.411	1	1	2	5	94.816	<1	3	1	5	117.83	8	4	1	0

Figure (A-6): XRD Card for Compound (Al_2O_3) .

Cu O
Copper Oxide
Ref: Swanson, Tatge, Natl. Bur. Stand. (U.S.), Circ. 539, I, 49 (1953)

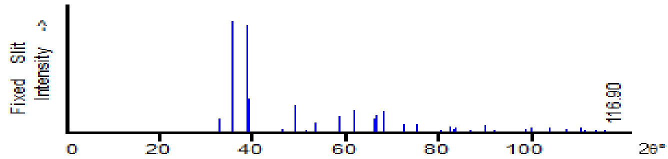

2θ	int-f	h	k	l	2θ	int-f	h	k	l	2θ	int-f	h	k	l
32.520	12	1	1	0	68.140	19	2	2	0	98.367	3	0	2	4
35.451	49	0	0	2	72.414	7	3	1	1	99.747	4	3	1	3
35.553	100	$\bar{1}$	1	1	75.022	6	0	0	4	101.86	<1	4	0	2
38.730	96	1	1	1	75.232	7	$\bar{2}$	2	2	103.50	4	$\bar{1}$	1	5
38.922	30	2	0	0	80.180	2	$\bar{2}$	0	4	107.10	3	4	2	0
46.308	3	$\bar{1}$	1	2	82.375	5	$\bar{3}$	1	3	109.45	<1	$\bar{1}$	3	3
48.761	25	$\bar{2}$	0	2	83.042	3	2	2	2	110.23	4	$\bar{4}$	2	2
51.345	2	1	1	2	83.348	2	3	1	2	111.26	2	$\bar{4}$	0	4
53.411	8	0	2	0	83.605	4	4	0	0	113.53	2	1	1	5
58.315	14	2	0	2	86.586	2	$\bar{4}$	0	2	115.65	2	1	3	3
61.569	20	$\bar{1}$	1	3	89.763	6	$\bar{1}$	3	1	116.89	1	$\bar{5}$	1	1
65.806	12	0	2	2	91.682	2	1	3	1					
66.227	15	$\bar{3}$	1	1	95.647	<1	2	0	4					

Figure (A-7): XRD Card for Compound (CuO) .

Ni O
Nickel Oxide
Ref: Wies, S., Eysel W., Mineral.-Petrograph., Institut der Universitaet Heidelberg, Germany, ICDD Grant-in-Aid, (1992)

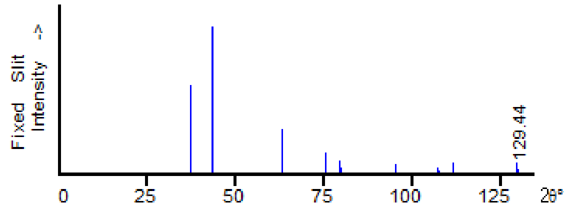

2θ	int-f	h	k	l	2θ	int-f	h	k	l	2θ	int-f	h	k	l
37.248	60	1	0	1	79.372	9	2	0	2	107.10	2	1	0	7
43.286	100	0	1	2	79.501	4	0	0	6	111.05	7	1	2	2
62.852	30	1	1	0	95.052	6	0	2	4	111.18	7	1	1	6
62.912	25	1	0	4	106.90	4	2	1	1	129.16	7	2	1	4
75.404	14	1	1	3	107.00	2	2	0	5	129.43	3	0	1	8

Figure (A-8): XRD Card for Compound (NiO) .

Zn O
Zinc Oxide
Ref: Vannerberg, Ark. Kemi, 14, 119 (1959)

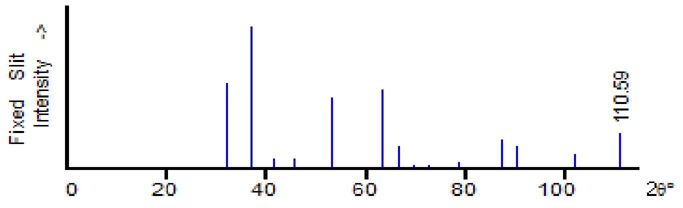

2θ	int-f	h	k	l	2θ	int-f	h	k	l	2θ	int-f	h	k	l
31.901	60	1	1	1	63.298	55	3	1	1	87.196	20	3	3	1
36.993	100	2	0	0	66.600	15	2	2	2	90.141	15	4	2	0
41.503	6	2	1	0	69.581	2	2	3	0	101.59	10	4	2	2
45.691	6	2	1	1	72.608	2	3	2	1	110.58	25	5	1	1
53.210	50	2	2	0	78.534	4	4	0	0					

Figure (A-9): XRD Card for Compound (ZnO) .

Cu Cl
Copper Chloride
Ref: Meisalo, V., Kalliomaki, High Temp. High Pressures, 5, 663 (1973)

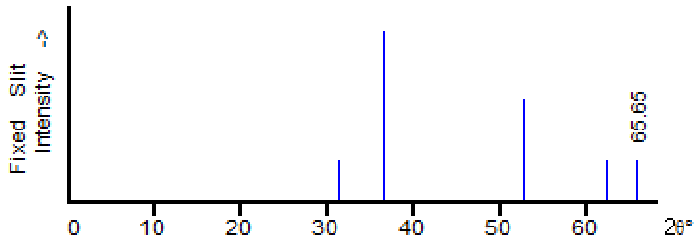

2θ	int-f	h	k	l	2θ	int-f	h	k	l	2θ	int-f	h	k	l
31.316	25	1	1	1	52.551	60	2	2	0	65.649	25	2	2	2
36.403	100	2	0	0	62.304	25	3	1	1					

Figure (A-10): XRD Card for Compound (CuCl) .

B2 O3
Boron Oxide
Ref: Berger, Acta Chem. Scand., 7, 611 (1953)

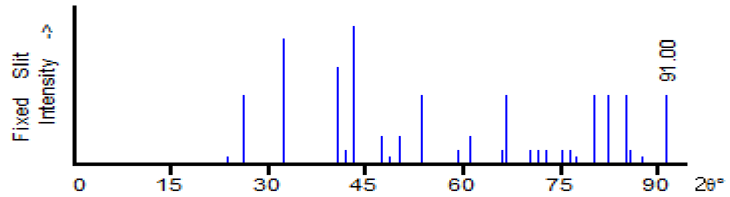

2θ	int-f	h	k	l	2θ	int-f	h	k	l	2θ	int-f	h	k	l
23.707	5	1	0	0	53.546	50	2	0	2	76.226	10	2	0	5
26.033	50	1	0	1	59.219	10	2	0	3	77.175	5	3	0	1
32.172	90	0	0	3	60.808	20	1	0	5	80.108	50	3	0	2
40.415	70	1	0	3	65.806	10	2	1	0	82.264	50	1	1	6
41.683	10	1	1	0	66.600	50	2	1	1	85.107	50	3	0	3
43.123	100	1	1	1	70.056	10	2	1	2	85.665	10	1	0	7
47.305	20	1	1	2	71.401	10	1	1	5	87.294	5	2	0	6
48.595	5	2	0	0	72.543	10	1	0	6	90.995	50	2	1	5
50.019	20	1	0	4	75.232	10	2	1	3					

Figure (A-11): XRD Card for Compound (B_2O_3) .

Appendix B

Figure (B): Planetary Balls Mill.

الخلاصة

نظرا إلى التطبيقات والصناعات التكنلوجيا العديدة للسبائك ذاكرة الشكل ذات أساس نحاس مكونه من Cu- 25 wt% Zn- 4 wt% Al يجعلها موضوعا بحثيا مثيرا للاهتمام ، وكذلك أمتلاكها العديد من الصفات والمميزات المهمة ومنها الكلفة المنخفضة مقارنة مع سبيكة نيكل – تيتانيوم ، سهولة تصنيعها وقابلية استعادة شكلها الاصلي . في الجزء العملي سوف ندرس تاثير اضافة العناصر السبائكيه النيكل (Ni) والبورون (B)، وايضا اوكسيد البورون (B_6O) للسبيكة على السلوك الميكانيكي والكيمائي لها . يُقـسم هذا العمل الى جزئين الجزء الاول هو يختص بالبنية المجهريه ,انواع الاطوار الظاهرة , درجات حرارة التحول وتاثير السبائك الذاكرة للشكل والخواص الكيمائيه للسبيكة الاساس ومع اضافة العناصر السبائكية نيكل (Ni)، وبورون(B). ان هذه السبيكة Cu-Zn-Al تم تحضيرها بطريقة ميتالورجيا المساحيق و تم ايضا اضافة العناصر السبائكيه لها والمتمثلة بالنيكل والبورون بنسبة وزنيه (0.5%، 0.7%، 1%) لكل عنصر. بعد عملية خلط المساحيق لمدة اربع ساعات تكبس بضغط مقداره 675 ميكا باسكال. واجريت عملية التلبيد للعينات المستخدمة في هذه الدراسة بفرن انبوبي تحت تحكم غاز الاركون بثلاث مراحل ، المرحلة الأولى (350 درجة مئوية) لمدة ساعتين ، المرحلة الثانية (550 درجة مئوية) لمدة ساعتين والمرحلة الثالثة (900 درجة مئوية) لمدة 4 ساعات . بعد ذلك اجريت العديد من الفحوصات مثل الفحص المجهري وحيود الاشعة السينية و المجهر الالكتروني الماسح و اختبار DSC وSME و اختبار التاكل للسبيكة الاساس والسبيكة بعد اضافة العناصر (Ni) و(B) .

لقد أثبت تحليل XRD والبنية المجهرية ان العينات المحضرة تتكون من طورين هما طور (α)يمثل طور المارتنسايت وطور الاوستنايت (βCu_5Zn_8) . كما بينت نتائج اختبار DSC بان درجات حرارة التحول (A_f,A_s) لسبيكة نحاس - زنك – المنيوم هي (228.32^0 سليزيه ، 326.93^0 سليزيه)على التوالي بينما اعلى درجة حرارة تحول في سبيكة نحاس - زنك – المنيوم–1% نيكل و سبيكة نحاس - الزنك – المنيوم–1% بورون هي (274.64^0 سليزيه ، 335.38^0 سليزيه) و (273.88^0 سليزيه ، 343.68^0 سليزيه) على التوالي . كما أظهرت نتائج Shape Memory Effect للسبيكة باضافة العناصر السبائكية (Ni) , (B) تكون افضل من السبيكة الاساس ، حيث كانت نتائج SME هي ٪ 29.1 عند نسبة ٪ 1 wt.(Ni) و ٪ 23.65 عند نسبة ٪ 1 wt. (B) .

تم اجراء اختبار التاكل للسبائك المحضرة قبل وبعد الاضافة بتقنية Potentiodynamic Polarization في محلول كلوريد لصوديوم بتركيز 3.5% ، واظهرت النتائج بان مقاومة التاكل تحسنت بنسبة 36% عند نسبة 1 wt% النيكل و 25% عند 1 wt% بورون ، حيث كان معدل التآكل (0. 033 mpy) و (0. 039 mpy) على التوالي ، علما ان معدل التأكل للسبيكة الاساس هو(0. 052 mpy) .تم اجراء فحص تشتيت بالأشعة السينية الطيفية لسبيكة نحاس-زنك – المنيوم الذاكرة للشكل الملبدة قبل وبعد اضافة النيكل و البورون تم اجراؤه للسطح العينات بعد عملية التأكل وذلك لغرض الحصول على التركيب الكيميائي للطبقة الواقية التي تغطي السطح واهمها (Al_2O_3),(Cu_2O) و (NiO) .

الجزء الثاني يدرس تاثير اضافة كميات مختلفه (1 wt%, 3 wt%, 5 wt%) من اوكسيد البورون على الخواص الميكانيكيه للعينات المحضرة قبل وبعد الاضافة ، حيث بينت النتائج بان افضل قيمة للصلادة الدقيقة (Hv.) هي 176.6 و 165.8 للعينات ذات التركيب الكيميائي Cu-25Zn-4Al-1Ni- 3%B_6O و Cu-25Zn-4Al-1B- 3%B_6O على التوالي. وايضا تم دراسة اختبار البلى الانزلاقي الرطب للعينات المحضرة قبل وبعد الاضافة عند الاحمال (2N, 5N , 10N) في درجة الحرارة الغرفة ، وأظهرت النتائج بان نسبة 3 ٪ اوكسيد البورون B_6O تعطى افضل مقاومة بلى للسبائك المحضرة خلال هذه الدراسة .

وزارة التعليم العالي والبحث العلمي
جامعة بابل– كلية هندسة المواد
قسم المعادن

تحسين السلوك الميكانيكي والتآكل لسبيكة نحاس -٢٥٪ زنك-٤٪ ألمنيوم الذاكرة الشكل

رسالة ماجستير مقدمة

إلى

مجلس كلية هندسة المواد/ جامعة بابل

كجزء من متطلبات نيل درجة الماجستير

في هندسة المواد /معادن

مقدمة من قبل

اسراء نايف كاظم عبيس

إشراف

أ. د. علي هوبي حليم | **أ.م. د. زهير طالب خليف**

٢٠٢١م